Chemical Weathering, Soil Development, and Geochemical Fractionation in a Part of the White Mountains, Mono and Inyo Counties, California

GEOLOGICAL SURVEY PROFESSIONAL PAPER 352-J

Chemical Weathering, Soil Development, and Geochemical Fractionation in a Part of the White Mountains, Mono and Inyo Counties, California

By DENIS E. MARCHAND

EROSION AND SEDIMENTATION IN A SEMIARID ENVIRONMENT

GEOLOGICAL SURVEY PROFESSIONAL PAPER 352-J

UNITED STATES GOVERNMENT PRINTING OFFICE, WASHINGTON: 1974

UNITED STATES DEPARTMENT OF THE INTERIOR

ROGERS C. B. MORTON, *Secretary*

GEOLOGICAL SURVEY

V. E. McKelvey, *Director*

Library of Congress catalog–card No. 73-600361

For sale by the Superintendent of Documents, U.S. Government Printing Office
Washington, D.C. 20402 – Price $1.35 (paper cover)
Stock Number 2401-02484

CONTENTS

ILLUSTRATIONS

TABLES

CHEMICAL WEATHERING, SOIL DEVELOPMENT, AND GEOCHEMICAL FRACTIONATION IN A PART OF THE WHITE MOUNTAINS, MONO AND INYO COUNTIES, CALIFORNIA

By DENIS E. MARCHAND

ABSTRACT

The White Mountain erosion surface truncates a variety of late Precambrian and Cambrian metasedimentary units and several Mesozoic plutonic bodies; it is overlain by Tertiary basalts. Present climatic gradients in the 30-square-mile study area are not pronounced, and thus weathering of diverse lithologies under a reasonably uniform semiarid subalpine environment may be studied here. The local vegetation, consisting primarily of sagebrush, bristlecone and limber pine, and associated perennial herbs, is relatively sparse and shows marked discontinuities across geologic contacts. Soils in the region are immature lithosols, usually less than 1 foot deep, but better developed soils may have formed prior to or during late Tertiary uplift, only to be stripped by subsequent erosion. A reworked rhyolitic late Pleistocene ash and local windblown fragments are abundant soil contaminants and complicate efforts to decipher mineralogical and chemical changes due to weathering.

Rock weathering in this region appears to be primarily a function of mineral composition and of the density and degree of physical rock flaws which serve as avenues for penetrating fluids. Physical breakdown, which tends to precede chemical weathering, seems as closely related to lithologic features as to climate. Since erosion is aided by rapid weathering, easily disintegrated rock types such as course-grained carbonate and adamellite and fissile shale have eroded to topographic lows while slow-weathering fine-grained carbonate, quartzose sandstone, basalt, aplitic dikes, and mafic inclusions have resisted erosion.

Reed Dolomite, a Precambrian unit, weathers by frost riving to polycrystalline, cleavage-bounded grains, except where the presence of thermally recrystallized rock has led to production of single-crystal fragments. Mineral weathering occurs in the sequence dolomite $\gg$ tremolite, epidote $>$ talc, K-feldspar, biotite $\geqslant$ apatite $>$ quartz and ilmenite. Percentage chemical losses from bedrock to soil are Mg $>$ Ca $>$ Sr $>$ Mn $\approx$ Fe, for carbonate-constituent elements. Authigenic calcite is apparently precipitated in the soil during dry seasons and partially dissolved during wet periods. Spring waters related in part to the dolomite show relative mobilities of Mg $>$ Ca $>$ Fe $>$ Mn. Ion-activity product computations indicate that these waters are undersaturated with respect to both calcite and dolomite. PCO_2 exceeds atmospheric values by over an order of magnitude and those of adamellite-derived waters by several times. Dolomite soil water extracts appear closer in pH to the spring waters than to rain or snow, although the soil water composition is obviously quite different from either of these fluids. Chemical changes in both solid and liquid phases related to the dolomite appear to begin along with physical breakdown in the early stages of rock weathering.

Adamellite of Sage Hen Flat weathers by frost riving along intergranular weaknesses, causing boulder exfoliation and accumulation of grus. This coarse material, largely unaltered except for minor Fe oxidation, later undergoes important chemical breakdown during its transformation to finer sized particles. Primary minerals weather in the sequence plagioclase (An_{25-30}) $>$ hornblende $>$ biotite, epidote $>$ microcline, plagioclase (An_{10-15}), allanite $>$ apatite, chlorite, magnetite $>$ ilmenite, muscovite, quartz, sphene $>$ zircon, resulting in percentage chemical losses from fresh rock to soil in the sequence Rb $\overset{?}{>}$ Na $\approx$ K $\approx$ Mg $>$ Sr $>$ Mn $\approx$ Ca $>$ Ba $>$ Si $>$ Al $\gg$ Fe $>$ Ti.[1] Kaolinite, and possibly some vermiculite, is forming from feldspar, biotite, and other silicates. Microprobe analyses of biotite indicate losses in the sequence Ba $\overset{?}{>}$ K $>$ Mg $>$ Fe $>$ Si $>$ Al; cations having eightfold to twelvefold coordination are most readily lost, then cations in octahedral coordination, and finally ions in sixfold and fourfold coordination. Microclines reveal losses of Na and K, and plagioclases show changes implying removal of Na $>$ Ca $>$ Si $>$ Al. Water saturation extracts from adamellite soils are distinct in composition from rain and snow water and from spring water in adamellite terrane. Relative mobilities of dissolved constituents in adamellite ground waters indicate changes with regard to bedrock of Ca $>$ Mg $\approx$ Na $\gg$ Si $\approx$ K $\geqslant$ Mn $\approx$ Fe $>$ Al. Owing to plant extraction, K and Al mobilities may be lower than bedrock-to-soil losses would suggest. High Ca and Mg mobilities could result from solution of carbonate grains blown into the soils.

Chemical equilibrium does not exist in the natural waters studied, but steady-state conditions are closely approximated in spring waters. Contact with weathering rock over a considerable space-time interval is apparently necessary for the achievement of a steady state, but this interval may decrease for mobile constituents in readily weathered minerals. The chemistry of spring waters related to all lithologies studied appears very sensitive to differences in source material.

Nine elements released by weathering appear to apportion themselves between vegetation, colloidal exchange, and solution as follows: Na, soln $\gg$ exch $>$ veg; Si, soln $\gg$ veg; Ca, exch $>$ soln $>$ veg; Mg, exch $>$ soln = veg; K, veg $\gg$ soln $>$ exch; Fe, Mn, P, veg $\gg$ soln; Al, veg $\ggg$ soln.

INTRODUCTION

Bedrock, soil, vegetation, natural waters, and the atmosphere are interrelated by a highly complex system of reactions and processes, some of which are shown in figure 269. To adequately understand such a system, a broad investigation is necessary, including study of the many related and potentially significant aspects. It

1. A question mark is used in conjunction with greater than or less than symbols in this paper to indicate uncertain position in the sequence.

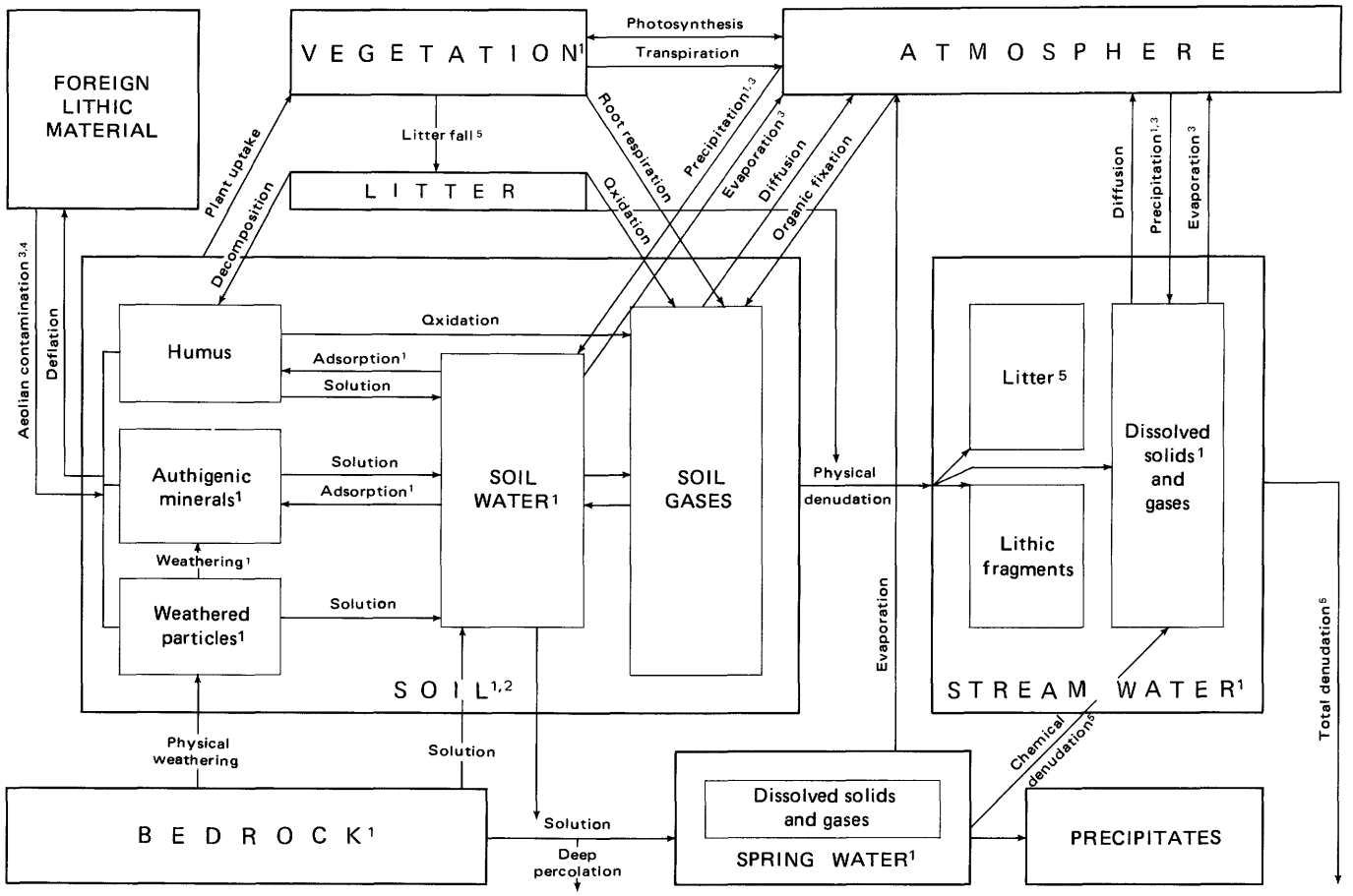

FIGURE 269.—Some reversible, irreversible, and cyclical processes associated with weathering and erosion. Footnotes refer to data given in this and other papers: [1]Total or partial chemical analysis; [2]Physical analysis; [3]Rate evaluation; [4]Physical analysis and rate evaluation (data in Marchand, 1970); [5]Rate evaluation (data in Marchand, 1971).

is impossible, for example, to clearly comprehend the transformation of bedrock into soil by studying changes in the mineral phases alone, for weathering involves important alteration of liquid and gas phases in contact with the minerals as well. This paper constitutes the fourth in a series of vegetational, erosional, and weathering studies in the southern White Mountains of eastern California (Marchand, 1970, 1971, 1973). The focus here is primarily on the chemical weathering of two widely distributed rock types, dolomite and adamellite, utilizing chemical and physical data from all of the five system components mentioned. Chemical analyses of bedrock, soils, plants, and natural waters permit estimates of the direction and magnitude of chemical fractionation in parts of the geochemical system described in figure 269.

The upland surface of the White Mountains, truncating a diversity of sedimentary and plutonic bodies and overlain locally by basalt, provides an excellent area in which to study the extent, sequence, and processes of weathering and soil development applied to many lithologies in a semiarid, subalpine environment. Quantitative chemical weathering studies have previously been largely confined to tropical or humid temperate regions, for example, Mead (1915), Goldich (1938), Cady (1951), Sherman and Uehera (1956), Hay (1959), and Wolfenden (1965). In such areas weathering has proceeded to such an extent that initial trends are difficult or impossible to recognize. Soils in the White Mountains are immature and clearly illustrate some of the early stages of the weathering process.

Gerald Osborn and Francis H. Brown assisted with sample collection and planetable mapping during the summer of 1966. J. Ross Wagner aided in preparing X-ray fluorescence pellets of bedrock and soil samples, conducting mineral separations, and in determining many physical and chemical soil parameters. Electron microprobe studies were conducted by Lary K. Burns. Joaquim Hampel determined Na and K in eight bedrock and soil samples by flame photometer. Barbara Lewis and James Clayton analyzed plant materials for inorganic constituents.

This paper represents a major portion of a Ph. D. dissertation carried out at the University of California, Berkeley, and financially supported by the U.S. Geological Survey. Many members of the Survey, especially

Ivan Barnes, John Hem, and Edward J. Helley, rendered indispensable aid and advice. The manuscript in its various stages of preparation was aided by the critical reading of F. J. Kleinhampl, John D. Hem, Richard L. Hay, Clyde Wahrhaftig, Peter W. Birkeland, and R. R. Tidball.

STUDY AREA

LOCATION AND DESCRIPTION

The White Mountains, often termed the northern Inyo Range in older publications, extend from Westgard Pass in eastern California north to Montgomery Peak (north of map shown in fig. 270) in western Nevada. White Mountain Peak (14,246 ft.) is the highest point in the range.

The area investigated encompasses approximately 30 square miles along the crest of the southern White Mountains, east of Bishop, Calif., in Mono and Inyo Counties (fig. 270). It is characterized by a gently undulating summit upland (fig. 271) sloping southward from 11,500 feet near Sheep Mountain to about 10,000 feet east of Bucks Peak (fig. 272). Summits such as

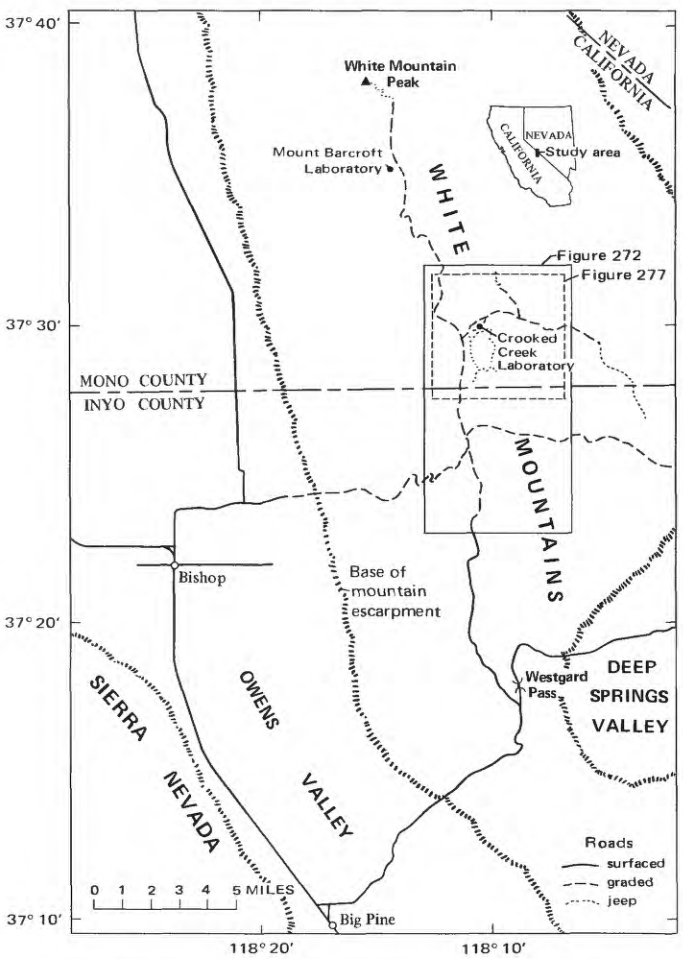

FIGURE 270.—East-central California and adjacent part of Nevada, indicating location of the study area and of the maps shown in figures 272 and 277.

FIGURE 271.—Part of the upland surface in the White Mountains. View north across Big Prospector Meadow. Outcrops of Andrews Mountain Member of Campito Formation in foreground; white tree-covered exposures in middle and far distance are Reed Dolomite.

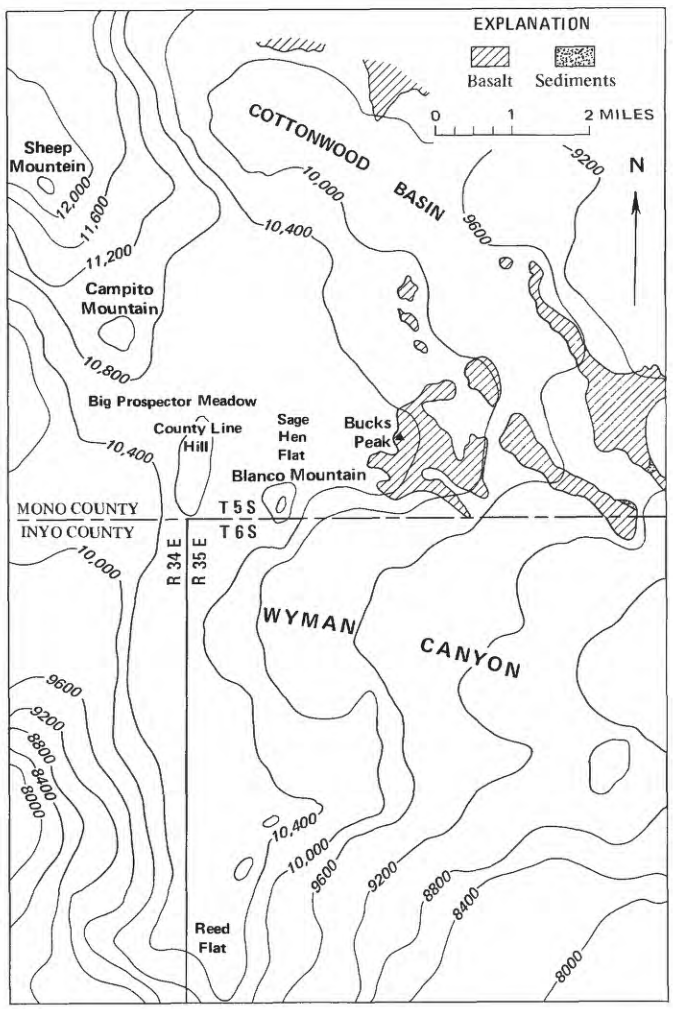

FIGURE 272.—Generalized topography (contours in feet above mean sea level) of a part of the southern White Mountains. Posterosion surface deposits shown locally.

Blanco Mountain, County Line Hill, and Campito Mountain stand 500 feet or more above this rolling surface. The steep western escarpment of the range, not included within the study area, descends 6,000–7,000 feet in 6 or 7 miles to the floor of the Owens Valley. The eastern flank slopes much more gradually, but is incised by a series of canyons as much as 1,000 feet deep, which drain southwestward to Deep Springs Valley and eastward to Fish Lake Valley.

PREVIOUS WORK IN THE REGION

The brief description of Spurr's (1903, p. 206–212) and Knopf's (1918) reconnaissance of the northern Inyo Range and eastern Sierra Nevada, which included a section on the stratigraphy of the Inyo Range by Edwin Kirk, marked the first geological studies of the White Mountains. Anderson and Maxson (1935) and Maxson (1935) described the physiography and Precambrian stratigraphy, respectively, of the northern Inyo Range. Recent work in the White Mountains led to publications on Precambrian and Cambrian stratigraphy, paleontology, and boundary problems by Nelson and Perry (1955), Nelson (1962), Taylor (1966), and Cloud and Nelson (1966). Anderson's (1937) arguments for the granitization in the formation of the Inyo batholith were challenged by Hall (1964) and Emerson (1966). McKee and Nash (1967) dated most of the plutonic bodies and several metamorphic units in the area by K/Ar methods, and Krauskopf (1968) discussed the complex intrusive history of the region. Cenozoic volcanism and tectonics were considered by Taylor (1965), and Dalrymple (1963) dated Tertiary volcanic rocks on the northwest edge of Deep Springs Valley. The Blanco Mountain 15-minute quadrangle (Nelson, 1963, 1966) and the Mount Barcroft (Krauskopf, 1971) 15-minute quadrangles were mapped. Hall (1964), Pittman (1958), and Gallick (1964) mapped parts of the White Mountain Peak, Mount Barcroft, and Blanco Mountain quadrangles. A general summary of the area's geologic history was provided by Nicholls (1965).

Geomorphic processes in the White Mountains were investigated by Powell (1963) and Kesseli and Beaty (1959), who studied desert flood conditions, and by Beaty (1959, 1960), who discussed slope evolution and gullying. LaMarche (1967, 1968) estimated erosion rates on the Reed Dolomite from tree-ring data and described spheroidal weathering in the carbonate rocks of the area.

Several members of the U.S. Geological Survey discussed dissolved constituents in snow (Feth, Rogers, and Roberson, 1964) and ground water (Feth, Roberson, and Polzer, 1964) in the eastern California region. Barnes (1965) studied the geochemistry of Birch Creek, which drains the southernmost part of the area and is similar in some respects to spring waters discussed here.

Pace (1963) and Nicholls (1965) summarized climatic data collected at the Mount Barcroft and Crooked Creek Laboratories of the White Mountain Research Station for the decade 1953–62.

CLIMATE

The White Mountains lie in the rain shadow of the Sierra Nevada and are generally characterized by a cold, dry climate (BWk to BSk of Köppen notation) with precipitation occurring largely in the form of snow and in sudden summer storms. Mean annual precipitation is about 13 inches at Crooked Creek and mean annual temperature is approximately 35°F.

Climatic data from the Crooked Creek and Mount Barcroft Laboratories (fig. 270) of the White Mountain Research Station are summarized in table 1. The Crooked Creek Station (10,150 ft.) is located in a valley at the approximate center of the study area; the Mt. Barcroft Station (12,470 ft.) lies on the upland surface about 5–6 miles to the northwest. Both stations are situated about 1 mile east of the range crest. Therefore climatic data from the two laboratories indicate differences due to elevation and exposure. Precipitation, relative humidity, and wind velocity are higher at Barcroft. Temperature and diurnal temperature change are greater at Crooked Creek, and a greater proportion of the total precipitation occurs as rainfall there. Both stations show principal wind directional maximums from the west and southwest and a lesser maximum from the north or northeast throughout the year. Major (1967, p. 119–122) evaluated climatic data at the two stations in terms of evapotranspiration and water balance.

Because pronounced geographical climatic gradients might produce similar trends in weathering intensities or soil development, it was desired to determine whether significant east-west or north-south climatic gradients exist today in the study area. For this reason five auxiliary weather stations (AWS) on the upland surface were maintained from June 1966 to August 1967 (fig. 273). The stations chosen were the Patriarch AWS, just south of the Patriarch picnic area; the Campito AWS, on the south flank of Campito Mountain; North Sage Hen AWS, on the north edge of Sage Hen Flat, above Crooked Creek Station; the Basalt AWS, on basalt cappings south of Crooked Creek Canyon; and the South Sage Hen AWS, on the southeast flank of County Line Hill. (See fig. 277 for locations.) Wind measurements recorded at Crooked Creek Laboratory were obtained from anemometers near the North Sage Hen AWS. All AWS sites were situated on relatively level topographic highs at spacings of 1½–3 miles.

TABLE 1.—*Summary of climatic means and extremes from Crooked Creek (10,150 ft) and Mount Barcroft Laboratories (12,470 ft) for the indicated periods*

	Crooked Creek Laboratory (1949–1965)												Crooked Creek Laboratory	Mount Barcroft Laboratory
	Jan.	Feb.	Mar.	Apr.	May	June	July	Aug.	Sept.	Oct.	Nov.	Dec.	1949–65	1953–65
Highest maximum temperature °F	52	51	52	62	69	76	76	74	72	76	61	57	76	72
Mean maximum temperature °F	30.1	31.7	32.7	40.7	46.9	58.3	65.2	63.9	58.4	50.3	40.6	34.3	46.1	35.5
Mean temperature °F	19.6	21.4	22.5	30.3	36.2	46.0	52.6	51.4	45.7	38.4	29.3	23.5	34.8	27.4
Mean minimum temperature °F	9.1	11.0	12.2	19.9	25.6	33.8	40.1	38.9	33.1	26.5	18.1	12.7	23.4	19.7
Lowest minimum temperature °F	−21	−21	−16	−10	2	12	22	17	10	−7	−13	−19	−21	−35
Mean diurnal difference °F	21.0	20.7	20.5	20.8	21.2	24.5	25.1	25.0	25.3	23.8	22.5	21.6	22.7	16.1
Largest diurnal difference °F	41	46	47	42	45	38	42	41	49	58	49	40	58	44
Smallest diurnal difference °F	1	4	5	3	2	9	10	8	6	6	2	3	1	2
Mean days 33°F or above	13.8	13.8	17.1	24.0	28.4	29.9	30.9	31.0	30.0	29.4	23.9	19.4	291.6 per yr	204.5 per yr
Mean 8 a.m. relative humidity (percent)	57.5	61.2	59.1	55.4	51.5	40.1	40.6	41.4	44.8	45.5	52.5	55.1	50.7	55.1
Mean 8 a.m. barometer mm Hg	517.6	517.7	516.4	518.1	519.2	522.5	526.1	525.6	524.3	523.1	521.3	520.1	[1]523.8	[1]481.3
Mean snowfall in	15.0	18.1	17.0	16.8	12.9	3.5	.4	.2	1.2	5.1	11.1	13.3	114.4 per yr	164.4 per yr
Mean snow depth in	10.2	15.5	16.5	11.0	2.4	.1	.0	.0	.0	.3	3.4	5.7	[1]4.7	[1]7.2
Highest snow depth in	72	74	94	62	47	12	1	3	1	12	30	50	94	73
Mean snow water in	1.51	1.62	1.38	1.63	1.11	.34	.04	.02	.12	.48	.92	.96	10.14 per yr	14.87 per yr
Mean rainfall in	.00	.00	.00	.00	.10	.06	1.30	.74	.48	.04	.00	.04	2.73 per yr	2.11 per yr
Mean total precipitation in	1.51	1.62	1.38	1.63	1.21	.40	1.34	.76	.60	.52	.92	1.00	12.87 per yr	16.98 per yr
Mean maximum wind (knots)	19.8	19.0	18.8	16.8	15.3	13.5	12.3	12.2	13.0	13.8	15.8	17.9	15.8	22.5
Maximum wind direction (percent):														
North	8.3	7.7	4.9	7.6	7.3	3.0	3.4	1.7	4.1	5.0	7.8	6.6	5.8	12.7
Northeast	10.3	16.8	11.4	10.3	14.2	10.3	8.0	7.2	5.8	11.8	13.6	12.3	11.0	5.6
East	2.3	3.6	2.2	2.7	1.4	4.8	4.1	6.1	5.4	3.8	3.0	2.4	3.5	5.4
Southeast	3.5	1.7	3.5	4.9	5.4	9.8	15.2	13.7	9.8	10.9	5.6	5.1	7.5	5.0
South	2.9	2.9	1.9	1.7	4.2	5.0	14.5	11.1	13.3	9.1	6.5	7.4	6.5	7.9
Southwest	26.1	15.7	23.5	29.9	25.1	32.7	25.1	33.9	29.1	27.3	24.2	23.4	26.2	17.0
West	32.4	36.0	33.8	33.1	31.5	27.7	26.1	22.3	26.9	25.8	29.4	27.1	29.6	39.9
Northwest	14.5	16.0	18.8	9.9	11.1	6.5	3.4	4.4	5.8	6.6	9.8	15.7	10.3	9.8

[1]1953–62.

FIGURE 273.—North Sage Hen Flat auxiliary weather station and dust trap. Evaporimeter to left of pole, thermometer in white container to right of pole, dust trap on top. Rain gage to left and rear of stand. View west, showing parts of the upland surface, with the Sierra Nevada in distance.

Four-inch-diameter sections of stovepipe, 2½ feet long and sealed at the bottom, were used as rain gages. Lightweight oil was added to minimize surface evaporation. Taylor maximum-minimum window thermometers, suspended inside white ½-gallon ice cream containers, were used for temperature readings. Relative evaporation rates were obtained with modified Piche evaporimeters (Waring and Hermann, 1966). Temperature and precipitation readings were taken at bimonthly intervals from June 20 through September 1966, at the end of October 1966, and at monthly intervals from June to August 1967. Evaporation readings were obtained only during the summer of 1966. Table 2

TABLE 2.—*Types of information obtained at Crooked Creek Laboratory and five auxiliary weather stations during the period June 1966 to August 1967*

Name	Abbreviation	Position relative to center of area	Elevation (ft)	Maximum-minimum temperature	Precipitation	Evaporation rate
Crooked Creek	CC	Center	10,150	Yes	Yes	No.
Basalt	B	East	10,200	Yes	Yes	Yes.
Campito	C	West	10,440	Yes	Yes	No.
North Sage Hen	NSH	Center	10,660	Yes	Yes	Yes.
South Sage Hen	SSH	South	10,740	No	Yes	Yes.
Patriarch	P	North	11,250	No	Yes	Yes.

summarizes types of data collected at each weather station.

A plot of temperature and evaporation rates for the auxiliary weather stations and Crooked Creek is shown in figure 274. The Campito and North Sage Hen AWS sites show nearly the same maximum and minimum temperatures; the Basalt commonly has lower maximums and higher minimums. All Crooked Creek temperatures fall below those obtained on the upland surface, often by as much as 10–15°F. Evaporation data are quite spotty owing to malfunctioning at several sites, but the Basalt AWS values tend to be highest, followed by North Sage Hen, South Sage Hen, and the Patriarch. The comparison suggests a slight trend toward increasing evaporation rates from west to east, possibly owing to decreasing elevation. Since temperatures do not appear to increase eastward, the increased evaporation may be the result of a lower relative humidity. A comparison of precipitation at the five AWS sites and Crooked Creek (fig. 275) indicates highest values at

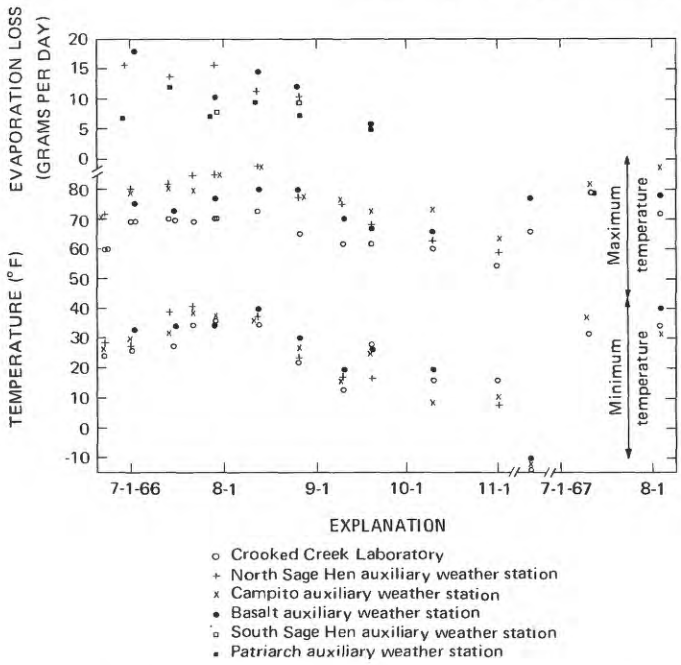

FIGURE 274.—Maximum and minimum temperature and relative evaporation rates at Crooked Creek Laboratory and five auxiliary weather stations in the study area.

Crooked Creek, closely followed by the Patriarch AWS. All the other sites received much less precipitation and tend to follow the order North Sage Hen > Basalt > Campito > South Sage Hen. There is a general trend of increasing precipitation toward the north, and higher values were recorded in the valley of Crooked Creek than on the surrounding upland surface, probably because the AWS sites were exposed to high winds which would tend to decrease catchment of precipitation and to deflate snow accumulations.

Crooked Creek data for wind velocity and direction, barometric pressure, and to some extent, relative humidity, approximate present-day climatic conditions for most of the study area. Absolute precipitation values at Crooked Creek are probably much more reliable than those obtained at the auxiliary stations, but the fact that the latter are much lower should not be dismissed altogether, for they suggest that Crooked Creek values may be high owing to drifted snow blown from adjacent slopes. To obtain representative temperature estimates for nearby upland surface areas, Crooked Creek maximum temperatures should be increased by about 10°F and minimum temperatures by about 5°F. In the northern part of the study area, precipitation and relative humidity are probably somewhat higher and temperatures slightly lower than further south owing primarily to differences in elevation. With this exception, present climatic gradients in the study area are not marked.

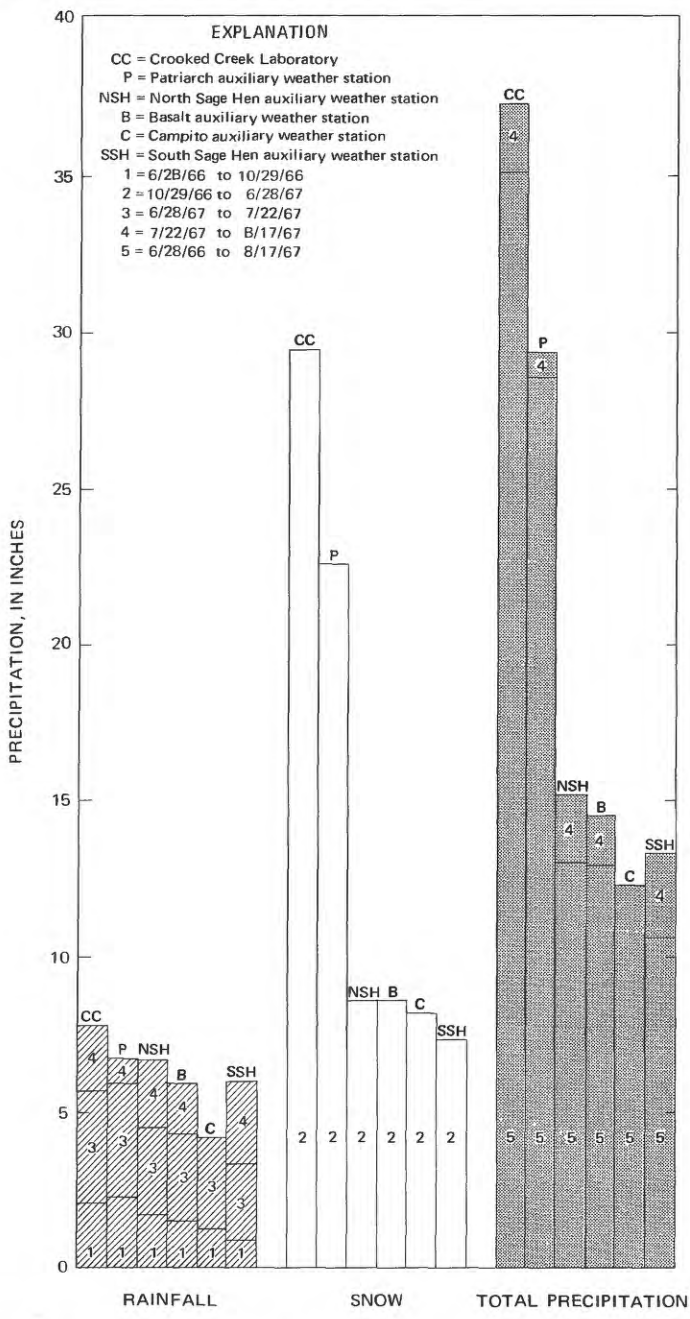

FIGURE 275.—Precipitation recorded at Crooked Creek Laboratory and at five auxiliary weather stations for the indicated periods.

VEGETATION

The flora of the study area includes the Bristlecone Pine Forest and Sagebrush Scrub plant community types of Munz and Keck (1959, p. 11–18). Toward lower elevations the vegetation passes into Pinyon Juniper Woodland, and at higher elevations into Alpine Fell Fields. Stands of bristlecone pine (*Pinus aristata*), limber pine (*Pinus flexilis*), and aspen (*Populus tremuloides*) make up a discontinuous tree canopy along the

crest of the range below about 11,500 feet. A continuous shrub understory on noncarbonate soils is dominated by sagebrush (*Artemisia tridentata* and *A. arbuscula*) and to a lesser extent by rabbitbrush (*Chrysothamnus viscidiflorus*), mountain mahogany (*Cercocarpus ledifolius* and *C. intricatus*), creambush (*Holodiscus microphyllus*), mountain misery (*Chamaebatiaria millefolium*), and currant (*Ribes velutinum*). Beneath this two-story canopy of trees and sagebrush scrub is a nearly ubiquitous but sparse cover of grasses and herbaceous perennials, mostly low to the ground and often inconspicuous.

Most areas are dry, but moister conditions occur locally along streams and near seeps and springs. Such sites are characterized by annual grasses as well as *Carex spp.* (sedges), *Cirsium drummondii* (thistle), *Artemisia ludoviciana* (sagebrush), *Castilleja miniata* (paintbrush), and several species of *Penstemon* (beardtongue), *Mimulus* (monkey flower), and *Oenothera* (evening primrose).

Many plant species in the White Mountains are partly controlled by substrate in their distribution (Marchand, 1973). Edaphic restriction is evident in all vegetational strata, from bristlecone and limber pine to the smallest perennials. The principal botanical discontinuities occur across carbonate-noncarbonate boundaries (fig. 276): dolomites and limestones support similar vegetation as do, with a few notable exceptions, noncarbonate lithologies. Vegetation on sandstone and shale, granitic bodies, and basalt shows subtle differences which are sufficiently consistent to permit identification of three noncarbonate plant communities, each characteristic of a given bedrock type.

FIGURE 276.—Vegetational contrast between dolomite outcrops and colluvium (foreground and right rear) and sandstone colluvium (darker colored). Sandstone is covered by sagebrush and numerous other perennials, dolomite by certain small perennial herbs and bristlecone pine.

GEOLOGY

A complex mixture of sedimentary, igneous, and metamorphic rocks constitute the bedrock of the southern White Mountains (fig. 277). The oldest strata in the region are a slightly metamorphosed Precambrian to Early Cambrian succession of sandstones, shales, limestones, and dolomites. The Precambrian Wyman Formation, consisting primarily of sandstone and shale with minor but conspicuous lenses of white limestone, is the oldest of this group. Overlying the Wyman is the Reed Dolomite, a massive and very pure carbonate rock. The Deep Spring Formation, composed of alternating members of carbonate rocks (both limestone and dolomite) and clastic sediments (quartzitic sandstone and shale) overlies the Reed. The next youngest formation is the Campito, consisting of a lower quartzose sandstone member, the Andrews Mountain, and an upper shale member, the Montenegro. The Precambrian-Cambrian boundary, coinciding with the base of the *Fallotaspis* Olenellid biozone (Taylor, 1966), occurs within the upper part of the Andrews Mountain Member. The youngest stratigraphic unit of the group is the Poleta Formation, a somewhat shaly carbonate.

This succession was tilted toward the west and then intruded by the adamellites of Sage Hen Flat (130–138 m.y. (million years)) and Cottonwood area (151-170 m.y.) during the late Mesozoic (McKee and Nash, 1967, p. 672). Early to middle Tertiary erosion resulted in the beveling of a surface of low relief across the region (fig. 278), although monadnocks of Reed Dolomite and Andrews Mountain sandstone stood well above the erosion surface during its development. Parts of this surface were subsequently covered by thin local sediment and extensive basaltic flows (figs. 272, 279), K/Ar dated by Dalrymple (1963) at 10.8 m.y.

In terms of late Cenozoic structure, the White Mountains are an eastward-tilted horst which exhibits relatively greater uplift on the west, where a steeply dipping fault zone bounding the range has undergone as much as 10,000 feet of normal displacement. The east margin is also faulted along the northwest side of Deep Springs Valley, but individual displacements here are about 1,000 feet or less. The basalts and underlying erosion surface are tilted and faulted up from 6,000 feet at the northeast end of Deep Springs Valley to 10,800 feet at Bucks Peak, showing that tectonic activity occurred later than 10.8 m.y. ago. Bateman and Wahrhaftig (1966) presented convincing evidence for regional uplift of east-central California and western Nevada between about 9 and 3.5 m.y. before present and formation of Owens Valley and other collapse structures along the axis of uplift during a period of downfaulting beginning about 2.5 m.y. ago. The "Waucoba Lake

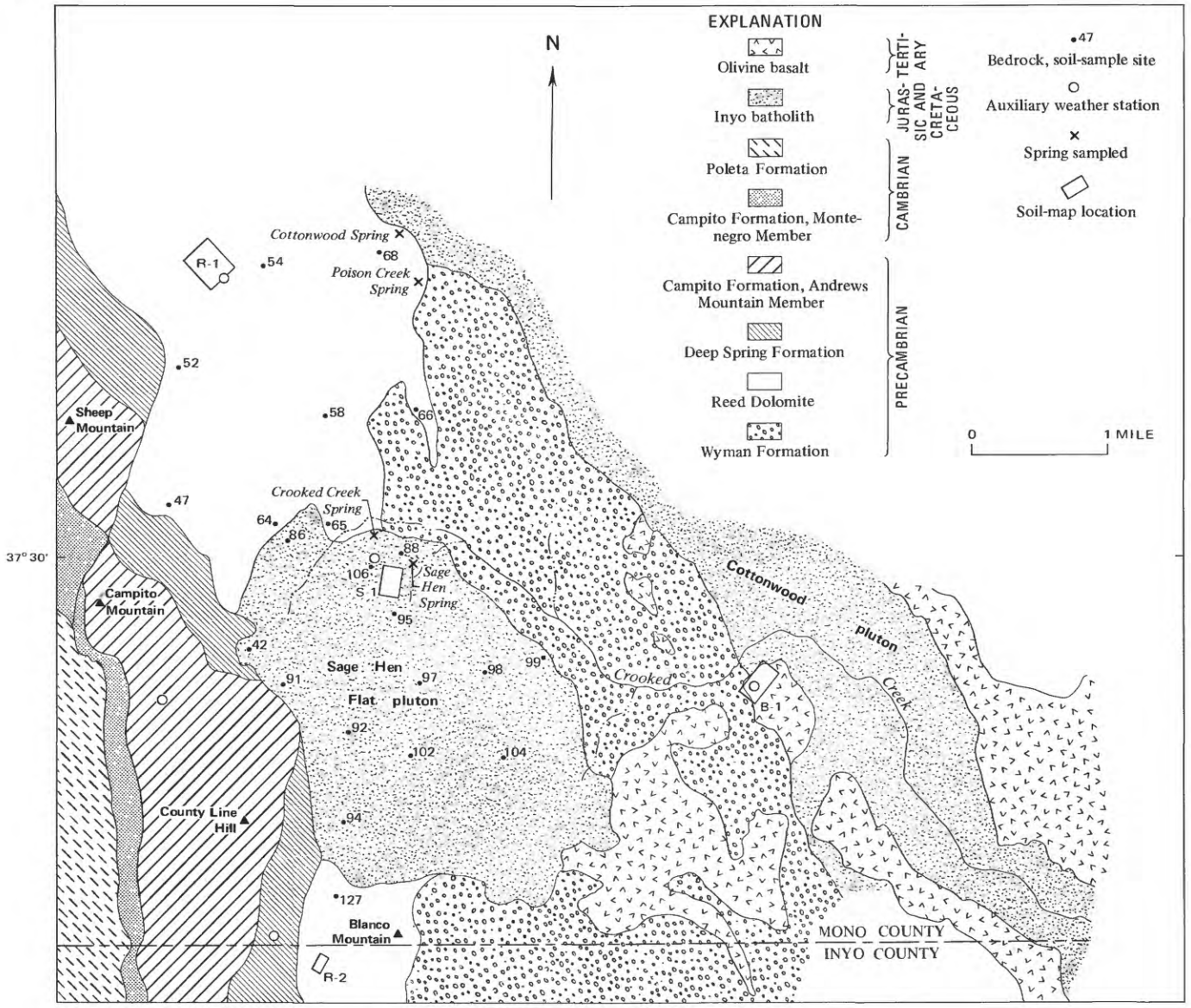

FIGURE 277.—General geology and sample locations in the study area.

Beds," exposed on the upthrown side of the frontal fault east of Big Pine, possess a predominantly Sierran mineralogy and apparently represent deposition in an early Pleistocene pluvial lake prior to the downfaulting of Owens Valley. The uppermost of several rhyolitic tuffs in the lakebeds has given a K/Ar age of 2.3 m.y. (Hay, 1966, p. 20). Coarse clastic debris from the White Mountains overlies and intertongues with the upper part of the lakebeds, which now dip westward at 5–7°, indicating some uplift of the range or downwarping of Owens Valley during the latter part of lakebed deposition, about 2.3 m.y. ago. The range-front faulting may have begun at this time, but cannot have preceded the lakebed deposition. Regional arching therefore appears to have preceded faulting by at least 1 million years in this area, although some uplift in the White Mountains may have occurred as recently as 2.3 m.y. before present.

Pleistocene glaciation along the eastern slope of the White Mountains north of the study area has incised cirques and U-shaped valleys into the upland surface and has left morainal and outwash deposits along the valley walls and floors. According to D. R. Powell (1967, oral commun.), recognizable glacial advances in the White Mountains appear to correlate with those of the eastern Sierra Nevada. Quaternary alluvium and terrace deposits are present along most of the major streams draining the range, especially on the east flank where gradients are gentler. Interbedded with terrace alluvium along Crooked Creek and its tributaries is a

FIGURE 278.—View north across Sage Hen Flat, showing degraded White Mountain erosion surface and outcrop areas of adamellite of Sage Hen Flat (light colored, foreground and middle distance), Reed Dolomite (white, tree covered), and Andrews Mountain sandstone (dark, left distance).

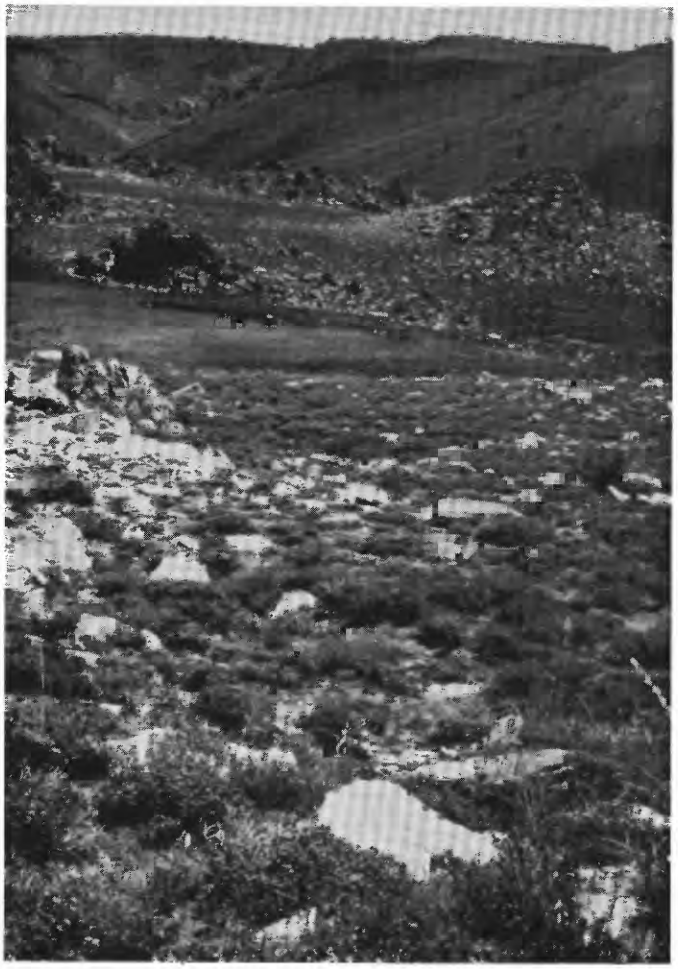

FIGURE 279.—View east from Sage Hen Flat, showing resistant basalt capping less resistant metasediments and granitic intrusive rock.

FIGURE 280.—Exposures of reworked rhyolitic ash interbedded with terrace alluvium along Crooked Creek. White layers are largely composed of pumiceous material.

white, reworked pumiceous ash (fig. 280), rhyolitic in composition and as much as 0.6 feet thick. Although glass shards and rhyolitic mineral fragments occur in soils throughout the area, no primary deposits have been seen. On the basis of major elements, trace elements, refractive indices, mineralogy, and physical appearance, the ash has been correlated with a source at Mono Craters (probable) or Mono Glass Mountain (possible), both located on the eastern Sierra Nevada slope south of Mono Lake (Marchand, 1968, 1970).

Those parts of the White Mountain erosion surface which have not been totally destroyed have been lowered several hundred feet to the level of Sage Hen Flat (fig. 278), Reed Flat (fig. 272), or similar areas of subdued, rolling topography by late Tertiary or Quaternary erosion. Frost heaving, solifluction (including altiplanation), nivation, and other periglacial phenomena continue to affect the range, becoming increasingly important toward higher elevations. Rillwash channels as much as 2 inches deep and debris accumulations behind trees, fallen limbs, bushes, and large boulders testify to the effectiveness of slope runoff processes, particularly on the relatively bare surfaces beneath bristlecone pine forest. Talus cones and stone stripes are frequent, particularly in the Campito Formation and other sandstones or shales. Although eastward draining canyons are gradually eroding headward into degraded remnants of the erosion surface, fairly extensive parts of the lowered surface are still relatively undissected and

often serve as a local or temporary base level for periglacial processes and slopewash. The effect of these circumstances is the accumulation of colluvium (consisting of weathered and unweathered rock, mineral, and organic material) on gentle slopes and in topographic lows on these surfaces.

To put present climatic data into perspective, it is necessary to consider the regional climatic and tectonic changes that have occurred in the area during the late Cenozoic. Any attempt at backward extrapolation of climatic conditions is extremely hazardous, especially in areas such as this where faulting and uplift have complicated an already complex series of fluctuations, but a few conclusions appear to be valid: (1) Cold, dry, climatic conditions such as those which currently characterize the area, and the more severe climates of glacial periods, are not conducive to rapid soil formation (for example, cf. Morrison, 1964, p. 114); (2) the White Mountains area was at a lower and presumably warmer elevation and probably did not lie in the Sierran rain shadow prior to regional uparching, between 9 and 3.5 m.y. ago; (3) considering the total duration of warm, wet, or warm and wet intervals which promote rapid weathering, it would appear likely that most of the total amount of soil formed on the White Mountain surface occurred prior to or during the regional uplift, perhaps augmented during extended interglacial periods. The immaturity of present soils indicates that most of the weathered debris has been stripped by erosion, but the extreme weathering of some soil grains may date from an earlier period of soil formation.

CHEMICAL WEATHERING AND SOIL DEVELOPMENT

Chemical weathering is so closely interrelated with physical weathering that it is sometimes difficult to distinguish their separate effects. Taken together these two processes are responsible, along with various organic effects, for the development of soil. Because of the close ties between physical and chemical processes in the evolution of soils, both aspects are considered here, although primary emphasis is placed on chemical weathering.

METHOD OF APPROACH

The immature soils in this area formed on four widespread parent materials. Because spring waters closely related to sandstone and basalt were not available and because changes in the liquid phase are important considerations in this study, detailed discussion is restricted to the Reed Dolomite and adamellite of Sage Hen Flat, two commonly recurring lithologies for which closely related spring waters could be obtained. For the dolomite and adamellite the sequence and degree of physical weathering is evaluated, and problems of soil contamination are discussed. Chemical weathering is approached from the perspectives of chemical and mineralogical changes in dolomite and adamellite and of chemical changes in liquid phases associated with each lithology.

FIELD METHODS

After the geologic and soil mapping of the area (figs. 277, 281–284), 84 sample sites, about 20 to each lithology, were chosen at relatively even spacings on Reed Dolomite, adamellite of Sage Hen Flat, basalt, and sandstone of the Andrews Mountain Member of the Campito Formation. (See fig. 277 for site locations.) Topographic highs were selected for sample locations to minimize contamination by slopewash, mass wasting, and aeolian processes. Soil samples encompassing the entire profile above the C horizon were collected at every site and fresh bedrock samples were also obtained on dolomite and adamellite sites. Eight surface soil pH measurements (determined using pHydrion paper and a Truog indicator kit) were made at each site within a 7-foot radius of the soil pit. The dimensions of the pit were measured as closely as possible, its volume was calculated, and the soil samples were weighed (air dry) after collection to obtain bulk density figures for the whole soil. Representative profiles were described, and field impregnations were made at several sites for dolomite, adamellite, and basalt soils. Over a 14-month period from June 1966 to August 1967, samples of rain, snow, and of spring waters related to the adamellite and dolomite were collected.

LABORATORY METHODS

Samples of both dolomite and adamellite were randomly selected for detailed chemical and mineralogical study in the laboratory. Minerals were identified primarily by petrographic microscope, aided by reflecting microscope for opaque minerals. Compositions of glass fragments were determined by immersion oils, universal stage, and electron microprobe. The microprobe was also used to assess chemical alteration within weathered minerals. Estimates of major mineral percentages in fresh adamellite were determined from point counts of stained thin sections. Percentages of minor mineral phases in adamellite, all dolomite constituents, and all minerals in sand fractions of soils were obtained from line counts of grain mounts, after two heavy-liquid separations. Silt- and clay-sized fractions were analyzed qualitatively and quantitatively by X-ray diffraction. Layer silicates were identified following the methods of Warshaw and Roy (1961). Contaminative rhyolitic glass in the silt range of soils was estimated visually in oil immersion mounts. X-ray fluorescence was employed in the chemical analysis of bedrock and soil samples. Standard sieve and pipette techniques were utilized in size analyses of 26 dolomite

and adamellite soils. Other analytical methods used are discussed at appropriate places in the report. For a more detailed account of procedures, precision, reproducibility, and comparisons of methods, the reader is referred to the section "Supplemental Information."

Table 3 summarizes the estimated precision of measurement for some of the analyzed quantities discussed in the text. All percentages in the text, tables, and figures are weight percent, unless otherwise noted.

TABLE 3.—*Estimated precision of measurement for some analytical quantities discussed in this paper*

[See also "Supplemental Information"]

Analytical method	Estimated range of precision (percent of given value)
X-ray fluorescence	±6
Grain counting:	
Major minerals	±5
Minor minerals	±10–15
X-ray diffraction (silts)	±15
Size distribution:	
Sieve range	±2
Pipette range (silt and clay)	±10
Plant ash analyses	±20 (usually < 10)
Analyses of water-saturation extracts	±25
NH_4Ac extract analyses	±20

DESCRIPTION OF SOILS

CLARIFICATION OF TERMS

In the White Mountains, as in other areas of high relief, absolute distinctions between residual soil and weathered colluvium are essentially arbitrary. Periglacial processes, as well as mass wasting, slopewash, and aeolian transport, are actively moving loose material into topographic lows. Many definitions of soil imply formation by in situ weathering alone (for example, cf. Brewer, 1964, p. 7–8), apart from the effects of erosion and deposition. For purposes of this discussion, the term "soil" will be expanded from this usage to include some colluvial and windblown material. In the present context, "soil" encompasses all weathered or slightly weathered surficial debris other than talus, stone stripe boulders, slopewash fans, alluvium, and sand dunes and necessarily includes debris that has undergone some slope transport, albeit of relatively short distance in many cases.

The White Mountains soils are almost exclusively poorly developed lithosols having general $A_{11}/A_{12}/C/R$ profiles less than 13 inches deep. Color, structural, or textural B horizons are faintly visible in a few profiles, but such occurrences are rare. Calcium carbonate crusts can be found on all lithologies, but are abundant only on dolomite soils. An irregular surface layer of relatively large fragments (A_{11} horizon), brought to the surface by frost heaving, is a common feature of most profiles, independent of parent material. Beneath this stratum is a layer of finer grained weathered material (A_{12} horizon), usually overlying large partly weathered fragments in a matrix of silt and sand (C). Fresh bedrock (R) is generally encountered within 1 or 2 feet of the top of the C.

Planetable maps of topography and maximum soil depth for representative areas within dolomite, adamellite, and basalt terranes are shown in figures 281–284. Maximum soil depth was taken as the greatest penetration of a 1-inch-diameter soil auger in repeated borings at a given location. These depths correspond to the approximate top of fresh bedrock, except in deep profiles where lateral friction on the auger made further penetration impossible. The map isochores indicate a general thinning over topographic highs and steep slopes and thickening in local depressions, especially on Sage Hen Flat. Soil thickness appears to be somewhat erratic on the basalt and dolomite. Two dolomite areas at different elevations show no appreciable differences in soil depth. In the Patriarch area, the thickest soils occur in minor interfluves, and the thinnest are found in the intermittent stream channels, suggesting that the latter are presently sites of erosion or slow weathering. This relation contrasts with that of Sage Hen Flat, where surficial material is thickest along topographic lows.

The application of lithologic names to soil units (that is, Reed Dolomite soil) represent informal usage only;

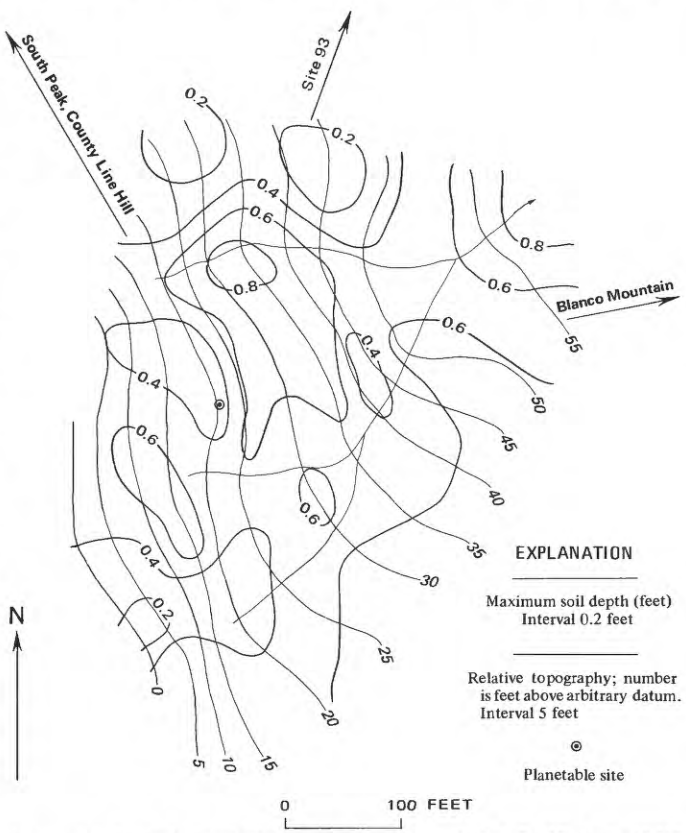

FIGURE 281.—Depth of soil and colluvium at planetable map site R–1, Reed Dolomite, 10,600 feet

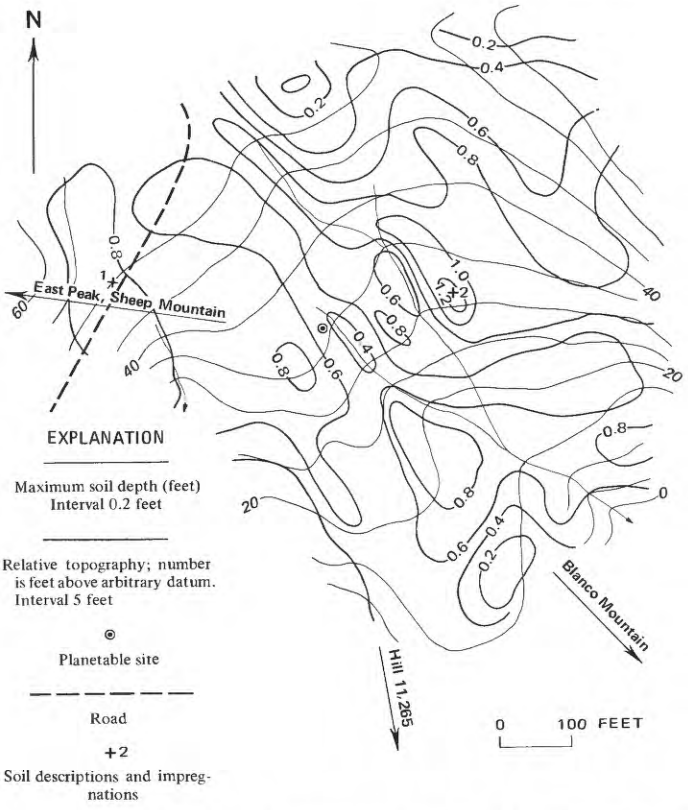

FIGURE 282.—Depth of soil and colluvium at planetable map site R–2, Reed Dolomite, 11,200 feet.

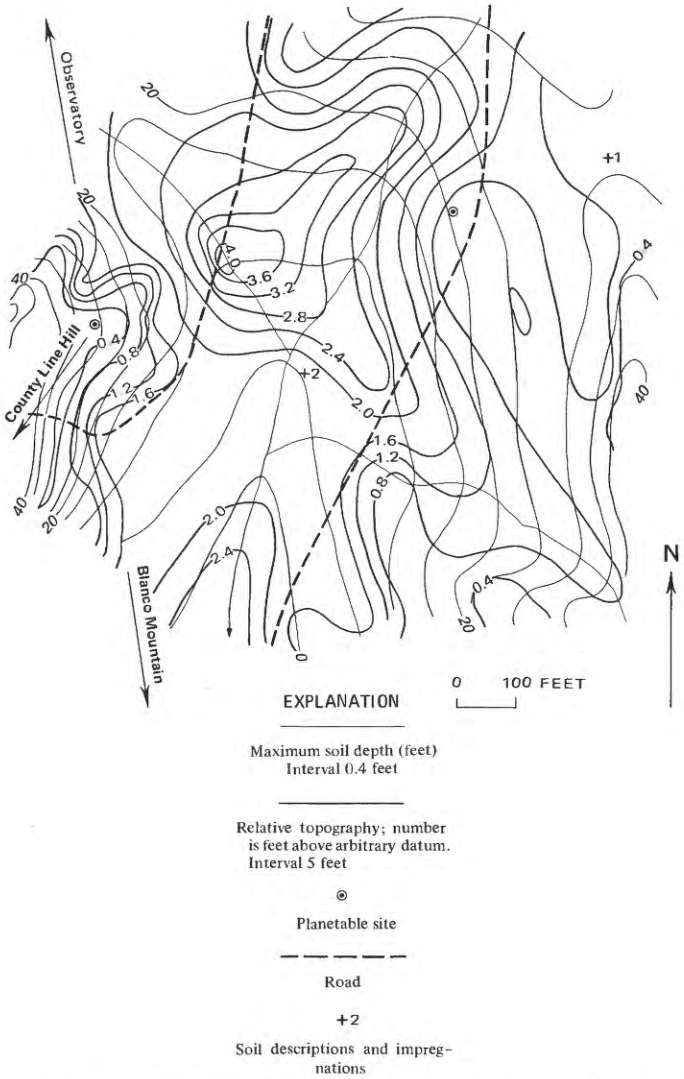

FIGURE 283—Depth of soil and colluvium at planetable map site S–1, adamellite of Sage Hen Flat.

no attempt has been made to formally designate or map soil series in this area.

REED DOLOMITE SOILS

Average soil profile thickness to Reed Dolomite bedrock, about 7 inches at sampled sites, is slightly greater than for other soil groups. White calcium carbonate surface crusts, usually discontinuous and less than one-half inch thick, are one of the most conspicuous features of the Reed profiles. Calcium carbonate is absent in lower parts of the A horizon, but occurs at the A–C interface and on nearly all rock fragments within the profile. Local O horizons, consisting of undecomposed and partially humified plant litter together with a few mineral grains occur sporadically beneath trees. Where O horizons are present, carbonate crusts are absent. Rock fragments concentrated near the surface in A_{11} horizons (fig. 285) usually appear quite fresh, except for minor solution pitting. Rock in the C horizon, however, is often so thoroughly decomposed that it is easily broken with a trowel. A_{12} horizons are occasionally quite red owing to oxidation of Fe-bearing minerals. Subangular blocky peds are common here, but structure in other horizons is generally single grained or massive. The pH may be below 7.0 in or near O horizons, but the normal range is between 7.5 and 8.2, appreciably higher than in noncarbonate soils. The pH tends to be high at the surface, lower in the A horizon, and high again near and within the C horizon, causing precipitation of calcium carbonate in localized areas of high pH within the soils.

ADAMELLITE SOILS OF SAGE HEN FLAT

The soils on adamellite of Sage Hen Flat are characterized by a general lack of large rock fragments above the C horizon. The surface horizon is commonly a grus, consisting of granules and coarse sand, and is usually less than 1 inch thick (fig. 286). Calcium carbonate crusts, although occasionally present, are not common and may result from solution of inblown carbonate grains. O horizons occur in forested areas. Sandy loam A_{12} horizons are infrequently underlain by weak color, structural, or textural B horizons, in which iron oxidation, subangular blocky structure, and very weak clay

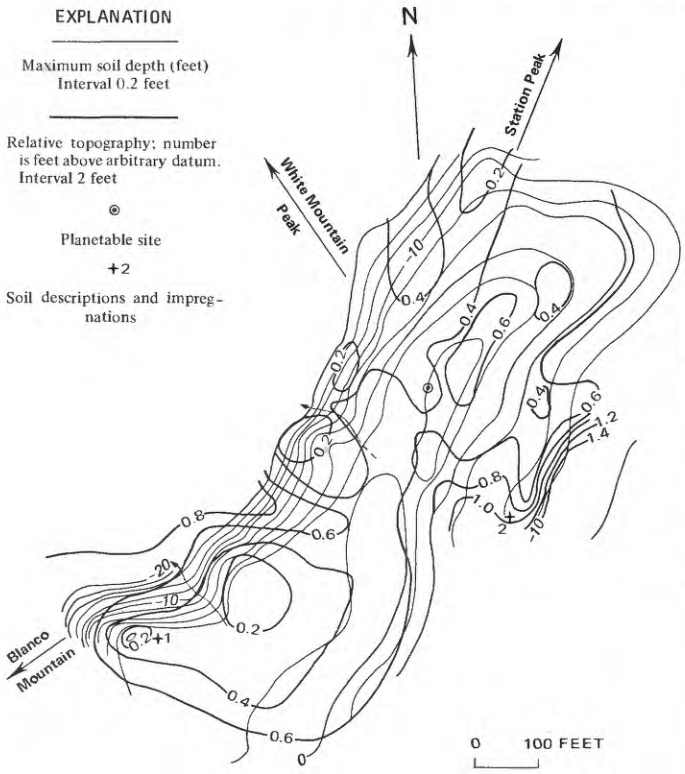

FIGURE 284.—Depth of soil and colluvium at planetable map site B–1, on basalt.

FIGURE 285.—Reed Dolomite soil pit showing accumulation of large fragments (A_{11} horizon) overlying finer grained A_{12} horizon.

films may be visible. The transition to the C horizon is often abrupt on topographic highs, but gradual in areas where the parent material is largely colluvial. Fragments in the C horizon may bear only thin weathering

FIGURE 286.—Soil pit in adamellite of Sage Hen Flat. Thin grus layer (A_{11} horizon) overlies A_{12} horizon, which tends toward a color and textural B at some sites. Lighter colored C horizon is transitional downward into unweathered colluvium (not shown).

rinds or may be quite thoroughly decomposed. Depth to bedrock averages about 6 inches on topographic highs.

BASALT SOILS

Basalt soil profiles average about 6 inches in depth and are characterized by good crumb structure in most A horizons and by a sharp A–C contact. Calcium carbonate crusts are rare, the surface layer generally consisting of coarse fragments or basaltic grus. Beneath this pavement is a vesicular gravelly loam to clay loam A_{12} horizon, as much as 4 inches thick, with subangular blocky peds. The lower part of the A horizon is often oxidized, but rarely is there other evidence of an incipient B horizon. Surface cracking and the degree of aggregation suggest higher clay contents than in other soils. Roots are uncommon, and O horizons are never present. The pH does not vary consistently with depth in the profiles.

ANDREWS MOUNTAIN SANDSTONE SOILS

Soils formed on the Andrews Mountain sandstones

and shales show a striking bimodal size distribution: Large rock fragments are concentrated at the surface near and within the C horizon, while sand, silt, and minor clay occur primarily in the A_{12} horizon. Calcium carbonate crusts are present locally but are not common. The A_{12} horizon is usually single grained or massive, although aggregation into crumbs may occur. The C horizon consists of colluvium or slightly weathered bedrock. As in other noncarbonate soils, the pH is generally 7.0 or slightly below and does not change systematically within the profile.

SOIL CONTAMINATION

Mineralogical analyses of five soils derived from the Reed Dolomite reveal from 3 to 73 percent of material, primarily volcanic glass, quartz, feldspars, biotite, and hornblende, that cannot be accounted for by weathering changes. The principal sources of this contamination are the pumiceous ash from the Mono Craters or Mono Glass Mountain (as much as 30 percent) and local windblown fragments (as much as 50 percent). The extent, nature, and implications of the soil contaminants were discussed elsewhere (Marchand, 1970). Their abundance necessitates considerable correction of soil data at most sites, as explained under "Chemical Weathering," and renders many soil samples uninterpretable in terms of weathering.

PHYSICAL WEATHERING

REED DOLOMITE

The Reed Dolomite is strongly jointed in one direction. Cross jointing is common, breaking the crystalline rock into angular fragments of about 3 feet to less than one-half inch in maximum dimension.

Bedrock grain size varies considerably depending on degree of recrystallization due to thermal metamorphism. Micrometer eyepiece examination of 16 bedrock samples indicate a mean diameter range of from 0.002 to 2 mm. Dolomite displaying spheroidal weathering has a bedrock grain size range from 0.125 to 2 mm, but angular dolomite is much finer grained, ranging from 0.002 to 0.125 mm.

Cumulative grain size frequency curves for 10 dolomite soil samples (fig. 287) show strong bimodal distributions indicative of immature weathering. The two modes are in fragments above 8 mm (jointed blocks) and in finer materials derived from the large blocks. For comparison, the range of bedrock grain size has been superimposed on the diagram. Triangular plots of dolomite, adamellite, and Andrews Mountain sandstone soils in terms of gravel, sand, and silt and clay, and of sand, silt, and clay are shown in figures 288 and 289, respectively. Gravel percentages vary greatly owing to extremely large fragments whose presence or

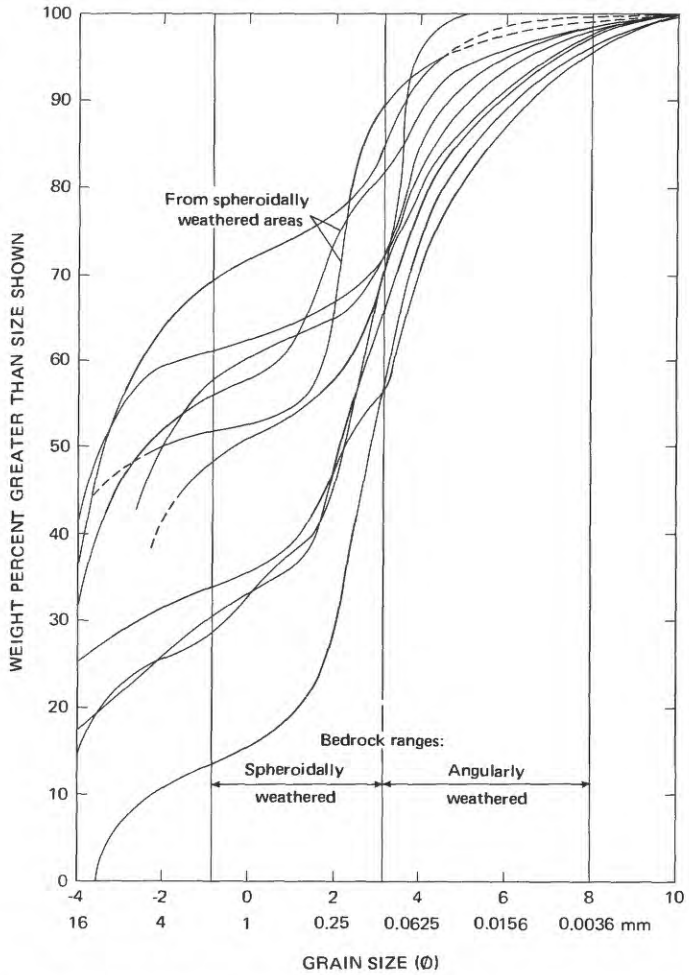

FIGURE 287.—Cumulative grain size frequency curves for dolomite soils and comparison with ranges in bedrock grain size based on samples from both spheroidally and angularly weathered sites.

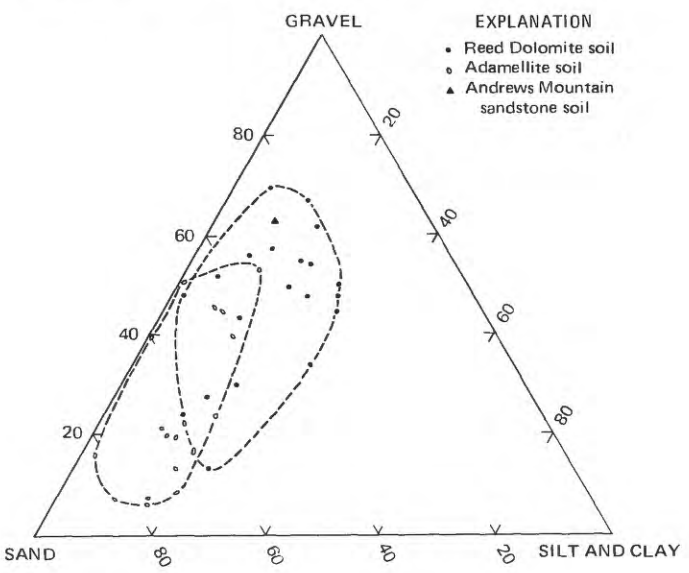

FIGURE 288.—Gravel-sand-silt and clay distribution for soil above the C horizon.

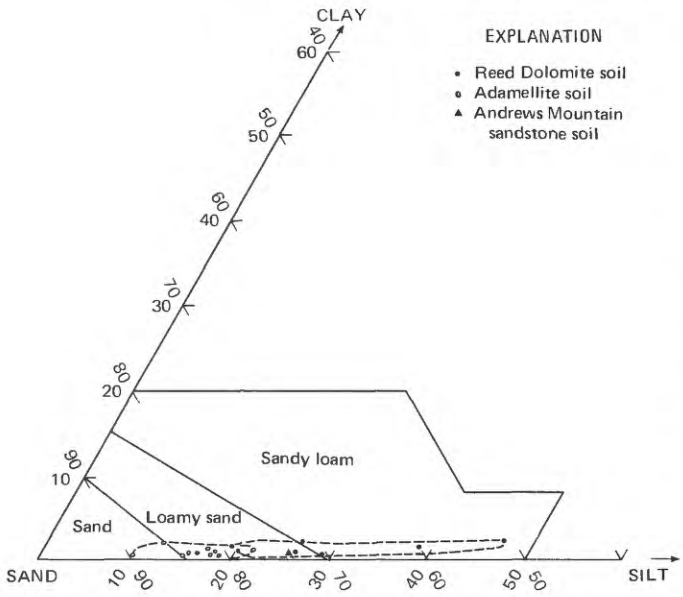

FIGURE 289.—Sand-silt-clay distribution for soil above the C horizon.

absence strongly influences the results. Relative amounts of sand, silt, and clay are more consistent.

The pattern of physical rock weathering after jointing and surface exposure appears to be a function of the earlier thermal history of the rock. Carbonates (both limestones and dolomites) adjacent to the Sage Hen and Cottonwood plutons tend to weather relatively rapidly to produce spheroidal boulders, whereas slower weathering of angular blocks characterizes carbonate terrane away from plutonic contacts. Most dolomite soils show maximums in the 2–4 phi interval, but several samples derived from thermally metamorphosed and spheroidally weathered dolomite have modes in the 1–2 phi range. Dolomite joint blocks have thus undergone two types of breakdown: (1) Fine-grained dolomite blocks have remained angular, and slow physical disintegration has produced smaller polycrystalline aggregates; (2) intergranular stresses within coarse-grained recrystallized dolomite developed during cooling from metamorphic conditions to subaerial temperatures have caused breakdown to single-crystal grains. This second weathering pattern was first noted and explained by LaMarche (1967), who contended that spheroidal forms are created by preferential attack at corners and edges of the more susceptible rock and are maintained by the greater porosity of the weathering block exterior. The author's observations corroborate those of LaMarche except that unrecrystallized dolomite commonly weathers to polycrystalline rather than monocrystalline grains as suggested by LaMarche, at least in the initial phase of physical weathering. Cleavages apparently afford an easier avenue of parting than the tightly held grain boundaries, except where contraction has created intergranular weaknesses.

ADAMELLITE OF SAGE HEN FLAT

Joints spaced as closely as 2–6 inches, but more commonly several feet apart, occur throughout the Sage Hen Flat pluton and tend to fall into two categories: A principal group trending north-northeast and dipping steeply to the southeast and a secondary group striking northwest and inclined to both northeast and southwest. Joint blocks are larger than in the dolomites and consequently have a lesser effect on weathering processes. Some joint openings and adjacent wallrocks have been silicified, sericitized, and tightly cemented with iron oxides. Such alteration is almost certainly deuteric or hydrothermal, as large crystals of mica have grown within feldspars adjacent to joint planes, in contrast with the fine-grained feldspar weathering products observed in soil thin sections. The altered joint planes and adjacent rock weather in positive relief with respect to adjacent adamellite (fig. 290), as do fine-grained mafic inclusions and aplitic dikes.

The medium-grained hypidiomorphic-granular texture of the adamellite locally tends toward porphyritic, but microscopic examination of 17 thin sections indicates that mean grain size never exceeds 4 mm. Average grain diameters commonly range from −0.5 to 3.5 phi.

In figure 291, cumulative grain size frequency curves for 10 adamellite soil samples and two grus samples are shown, along with the superimposed average and extreme ranges of bedrock grain size. With few exceptions, the adamellite soils are unimodal, the maximum frequency occurring between 2 and 9 phi in most samples. This mode falls within the mean bedrock range, sug-

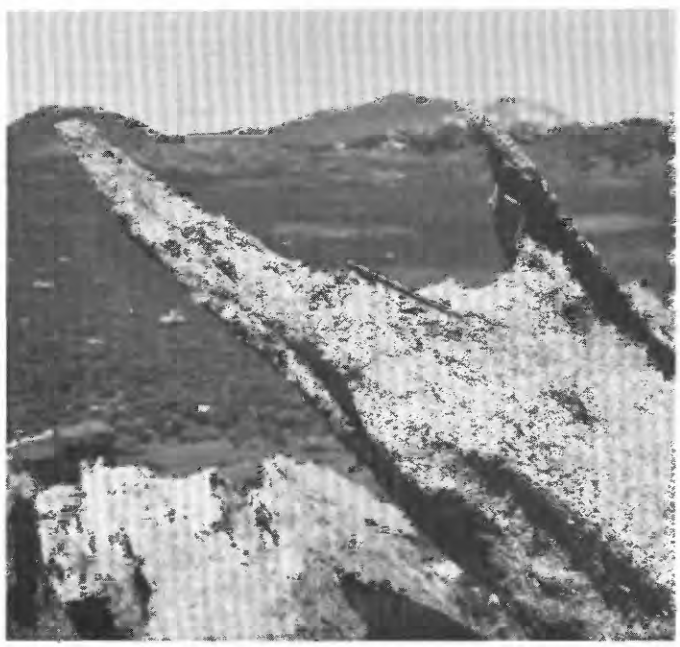

FIGURE 290.—Weathered adamellite outcrop on Sage Hen Flat. Note relative resistance of altered joint planes. Pencil gives scale.

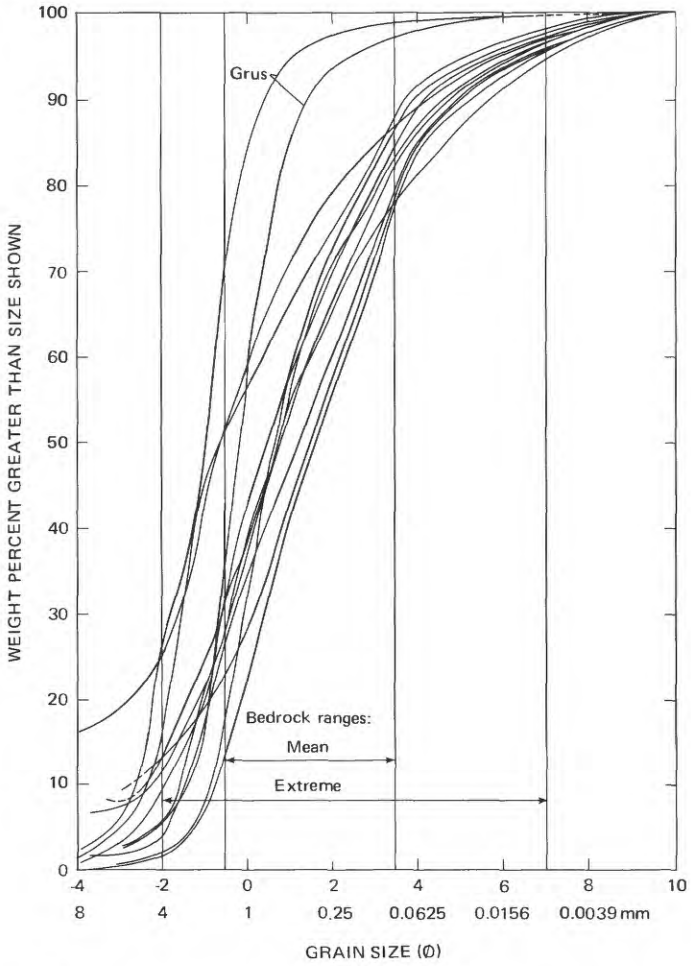

FIGURE 291.—Cumulative grain size frequency curves for adamellite soils and comparison with ranges of bedrock grain size.

gesting a tendency toward production of single-crystal grains by physical weathering. Two grus samples, however, collected beneath exfoliating boulders, show modes of -1–0 phi. This material is commonly composed of polycrystalline aggregates and occasional large grains.

On textural triangular diagrams (figs. 288, 289), adamellite soils of Sage Hen Flat plot closer to the sand component and farther from the gravel and silt components than do the Reed soils. Large joint blocks are rare in the adamellite soils, unlike the dolomite soils. Silt-sized grains are not common in fresh adamellite and have not been produced to any notable degree by weathering.

A two-stage process of physical weathering is suggested by the data. An initial breakdown into polycrystalline grus, occurring at the weathering surface of rock masses, is followed by a size reduction to monomineralic grains within the soil profile.

MECHANISMS OF DISINTEGRATION

Of the many mechanisms suggested for physical weathering and exfoliation, repetitive freezing of interstitial water seems the most applicable to relatively cold regions such as the White Mountains. At Crooked Creek Laboratory, temperatures descend below freezing on an average of about 220 days per year, and most of the precipitation occurs during the winter.

A striking feature of physical disintegration in the study area is that the same process applied to several lithologies has resulted in differing soil grain size distributions. This observation and the similarity of grus development from granitic rock here with that in much wetter and warmer areas suggest that rates and products of physical weathering may be as much a function of inherent lithologic properties as of climatic conditions. For frost riving to be effective, water must be able to penetrate the rock. The fact that coarse-grained lithologies weather more rapidly than fine-grained rocks of the same composition lends credence to LaMarche's (1967) hypothesis that contraction of large mineral grains during cooling from elevated temperatures may result in weakened intergranular bonds, affording access to water during weathering. Grain size may thus be one factor causing plutonic rocks to weather more rapidly than basalt: A larger grain will contract more than will a smaller grain having cooled the same amount, creating wider intergranular spaces or, if no separation occurs, greater intergranular tensional stresses. Fissility, grain adhesion and cohesion, and jointing may also be important factors in determining degree of water penetration.

It is not the author's intent to imply that the contraction mechanism is the only likely cause of grus formation. Wahrhaftig (1965, p. 1178–1179) suggested that alteration of biotite to swelling clays may aid in splitting apart intrusive rock into granular fragments. Evidence presented in the following pages indicates that expandable clays are not an important biotite weathering product in this area, but Helley (1966) showed that biotite can swell without being chemically altered. The absence of biotite or similar alterable minerals in the dolomite, however, necessitates an explanation other than presence of expandable minerals in this case.

An interesting aspect of erosion in the White Mountains is the striking correlation between erosional resistances and the manner of physical weathering in various lithologies. Fine-grained carbonate, quartzose sandstone, basalt, and aplitic dikes and mafic inclusions within the plutons are relatively resistant to erosion. These lithologies tend to produce immature soils having bimodal size distributions, large fragments representing one of the modes. Physical breakdown of such mat-

erial into fine particles is obviously very slow and the larger blocks are not easily eroded. Recrystallized carbonates, plutonic rock, and shales are much less resistant to physical weathering. These lithologies tend to yield submature soils lacking strong bimodal size distributions and containing sand-, silt-, and clay-sized particles which can be removed by rillwash and sheetwash. Thus erosion is faster in areas underlain by coarse-grained or fissile rock types (Marchand, 1971).

CHEMICAL WEATHERING

CHANGES IN THE SOLID PHASES

MINERALOGICAL CHANGES

Reed Dolomite

The Reed Dolomite is close to a pure carbonate, containing less than 0.5 percent of minerals other than dolomite (table 4). Talc comprises as much as 0.46 percent, but is generally less than 0.1 percent. Ilmenite, quartz, K-feldspar, plagioclase, apatite, epidote, and garnet are often present in trace amounts, and tremolite occurs in two of the five samples studied quantitatively. Although never observed in thin sections or oil immersion mounts, a few grains of biotite, hornblende, and magnetite were found in several grain mounts, possibly as a result of sieve contamination. Traces of chlorite and sericite were identified by X-ray diffraction of dolomite residues.

Table 4.—*Mineral weight percentages in five Reed Dolomite bedrock samples, based on line counts of grain mounts*

	54	68	47	65	127
Dolomite	99.51	99.68	99.97	99.96	99.93
Talc	.46	.090	.0336	.0067	.065
Tremolite	------	------	.0005	.0010	--------
Ilmenite	.0496	.0214	.0143	.0117	.006
Magnetite	.01	Trace	------	------	--------
Quartz	.0012	.0001	.0119	.0008	.001
K-feldspar	.0002	------	.001	.0013	.00003
Plagioclase	.0004	.20	.004	------	.001
Biotite	.0007	.005	.0003	.0013	--------
Hornblende	------	.0003	.0005	.0004	.00012
Apatite	------	.0058	.0002	.0004	.00012
Epidote	------	------	.0001	.0004	--------
Garnet	------	.0001	.0001	.0009	--------
Chlorite	------	------	------	.0014	--------
Zircon	.0003	.0002	------	------	--------

Oil immersion and grain mounts of 3–8 phi (125–4 μm) size fractions of five dolomite soils were examined for degree of etching or alteration of primary noncontaminative grains. Dolomite is strongly etched in all samples and in all size fractions (fig. 292), although effects are increasingly evident in finer particles. Tremolite is consistently etched, especially at the grain terminations, its degree of weathering being generally comparable to or slightly less than that of hornblende in adamellite soils. The weathering of talc is variable: In some samples it appears to be quite fresh, but in others has produced extremely irregular grain boundaries (fig. 293). K-feldspar, plagioclase, and biotite show minor

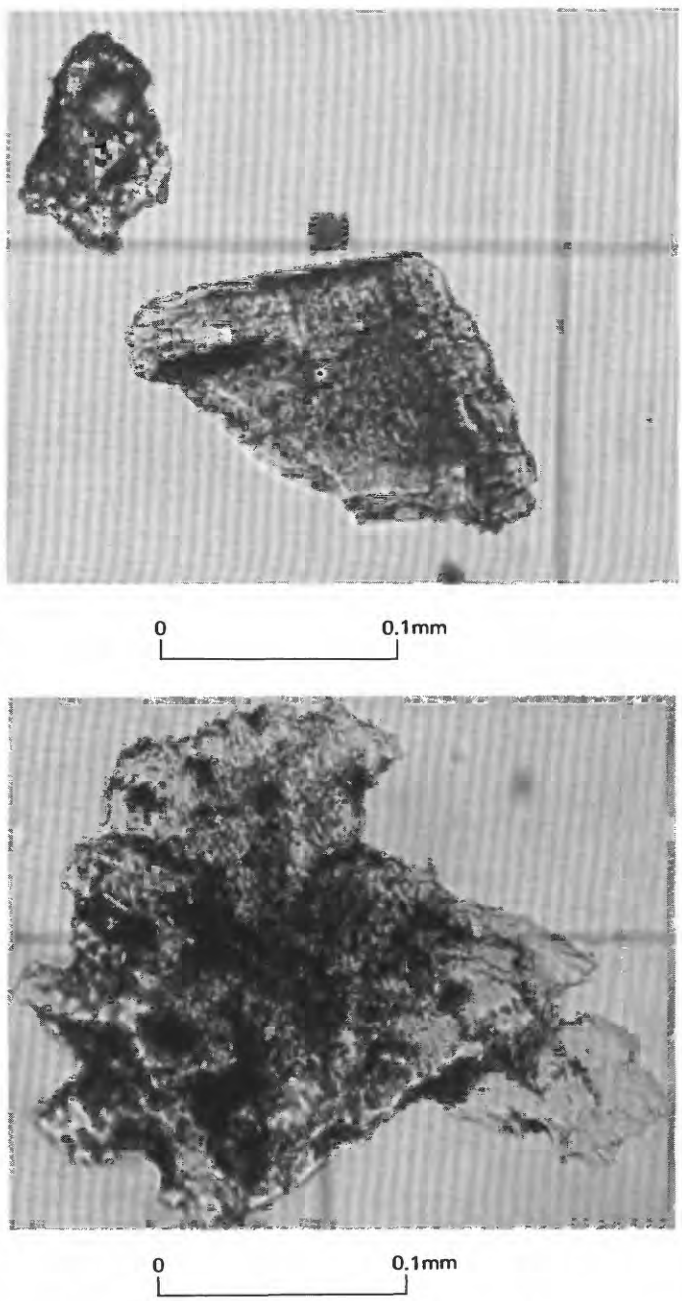

Figure 292.—Dolomite. *A*, Fresh, crushed bedrock (#47). Plane light. *B*, Etched, embayed, altered soil grain (#68 soil, fine sand). Plane light. Note tendency of etching to follow cleavage directions.

weathering alteration. Apatite grains are often rounded, showing effects of some solution. Quartz and ilmenite show little or no alteration, with the exception of very minor oxidation around the edges of a few ilmenite fragments. A general four-category weathering sequence, based on the preceding observations, is shown in figure 294. Attempts to quantify the sequence through grain counts proved unsuccessful owing to the abundance of contaminants.

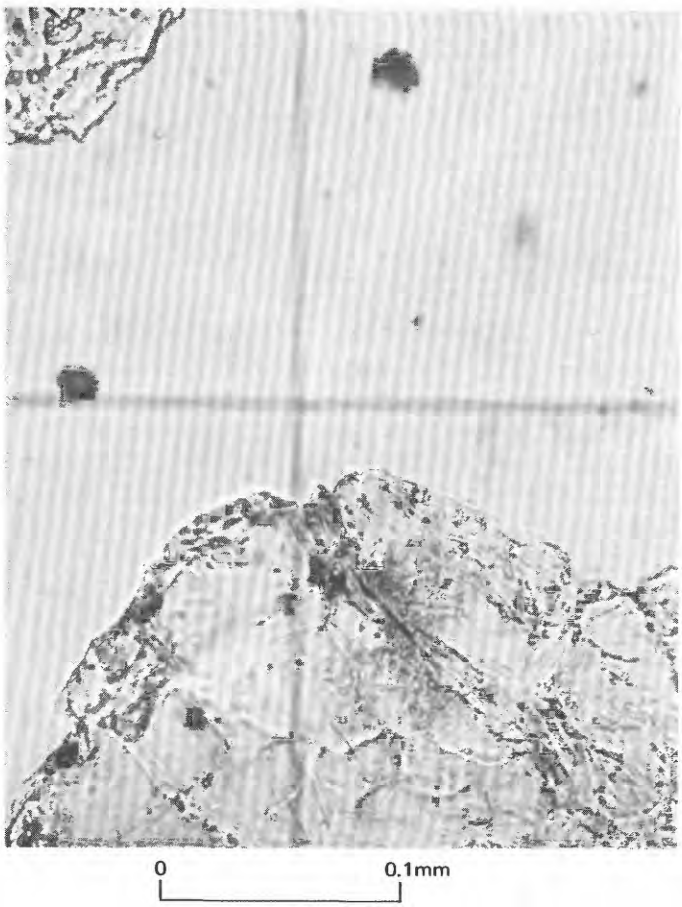

FIGURE 293.—Talc. *A*. Fresh crushed bedrock talc (#47). Plane light. *B*, Soil talc grains (#47 soil, crushed, 50–230 mesh). Grains to upper left are not strongly etched, but lower right grain shows large embayment. Plane light.

The only mineral that is definitely authigenic in Reed soils is calcite, which appears in both silt and clay fractions of about half of the analyzed samples. Several soil samples contain 7 A, 10 A, and 14 A layer silicates in both silt and clay fractions. These clay minerals are not

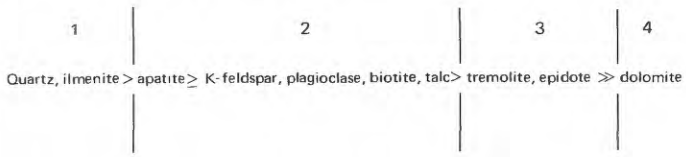

FIGURE 294.—Mineral weathering sequence in Reed Dolomite soils, in order of decreasing resistance. Based on visual comparison of bedrock and noncontaminative soil grains. Vertical lines separate major divisions of resistance.

believed to be authigenic; they possibly represent the chlorite and sericite originally present in the dolomite, plus aeolian additions from the surrounding terrain.

ADAMELLITE OF SAGE HEN FLAT

The mineralogy of the Sage Hen Flat pluton is typical of an adamellite. Quartz, microcline, and plagioclase make up more than 90 percent of the rock; biotite ranges from 3 to 7 percent; hornblende, muscovite, chlorite, epidote, sphene, ilmenite, and magnetite account for as much as 4 percent of the total; and allanite, zircon, apatite, and tourmaline are commonly present in trace amounts. A few pyrite grains were noted under the reflecting microscope.[2] Mineral percentages in five adamellite bedrock samples are given in table 5, and chemical compositions of principal minerals in the pluton are given in table 6.

Minerals in the silt and fine-sand fractions of Sage Hen soils and in soil thin sections were examined for size reduction and weathering modifications of margins, as compared with fresh bedrock grains. Plagioclase of composition An_{25-30} in the cores of zoned crystals is generally the most strongly weathered mineral in adamellite soils (fig. 295); fine-grained alteration products, chiefly kaolinite, sometimes make up much of the original plagioclase. Hornblende grains frequently possess no unmodified boundaries, the terminations

TABLE 5.—*Mineral weight percentages in five adamellite bedrock samples from Sage Hen Flat based on point counts of stained thin sections*

	86	101	94	97	105
Quartz	29.2	30.2	23.9	30.8	39.7
K-feldspar	25.8	19.1	25.4	25.7	23.4
Plagioclase	37.9	41.0	38.8	33.5	26.9
Biotite	6.7	5.4	5.5	3.2	7.1
Chlorite	.022	.24	.42	.102	.32
Muscovite	.05	.3	2.1	1.2	1.62
Hornblende	.13	------	.61	.008	------
Epidote	.057	.75	.76	2.8	.39
Allanite	.0004	.088	.18	Trace(?)	.018
Sphene	.0081	1.10	.32	.0003	.0854
Zircon	.0064	.008	.0005	------	.0037
Ilmenite	.0036	.60	.0095	.105	.42
Magnetite	.0016	1.27	1.98	2.65	Trace.
Apatite	.015	.025	.01	.003	.025
Tourmaline	------	------	.03	------	------

[2]Sulfides are localized along joints and near the margin of the pluton and are consequently not common in the samples examined. All nonmagnetic opaque minerals are therefore combined under the term "ilmenite" for the purposes of this discussion. The weathering of local sulfide concentrations, however, is of definite importance, as evidenced by significant sulfate values in spring waters draining the pluton.

TABLE 6.—*Chemical compositions of 10 major minerals in the adamellite of Sage Hen Flat*

[Methods of determination as indicated. All Fe assumed to be in ferric state]

	Electron microprobe (percent)											U Stage	Oil immersion		
													Indices of refraction		
	An	Ab	Or	Annite (Fe biotite)	Phlogopite	K	Ca	Mg	Fe	Al	Ti	An	Nx′	Ny	Nz′
Plagioclase:															
Maximum	30.5	88.2	2.1						.3			29			
Minimum	10.5	66.9	.4						.1			15			
Mean	20.9	77.2	1.1		(Ba=0.0)				.3						
Microcline:															
Maximum	.2	12.7	95.8						.3						
Minimum	.0	2.4	85.4						.1						
Mean	.0	7.1	93.7		(Ba=0.0)				.2					1.522	1.525
Biotite:															
Maximum				48.8	44.4	7.7									
Minimum				40.6	31.5	7.0									
Mean				43.4	38.1	7.5	(Ba=0.79)							1.633	
Chlorite:															
Maximum							Trace	10.0	19.8						
Minimum							.0	8.9	18.2						
Mean							.0	9.5	18.6					1.624	
Hornblende:															
Maximum							7.6	8.5	10.4						
Minimum							7.0	7.3	9.2						
Mean							7.3	7.7	9.9						
Epidote:															
Maximum							17.2	.0	9.9						
Minimum							16.0	.0	8.5						
Mean							16.5	.0	9.2					1.756	1.773
Allanite:															
Maximum							9.4		12.7	9.3					
Minimum							7.1		10.9	7.0					
Mean							8.0		11.5	8.2			< 1.775	1.772	>1.775
Sphene:															
Maximum							24.5	.0	1.5	0.8	19.8				
Minimum							21.7	.0	1.1	0.6	18.7				
Mean							23.3	.0	1.2	0.7	19.1		1.898	1.941	>2.00
Magnetite:															
Maximum								.08	71.7		.19			No	Ne′
Minimum								.00	70.4		.10		Apatite	1.630	
Mean								.01	70.8		.13		Tremolite	1.624	1.610
Ilmenite:															
Maximum								.15	33.0		27.9				
Minimum								.01	31.0		24.9				
Mean								.05	32.2		27.2				

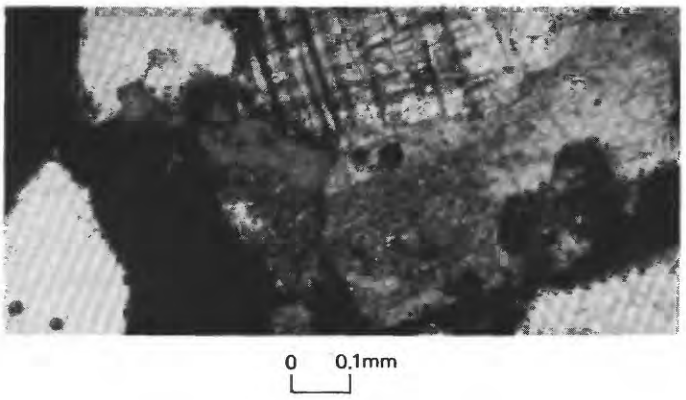

FIGURE 295.—Weathered grains in adamellite soil thin section. Core of plagioclase (lower center to right center) is considerably altered. Microcline (upper center and upper right) has parted along cleavages and shows slight alteration. Quartz (left) is fresh. Crossed nicols.

often displaying considerable etching. Many grains show no such effects, however, suggesting that the more severely etched fragments, and perhaps the dolomite soil talc grains as well, may owe their modifications to an earlier and more intense period of weathering. Along edges and cleavages biotite (fig. 296) is altering to secondary products, which are discussed in the section

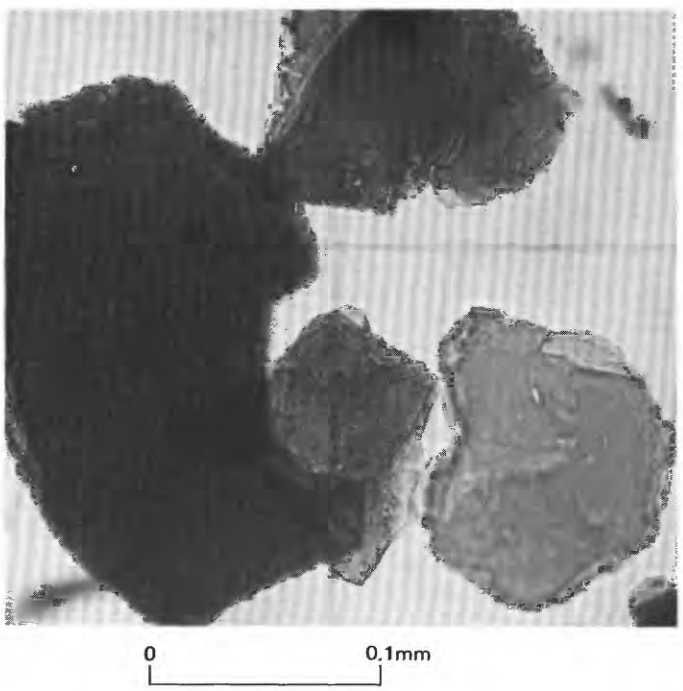

FIGURE 296.—Soil biotite grains (#86 soil, fine sand), showing both altered (upper left and upper center) and relatively unaltered margins (lower center). Plane light.

"Biotites." Biotites and epidotes have lost appreciable portions of their original margins, but irregular grain boundaries are only occasionally found on soil allanites. Microcline (fig. 295) and An_{10-15} plagioclase in the rims of normally zoned fragments commonly show some alteration to clay. Chlorite and apatite grains are frequently rounded, but are never deeply etched. Ilmenite and magnetite, especially the latter, may show minor external oxidation, but such changes are not common. Sphene, quartz (fig. 295), and muscovite display very little evidence of etching or alterations, but irregular boundaries not seen in bedrock grains are occasionally present. Soil zircons show perfectly euhedral margins. A seven-category weathering sequence for minerals in adamellite soils, based on the preceding evidence, is given in figure 297. In any given sample, a mineral may deviate from the sequence by one category, either above or below, but in general the order is consistent in all the samples studied. As in the case of the dolomite soils, quantitative mineral weathering studies were complicated by contaminants and yielded no substantial information not given by figure 297. In figure 305, mineral percentage changes with respect to bedrock are shown for the sand and silt fractions of #94 soil, a relatively uncontaminated site.

Qualitative data for phyllosilicates in the silt and clay fractions of some adamellite soils are summarized in table 7. Sericite, normal chlorite, and septechlorite are present in the silt fraction as well as in the clay and may be metamorphic or hydrothermal. Kaolinite and vermiculite are confined to clay fractions. As kaolinite occurs only in the adamellite soils, it is believed to be authigenic, but the vermiculite occurs widely and may have been partially or entirely added by aeolian processes. A small amount of montmorillonite is present in the clay fraction of one sample. The presence of several coexisting authigenic clay minerals, perhaps forming from different primary phases, is not inconsistent with the immature nature of the White Mountains soils.

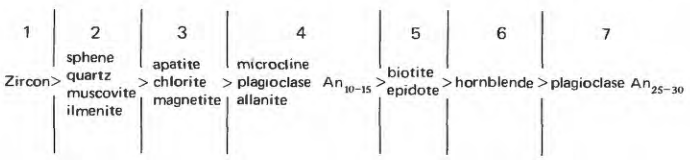

FIGURE 297.—Mineral weathering sequence in adamellite soils of Sage Hen Flat, in order of decreasing resistance. Based on visual comparison of bedrock and noncontaminative soil grains. Vertical lines separate major divisions of resistance.

ELECTRON MICROPROBE STUDIES OF ADAMELLITE MINERAL WEATHERING

Seven minerals from adamellite bedrock, grus, and soil on Sage Hen Flat were chemically analyzed by electron microprobe. Biotite showed major weathering alteration; microcline, plagioclase, allanite, and some magnetite gave detectable changes; ilmenite and sphene yielded no measurable variations because of weathering.

BIOTITES

Biotite analyses reveal progressively lowered contents of K, Ba, Mg, and Si and increases in Fe and Al, from bedrock to grus to soil (table 8). Biotite in grus is chemically similar to fresh bedrock biotite, but both of these differ markedly from soil biotite grains (1–3 phi), suggesting that little chemical weathering of biotites occurs prior to or during grus formation. Decreases in grus Mg with respect to bedrock is apparently due to primary solid solution substitution of Fe for Mg rather than weathering losses. Some grus biotites, however, are obviously breaking apart along cleavages prior to chemical alteration.

In terms of lattice sites, the biotite cations in 8–12-fold coordination appear to be the most vulnerable to weathering attack, followed by cations in octahedral coordination. (The values of table 8 assume no ferric iron is present and that all ferrous iron is in octahedral coordination.) Ions in sixfold and fourfold coordination taken together show little evidence of change. Within the 8–12-fold coordination sites, Ba appears to be more

TABLE 7.—*Layer silicates in silt and clay fractions of some adamellite soils*

[× = present; 0 = absent; n.d. = not determined. Clay is $< 2\mu$ m soil fragments]

Sample number	42	86	88	91	92	94	95	97	98	99	101	102	106
Kaolinite:													
Silt	n.d.	0	n.d.	n.d.	n.d.	0	n.d.	0	0	0	0	0	0
Clay	×	0	×	×	×	n.d.	×	×	×	n.d.	n.d.	n.d.	n.d.
Chlorite and (or) septechlorite:													
Silt	n.d.	×	n.d.	n.d.	n.d.	×	n.d.	×	0	×	(?)	×	×
Clay	×	×	0	0	0	n.d.	0	0	0	n.d.	n.d.	n.d.	n.d.
Vermiculite:													
Silt	n.d.	0	n.d.	n.d.	n.d.	0	n.d.	0	0	0	0	0	0
Clay	0	×	0	×	0	n.d.	×	×	0	n.d.	n.d.	n.d.	n.d.
Montmorillonite:													
Silt	n.d.	0	n.d.	n.d.	n.d.	0	n.d.	0	0	0	0	0	0
Clay	0	0	0	0	0	0	0	0	0	0	n.d.	0	×(?)
Sericite:													
Silt	n.d.	×	n.d.	n.d.	n.d.	×	n.d.	×	n.d.	×	×	×	×
Clay	×	×	×	×	×	×	×	×	×	×	n.d.	×	(?)
Biotite:													
Silt	n.d.	×	×	×	×	×	×	×	×	×	×	×	×
Clay	×	×	×	×	×	×	×	×	×	0	n.d.	×	(?)

TABLE 8.—*Averaged electron microprobe analyses of fresh and weathered biotites*

[CN=coordination number with respect to oxygen]

Source of analyzed grains	Elemental percentages						Total of analyzed elements as oxides[1] (percent)	Total: Annite + phlogopite[1] molecules	CN=8 to 12	CN=8	CN=4 to 6	CN=8 to 12	CN=8	CN=4 to 6
	K	Ba	Mg	Fe	Al	Si			K+Ba	Mg+Fe	Si+Al	K/Ba	Mg/Fe	Si/Al
Fresh bedrock	7.5	0.79	6.9	14.9	7.5	16.7	90.4	81.6	8.3	21.8	24.2	9.5	0.46	2.22
Grus	7.3	.51	5.8	15.8	6.7	16.5	87.3	81.6	7.8	21.6	23.2	14	.37	2.46
Soil (1–3ϕ)	5.8	.10	4.4	15.7	13.7	10.5	82.9	73.3	5.9	20.1	24.2	58	.28	.77

[1]Assuming all Fe in ferrous state

easily mobilized than K, but the extremely low Ba counting rate precludes any definite conclusions. Mg in the octahedral site is obviously more mobile than Fe, and Si, largely located in the sixfold to fourfold site, is much more readily removed than Al, which occurs in both octahedral and tetrahedral positions.

Microprobe analyses are usually grouped and averaged to compare changes in more than three elements, because only three elements may be analyzed simultaneously and because it is virtually impossible to return to the same location on the same grain in a subsequent analysis. Soil grains may often contain appreciable unaltered parts, however, and primary compositional differences between grains may obscure changes due to weathering. Comparisons were made between weathered and fresh parts of the same soil grain to eliminate those problems. Ratios of K/Fe and Mg/Fe along five typical transects across soil biotites, both parallel and perpendicular to the (001) cleavage, are reproduced in figures 298 and 299. Several conclusions seem apparent from the data: (1) Lower K/Fe and Mg/Fe ratios invariably occur either along edges or cleavages, but every edge and cleavage does not show changed ratios, (2) traverses perpendicular to the basal cleavage are more variable than transects parallel to cleavages, and (3) K losses with respect to Fe are generally more frequent and larger than those of Mg. Examination of the original data (not shown) reveals a relatively constant Fe percentage across the grains, indicating that Fe losses are comparatively minor. Decreased K/Fe and Mg/Fe ratios therefore reflect absolute losses, an observation consistent with the data of table 8. Some red-brown to yellow-brown Fe oxidation, though, was observed in soil biotites examined under the petrographic microscope, especially along grain margins.

To gain further information concerning the end product of biotite weathering, analyses of fresh and altered portions of soil biotites for Si, Al, and Ba were also conducted (table 9), using a finely focused electron beam. The Si/Al ratio drops from above 2 in fresh portions to less than 1, and even approaches 0 in the fine-grained alteration products that commonly occur adjacent to edges and cleavages. Ba also shows somewhat lower values in the alteration products. The Mg losses

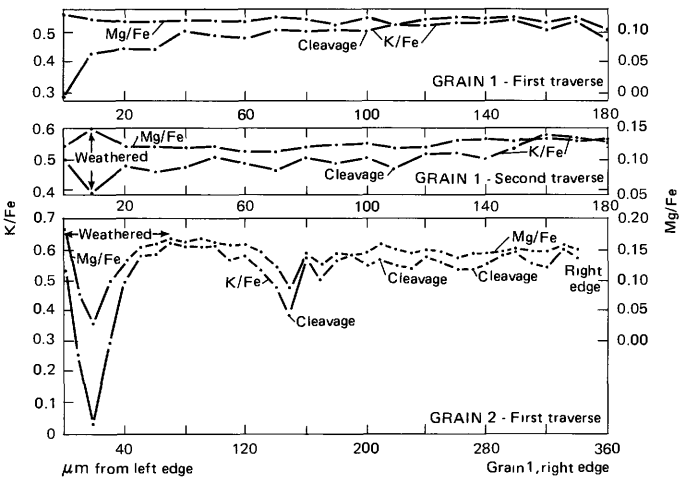

FIGURE 298.—Electron microprobe traverses normal to (001) cleavage of two soil biotite grains.

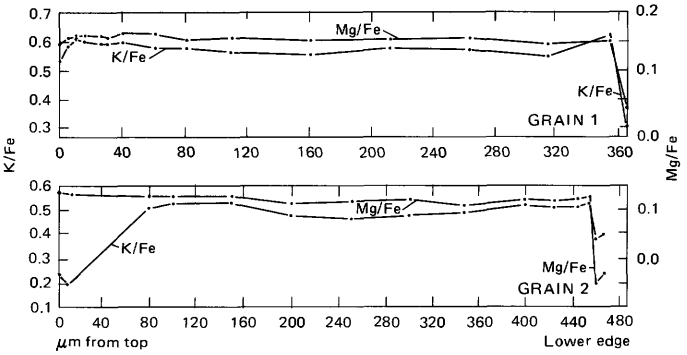

FIGURE 299.—Electron microprobe traverses parallel to (001) cleavage of two soil biotite grains.

TABLE 9.—*Individual electron microprobe analyses, in weight percent, of altered and relatively fresh parts of soil biotites*

Ba	Si	Al	Si/Al	Description	Number of analyses
0.10	16.70	7.38	2.26	Fresh	1
.30	16.57	7.55	2.19	do	4
.00	7.44	9.17	.81	Alteration product	1
.16	11.54	14.80	.78	do	1
.04	10.33	15.10	.68	do	1
.36	9.91	18.57	.53	do	1
.00	1.88	16.88	.11	do	1
.00	.86	22.43	.04	do	1
.00	.67	29.91	.01	do	1

and Si/Al ratios rule out vermiculite and montmorillonite as possible weathering products. The Si/Al ratios suggest that complete alteration to gibbsite may have occurred, but microprobe analyses of porous and probably hydrous materials such as these must be regarded with some caution. Four Si/Al values fall between 0.5 and 1.0, and 1:1 clays (but not gibbsite) were detected in X-ray diffraction patterns of soil and clay fractions; so, the formation of kaolinite from biotite, if only as a temporary weathering product, seems a more likely possibility. Presence of colloidal, noncrystalline aluminum hydroxide may account for the low Si/Al ratios.

Feldspars

Microscopic evidence indicates that plagioclase, especially the more calcic zones, and microcline are altering to clays. The soil feldspars analyzed by the microprobe are much less severely altered than feldspars observed in some soil thin sections and grain mounts; so, chemical differences between averaged microprobe analyses of fresh bedrock grains and soil fragments (table 10) are not striking.

Table 10.—*Averaged electron microprobe analyses, in weight percent, of feldspars from fresh adamellite bedrock, grus, and soils*

	K	Ba	Na	Ca	Fe	Total: An+Ab+Or	Number of grains analyzed
Microcline:							
Fresh	13.2	0.0	0.53	0.01	0.2	99.8	1
Grus	13.0	.0	.57	.01	.2	99.2	4
Soil	13.0	.0	.31	.00	.2	96.4	2
Plagioclase:							
Fresh	.1	.0	6.9	2.9	.3	99.4	4
Grus	.2	.0	6.4	3.3	.0	98.0	2
Soil	.1	.0	6.5	3.4	.1	98.4	8

The analyzed microclines appear to have undergone some chemical losses during weathering, as evidenced by the 3.4 percent decrease in molecular totals (An+Ab+Or), from bedrock to soil. Microcline grains from grus samples, like biotites (table 8), do not appear to be appreciably weathered. Microprobe transverses across K-feldspars from seven grus and soil samples (data not shown) suggest that lattice deficiencies, indicated by low molecular totals, most commonly occur near grain edges and that low Na and K values tend to be associated with these deficiencies. Primary crystal zonation, however, often obscures weathering losses.

Zoning is so prominent in the plagioclases that weathering changes are largely masked, but the molecular totals of table 10 indicate that losses due to weathering have occurred and that sodium may be the most mobile constituent. Plagioclases from both grus and soil appear to show detectable deficiencies of molecular totals. A very small electron beam was used to analyze fine-grained plagioclase alteration products within soil grains for Si and Al (fig. 300). The marked

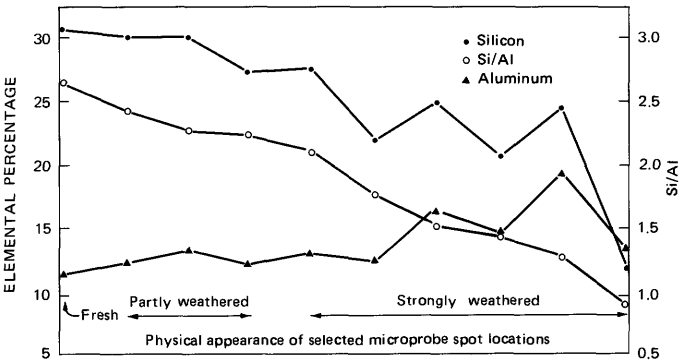

Figure 300.—Electron microprobe analyses of 10 parts of a single plagioclase grain.

decrease in Si/Al ratios from 2.7 in fresh portions to about 1–1.5 in altered areas suggests that kaolinite may be the principal weathering product. As weathering proceeds, Si percentages appear to decrease more rapidly than Al percentages increase, such that Si + Al steadily decreases.

Other Minerals

Analyses of fresh and weathered allanite, magnetite, ilmenite, and sphene are compiled in table 11. The one soil allanite examined is lower in Ca and Al and higher in Fe percentage than fresh grains. Analytical results from 35 magnetite and ilmenite grains in both bedrock and soil gave little indication of weathering changes, but a few magnetite grains showed some visible alteration and less Fe (apparently due to oxidation) near their margins. Soil and bedrock sphenes gave virtually identical chemical analyses, and traverses across soil grains showed no significant variations.

Table 11.—*Electron microprobe analyses, in weight percent, of four minerals from fresh adamellite of Sage Hen Flat and from derived soil*

	Ca	Mg	Fe	Al	Ti	Number of analyses
Allanite:						
Fresh	8.0	----	11.5	8.2	----	12
Soil	6.5	----	12.9	6.7	----	1
Magnetite:						
Fresh	----	0.00	70.8	----	0.13	13
Soil	----	.03	72.6	----	.25	10
Ilmenite:						
Fresh	----	.05	32.2	----	27.2	11
Soil	----	.26	30.0	----	29.4	1
Sphene:						
Fresh	23.3	.0	1.2	.7	19.1	11
Soil	23.8	----	----	.9	19.0	2

Chemical Changes from Bedrock to Soil

Chemical analyses of bedrock and soil samples were conducted by X-ray fluorescence techniques to assess the degree and sequence of bulk chemical changes due to weathering. For the adamellite and its derived soils, the U.S. Geological Survey samples G–1, G–2, GSP–1, AGV–1, BCR–1, and W–1 were used as standards. The U.S. Bureau of Standards' Dolomite #88 and five Reed

bedrock and soil samples analyzed by Ken-ichiro Aoki, Tohoku University, Japan, were used as standards for the dolomite group.

Reed Dolomite

Arithmetic means and standard deviations for analyses of dolomite bedrock, soil greater than 2 mm, soil less than 2 mm, and soil less than 62 μm are given in table 12. Standard deviations refer to differences between samples collected at different locations rather than to analytical precision (replicate analysis).

The principal reason for collection of numerous and widely distributed bedrock and soil samples was to obtain an indication of chemical and mineralogical variability within each parent material and soil, such that changes due to weathering could be clearly differentiated from apparent changes caused by sampling deficiencies. Unfortunately, careful study of soil mineralogy shows most of the Reed soil samples to be contaminated by both rhyolitic ash and local materials to the extent that corrections for contamination would be meaningless. The effects of external aeolian addition are also indicated by the large increases in Na and K in the finer size fractions of the soils. Only one sample for which the mineralogy was determined, #65 soil less than 2 mm, appears to be little affected by contamination. Corrections for the minor chemical effects of the tuff and local contaminants in this sample were made using weighted averages of glass and contaminative mineral percentages[3] in the sand and silt fractions (percentage clay was less than 1 percent and was therefore neglected in the calculations). Chemical composition of minerals and glass used to correct the original soil analysis are given, together with sources of information, in table 13. Local contaminants in this sample are assumed to be derived from the nearby Sage Hen Flat pluton. Soil analytical values from which corrections had been subtracted were recalculated to the previous oxide percentage total and converted back to elemental percentages. Total estimated contamination in #65 soil less than 2 mm is only 3.9 percent, and thus any errors due to inaccurate amounts of correction are relatively small.

Absolute losses (weight percent in bedrock minus weight percent in soil) are shown for the five carbonate-component elements in mean soil greater than 2 mm (hereafter termed "soil gravel") and #65 soil less than 2 mm (corrected for both ash and local contaminants) on the left side of table 14. To eliminate differential effects of heavy and light elements, the absolute losses are divided by atomic weight in the adjacent columns. Percentage losses with respect to bedrock, determined as

$$\text{percentage loss} = \frac{\text{weight percent in bedrock-weight percent in soil}}{\text{weight percent in bedrock}}$$

are shown in bar graph form in the left side of figure 301. Both calculations were made holding constant the percentage of Zr, the most stable element during the weathering process for the samples studied here. Undoubtedly Zr percentage does change between bedrock and soil, but this assumption permits relative comparison of all elements investigated, the principal concern of this study. The soil gravel fraction is assumed to be little affected by contamination, and #65 soil less than 2 mm has been corrected for all external additions; so, these two soil analyses should be chemically representative of Reed terrane. Elemental absolute losses from dolomite bedrock to soil follow the sequence Ca > Mg $\ggg$ Fe $\gg$ Mn $\gg$ Sr, a trend strongly controlled by bedrock composition. When atomic weight is taken into account, the position of Ca and Mg in the sequence converge or trade places, but other relations remain

[3]The methods by which percentages of ash and aeolian contaminants were determined has been discussed elsewhere (Marchand, 1970) in some detail.

TABLE 12.—*Chemical analyses, in weight percent except as noted, of Reed Dolomite bedrock and soils*

[Data are from X-ray fluorescence techniques except as noted. n.d.=not determined; S.D.=standard deviation. Soil analyses are not corrected for contamination]

	Bedrock			Soil > 2 mm			Soil < 2 mm			Soil < 62 μm		
	Mean	S.D.	Number of samples	Mean	S.D.	Number of samples	Mean	S.D.	Number of samples	Mean	S.D.	Number of samples
Si	0.11	0.07	7	0.80	0.10	2	13.24	5.84	6	22.01	1.00	5
Ti	.0069	.0050	6	.022	.002	2	.20	.11	6	.40	.02	5
Zr ppm	6.5	5.3	4	13	3	2	104	51	5	246	31	5
Al	.092	.059	6	.38	.06	2	4.15	1.70	6	7.16	.28	5
Fe	.26	.09	12	.36	.005	2	1.83	.62	11	3.13	.06	5
Mn	.055	.020	12	.08	.01	2	.11	.031	11	.12	.02	5
Mg	12.46	.43	7	11.01	.16	2	5.67	1.57	6	2.21	.38	5
Ca	21.52	.93	12	22.54	.43	2	12.93	4.16	11	8.38	.88	5
Ba	.00	.00	6	.00	.00	2	.028	.012	5	.06	.004	5
Sr ppm	56	7	6	62	3	2	124	27	5	222	17	5
Na[1]	.027	.003	2	.0550	.003	2	.755	.395	2	n.d.	n.d.	0
K[1]	.011	.006	2	.0545	.0055	2	1.281	.335	3	n.d.	n.d.	0
Rb ppm	.81	2.00	8	1.10	.50	2	25.8	11.7	11	51.0	4.0	5
P[2]	.0175	.0085	2	n.d.	n.d.	------	.0545	------	2	n.d.	n.d.	0
Oxide total[3]	------	------	[4]98.63	------	------	[4]97.69	------	------	[5]101.39	------	------	[6]94.63

[1]Flame photometer analyses by Joaquin Hampel.
[2]Wet chemical analyses by Ken-ichiro Aoki.
[3]CO_2 taken as stoichiometric. Iron computed as Fe_2O.
[4]Includes H_2O+ and H_2O- analyzed by Ken-ichiro Aoki for three samples.
[5]Includes H_2O+ and H_2O- analyzed by Ken-ichiro Aoki for two samples.
[6]Does not include H_2O+ and H_2O-.

TABLE 13.—*Chemical compositions, in weight percent except as noted, of minerals and glass in soils used to correct chemical analyses*

[Probe analyses supplemented by data from Deer, Howie, and Zussman (1952a, b; 1963a, b), as indicated, except analyses for volcanic glass and biotite, which are supplemented by data from Carmichael (1967, p. 50 and 52, respectively)]

	Volcanic					Plutonic (local)					
	Glass	Sanidine	Plagioclase	Biotite	Quartz	Microcline	Plagioclase	Biotite	Hornblende	Epidote	Chlorite
		Sample 10 sanidine (1963b, p. 41)	Sample 7 albite (1963b, p. 108)			Sample 13 microcline (1963b, p. 39)	Sample 8 oligoclase (1963b, p. 113)	Sample 5 igneous biotite (1963a, p. 58)	Sample 17 hornblende (1962b, p. 277)	Sample 8 epidote (1962a, p. 198)	Sample 18 chlorite (1963a, p. 141)
Si	35.31	30.7	30.2	16.8	46.75	30.1	29.6	16.3	22.5	17.4	12.0
Ti	.04	------	------	3.2	------	------	.01	2.4	.6	.05	.53
Zr ppm	106	------	------	------	------	------	------	------	------	------	------
Al	6.58	10.0	10.6	6.7	------	10.1	12.1	8.1	3.1	12.8	11.2
Fe	.97	.0	.64	16.4	------	.2	.06	[1]14.8	[1]9.9	[1]9.2	[1]18.6
Mn	.04	------	------	.3	------	.01	------	.3	.3	[1].03	.27
Mg	.02	.1	.19	6.4	------	.02	------	[1]6.4	[1]7.7	------	[1]9.5
Ca	.43	.1	[1]1.9	.01	------	------	[1]3.0	.8	[1]7.3	16.5	.11
Sr ppm	5	------	------	------	------	------	------	------	------	------	------
Ba	None	.4	------	.4	------	------	------	------	------	------	------
Na	3.00	3.0	[1]6.9	.5	------	[1].6	[1]6.8	.3	1.1	------	------
K	3.89	[1]10.9	[1]1.2	7.4	------	[1]12.8	[1].1	[1]7.4	.6	------	------
Rb ppm	190	------	------	------	------	------	------	------	------	------	------

[1]Analyzed by electron microprobe.

TABLE 14.—*Absolute losses, in weight percent, of chemical constituents from bedrock to soil, assuming constant Zr percentage*

[Figures in parentheses under mean dolomite column are losses expressed as percentages of #65 bedrock-to-soil losses for the given elements]

Element	Dolomite				Adamellite	
	Mean dolomite bedrock minus mean dolomite soil > 2 mm		#65 bedrock minus #65 soil < 2 mm[1]		#94 bedrock minus #94 soil < 2 mm[1]	
	Absolute loss	Loss/ atomic weight	Absolute loss	Loss/ atomic weight	Absolute loss	Loss/ atomic weight
Si	------	------	------	------	−16.67	−0.5934
Al	------	------	------	------	−4.33	−.160
K	------	------	------	------	−2.12	−.0542
Na	------	------	------	------	−1.77	−.0770
Fe	− 0.08(67)	−0.001	−0.12	−0.0022	−.98	−.017
Ca	−10.25(57)	−.256	−17.99	−.449	−.92	−.023
Mg	−6.96(65)	−.286	−10.72	−.441	−.43	−.01
Ti	------	------	------	------	−.09	−.002
Ba	------	------	------	------	−.07	−.0005
Mn	−.015(54)	−.00027	−.028	−.00051	−.05	−.0009
Sr	−.0025(65)	−.000028	−.0038	−.000043	−.0368	−.000420
Rb	------	------	------	------	−.0041	−.000047

[1]Corrected for both ash and local contaminants.

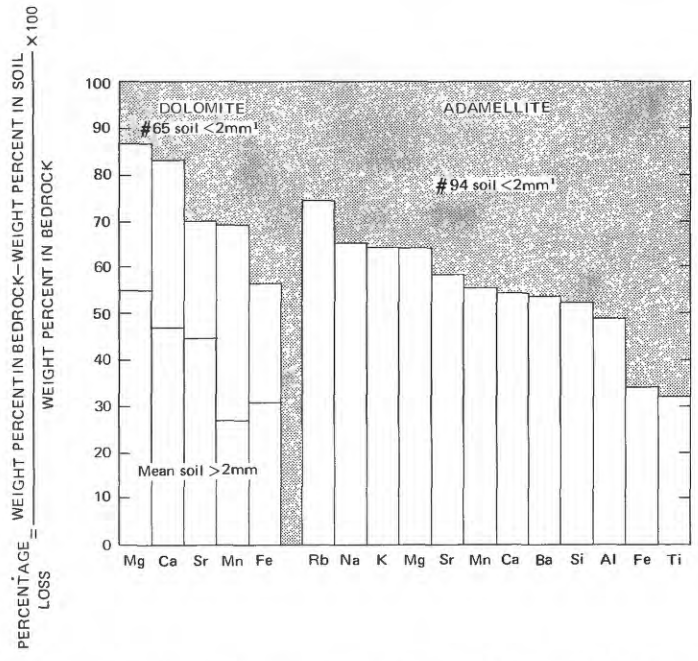

FIGURE 301.—Percentage chemical losses for the indicated Reed Dolomite and adamellite soils of Sage Hen Flat with respect to bedrock, assuming constant Zr percentage. [1]Corrected for both ash and local contamination.

essentially unchanged. Percentage losses, a more significant indication of weathering mobility, occur in the sequence $Mg > Ca > Sr > Mn \overset{?}{\approx} Fe$. In the percentage loss calculation, the atomic weight factor is automatically taken into account. Loss of Mg relative to Ca, as indicated by the percentage losses, is in agreement with the presence of secondary calcium carbonate in dolomite soils. Comparisons of both absolute and percentage losses indicate that, of the five elements shown (with the possible exception of Mn), well over half of the total elemental losses in bedrock to soil less than 2 mm occur during the transformation of bedrock into soil gravel. Obviously chemical breakdown of the dolomite begins almost simultaneously with physical disintegration in the early stages of the carbonate weathering process.

Sections cut through spheroidally weathered dolomite fragments occurring at the surface or within the soil profile commonly show an abrupt change from fresh light cream to pink crystalline dolomite outward into a

porous gray or white concentrically layered weathering rind (fig. 302). Under the petrographic microscope, alternating layers of fresh dolomite and a fine-grained alteration product are evident within the rind. Electron microprobe analyses of one of the rinds for Ca, Mg, Mn, and Fe and microprobe transects from unaltered dolomite into the rind (figs. 303, 304) indicate that the weathering product is a very pure calcite, as shown in the following table.

	CaO	MgO	MnO	FeO
Fresh dolomite ----------percent----	30.2	20.6	0.3	0.2
Alteration product ------percent----	54.1	.3	.2	.1

Leaching of Mg and deposition of calcite are undoubtedly responsible for the development of carbonate horizons and other calcium carbonate accumulations in dolomite soils. Fe and Mn are more variable within the rind, but appear to occur in approximately equal concentrations in both dolomite and calcite.

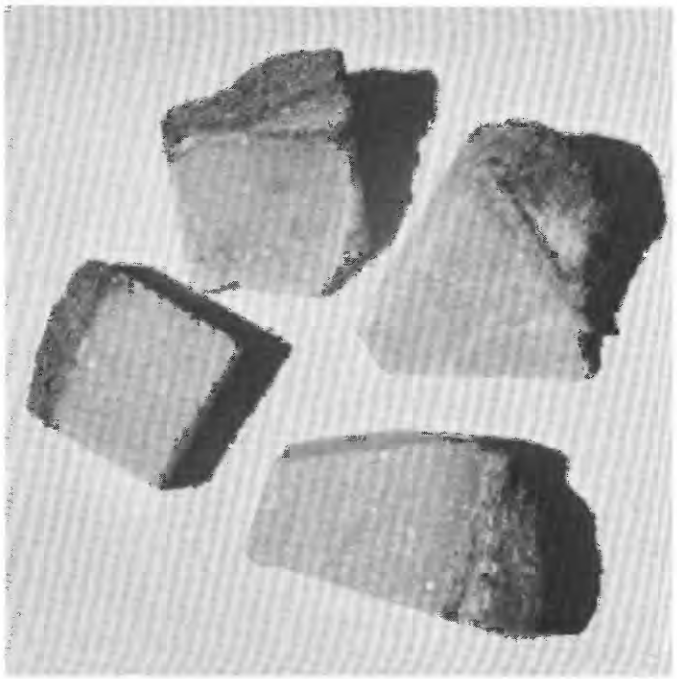

FIGURE 302.—Rock saw chips showing weathering rind on spheroidally weathered dolomite (#68) analyzed by electron microprobe. Rind is about 0.2 inch thick.

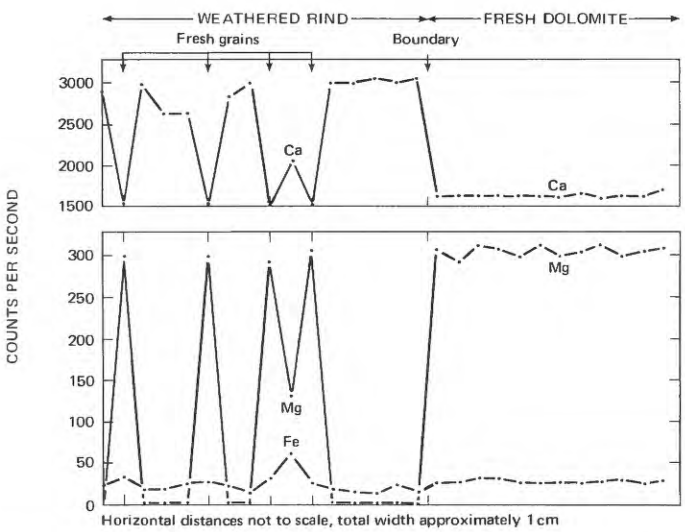

FIGURE 303.—Electron microprobe transect showing Ca, Mg, and Fe variation across an alteration rind in spheroidally weathered Reed Dolomite (#68).

ADAMELLITE OF SAGE HEN FLAT

Mean analytical values for bedrock, grus, soil less than 2 mm, and soil less than 2 μm are given in table 15. The grus values are generally comparable to those of the bedrock, and where they differ, the direction of change suggests primary variability rather than weathering. Therefore, in the third column of table 15, means weighted on the basis of number of samples have been calculated for both bedrock and grus and were used as the bedrock values in all further computations.

As in the case of the Reed, almost all adamellite soils are greatly contaminated by both rhyolitic ash and local debris. The first step in preparing the soil analyses for interpretation was to correct for the contaminating ash. After ash correction, only #94 < 2 mm gave a reasonable sequence of bedrock-to-soil mineralogical changes, on the basis of grain counts (fig. 305), suggesting ab-

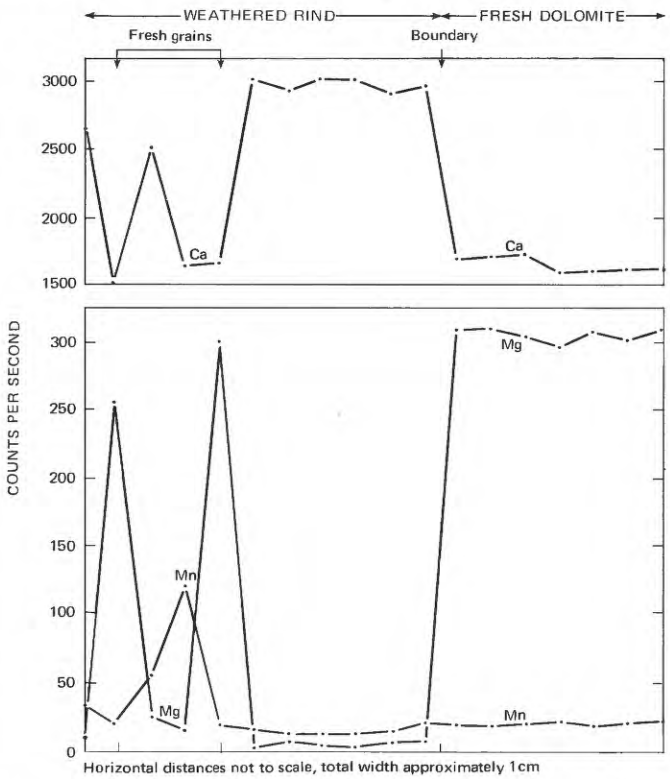

FIGURE 304.—Electron microprobe transect for Ca, Mg, and Mn across dolomite weathering rind (#68).

TABLE 15.—*Averaged values for X-ray fluorescence chemical analyses, in weight percent except as noted, of adamellite bedrock and soils of Sage Hen Flat*

[S.D.=standard deviation; n.d.=not determined. Soil analyses are uncorrected for contamination]

	Bedrock		Grus		"Bedrock" (= weighted average of bedrock and grus; see text)		Soil < 2 mm		Soil < 62 μm	
	Mean	S.D.	Mean	S.D.	Mean	S.D.	Mean	S.D.	Mean	S.D.
Si	32.39	0.98	31.16	1.67	31.79	1.08	31.51	0.61	28.21	0.85
Ti	.24	.04	.23	.04	.24	.04	.32	.05	.51	.03
Zr ppm	164	32	123	16	152	27	217	49	517	65
Al	8.36	.41	8.94	.50	8.53	.44	8.03	.55	8.38	.22
Fe	2.16	.56	1.55	.04	1.99	.41	2.77	.62	4.53	.50
Mn	.06	.02	.05	.04	.06	.03	.08	.02	.12	.01
Mg	.46	.18	.31	.03	.42	.14	.56	.12	1.32	.22
Ca	1.44	.29	1.45	.09	1.44	.23	1.32	.17	2.24	.12
Ba	.12	.02	.15	.05	.13	.03	.10	.01	.08	.01
Sr ppm	600	111	533	129	581	116	455	91	321	21
Na	2.70	.24	2.53	.23	2.65	.24	2.19	.14	1.57	.10
K	3.20	.45	4.41	.84	3.55	.56	3.00	.24	2.97	.06
Rb ppm	53.9	12.9	65.3	12.8	57.1	12.9	59.8	8.0	67.3	1.9
P	[1].048	------	n.d.	------	[1].048	------	[2].0455	------	n.d.	------
C	[1]none	------	n.d.	------	[1]none	------	[2].001	------	n.d.	------
H	[1].053	------	n.d.	------	[1].053	------	[2]2.04	------	n.d.	------
Oxide total[3]	100.20	------	97.73	------	99.32	------	100.47	------	94.89	------
Number of total analyses	10	------	4	------	14	------	6	------	5	------
Number of partial analyses	8	------	0	------	8	------	5	------	2	------

[1]Based on one wet chemical analysis by Ken-ichiro Aoki.
[2]Based on two wet chemical analyses by Ken-ichiro Aoki.
[3]Fe calculated as Fe_2O_3; H_2O+, H_2O-, P_2O_5, CO_2 not analyzed in grus and < 62 μm soil samples.

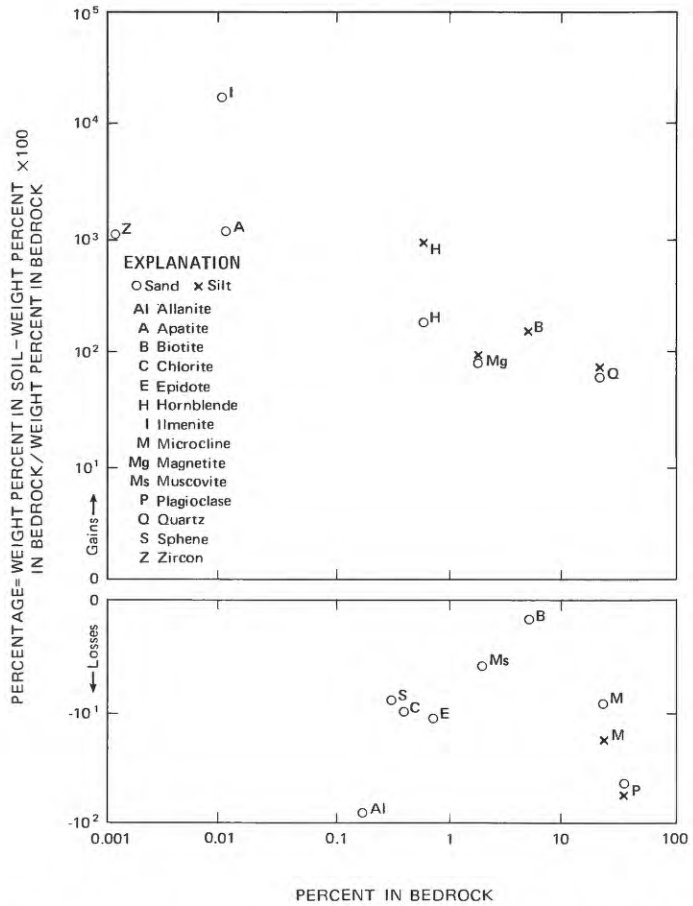

FIGURE 305.—Mineral percentage changes with respect to bedrock in two size fractions of a relatively uncontaminated adamellite soil (#94), after ash corrections.

sence of significant local contamination. All major minerals except biotite and hornblende appear in place in the #94 sand and #94 silt mineral sequences, based on the observed weathering sequence (cf. fig. 297). By using percentage changes consistent with those of quartz, microcline, and plagioclase and with the observed weathering sequence, corrections were computed for biotite and hornblende in the less-than-2-mm fraction of #94 soil, as shown in the left part of table 16. Chemical corrections using the values of table 13 assume that the biotite and hornblende came from the Sage Hen Flat pluton or do not differ greatly from that of the pluton. The adjustments, including those from the ash, were subtracted from the original analysis of #94 soil, followed by correction to the previous oxide total and reconversion to elemental values, as shown in the right part of table 16.

Chemical changes due to weathering at site 94 may now be assessed from bedrock and corrected soil analyses. Absolute losses and losses divided by atomic weight from #94 bedrock to less-than-2-mm soil are given on the right side of table 14. Percentage losses with respect to bedrock, computed from concentrations in weight percent and assuming constant Zr percentage, are presented graphically in figure 301 (right side). Bedrock-to-soil absolute losses occur in the sequence Si ≫ Al > K > Na > Fe > Ca > Mg ≫ Ti > Ba > Mn > Sr ≫ Rb, in close accordance with bedrock abundances. Absolute losses adjusted for atomic weight yield a slightly different sequence, Si ≫ Al > Na > K > Ca > Mg >

TABLE 16.—*Adamellite sample 94–bedrock chemical analysis and adjustment of < 2-mm-soil analysis for ash and local contamination by biotite and hornblende*

[All analytical data in weight percent, except as noted]

	Calculated percent change (fig. 305)	Assumed percent change	Percent in bedrock	Percent in soil	New soil value	Difference	Weighted average	Local component	Ash component	Original analysis	Corrections for ash	Corrections for local contaminants	Analysis corrections	Oxides	Recalculated to previous 13 element total	Corrected element values	Bedrock analysis
94 sand:																	
Biotite	−1.8	−30	6.7	8.2	4.7	−3.5											
Hornblende	+200	−40	.13	.42	.08	−.34											
94 silt:																	
Biotite	+170	−35	6.7	15	4.4	−10.6											
Hornblende	+1,050	−45	.13	7	.07	−6.93											
94 soil < 2 mm:																	
Biotite							−4.7	−4.4	−0.27								
Hornblende							−.97	−.97									
Si										31.13	−8.59	−0.94	21.60	46.21	65.66	30.70	31.72
Ti										.40	−.02	−.11	.27	.45	.64	.38	.28
Zr ppm										308	−24		284	384	546	404	198
Al										8.35	−1.62	−.39	6.34	11.98	17.02	9.01	8.75
Fe										3.75	−.26	−.75	2.74	3.92	5.57	3.90	2.89
Mn										.09	−.01	−.02	.06	.08	.12	.09	.09
Mg										.71	−.02	−.36	.33	.55	.78	.47	.66
Ca										1.29	−.10	−.11	1.08	1.51	2.15	1.54	1.67
Ba										.09	−.005		.085	.095	.135	.12	.13
Sr ppm										368	−1		367	434	617	522	624
Na										2.07	−.73	−.02	1.32	1.78	2.53	1.88	2.69
K										2.95	−.99	−.34	1.62	1.95	2.77	2.30	3.25
Rb ppm										62.3	−43		19.3	42.2	60.0	27.4	54.0

Fe ≫ Ti > Mn > Ba > Sr ≫ Rb. Percentage losses, the most significant indicator of chemical behavior during weathering, follow the sequence Rb $\overset{?}{>}$ Na ≈ K ≈ Mg > Sr > Mn ≈ Ca > Ba > Si > Al ≫ Fe > Ti. The placement of Rb within the latter sequence is somewhat uncertain owing to its low concentration in both bedrock and soil and to its susceptibility to contamination from biotite, feldspars, and glass.

Examination of figure 301 shows that percentage chemical losses generally follow the sequence alkali metals > alkaline earths > Si > Al > metals. Some notable differences in element mobility between the dolomite and adamellite are also evident. Greater absolute amounts of Sr, Fe, and Mn are lost from adamellite than from dolomite, whereas Ca, Mg, Sr, Mn, and Fe all undergo greater percentage losses from dolomite bedrock to less-than-2-mm soil than from adamellite bedrock to less-than-2-mm soil. The soluble dolomite obviously releases all its constituent elements more readily than they can be weathered from silicate and oxide phases in the plutonic rock.

The preceding interpretations are based on bedrock-to-soil changes recorded at only two sites, although mean dolomite soil gravel values and microprobe analyses of both dolomite and adamellite minerals give additional confidence to the patterns of chemical weathering. The extensive soil contamination rendered study of all other samples virtually meaningless. For confirmation of the chemical weathering sequences suggested by the limited data provided by bulk changes in the solid phases, it was necessary to examine the chemical composition of natural waters related to both dolomite and adamellite.

CHANGES IN THE LIQUID PHASE

Chemical weathering usually occurs only in the presence of a liquid phase which is undersaturated with respect to the altering phases. A considerable amount of information concerning processes and sequences of decomposition can be obtained from observations of progressive chemical changes in water as it passes from the form of precipitation into soil water and finally into ground water and springs. The following discussion considers the chemical nature of rain and snow water, soil water extracts, and spring waters related to both dolomite and adamellite, the saturation pH and exchangeable cations of the soils, and finally the significance of geochemical differences between the various fluids in terms of chemical weathering.

CHEMICAL COMPOSITION OF PRECIPITATION

Four rain samples and four snow samples, obtained during the period July 30, 1966, to June 29, 1967, were collected in plastic-lined pans and filtered through 0.45-μm filter membranes into airtight polyethylene containers. The analytical data[4] for these samples, together with mean values for Sierra Nevada snow, are given in table 17. The White Mountains samples tend to

[4]The procedures of Barnes (1964) were followed for field determination of pH and alkalinity for all water samples. All other chemical analyses of water were performed by the U.S. Geological Survey.

TABLE 17.—*Chemical analyses, in milligrams per liter except as noted, of precipitation collected near Crooked Creek Station and comparison with analyses of snow from the east slope of the Sierra Nevada*

[Mean for snow from Feth, Rogers, and Robinson (1964, p. 18–26)]

	Crooked Creek Station			Mean for snow, east slope of Sierra Nevada
	Mean[1] ± standard deviation	Maximum	Minimum	
Specific conductance μmhos	7 ±3	11	4	
K	.14 ±.10	.31	.06	.41
Na	.34 ±25	.90	.16	.43
Ca	.36±.12	.57	.23	.84
Mg	.9 ±.07	.22	.034	.19
Ba	<.5			
Mn	.003 ±.002	.006	.000	[2].00
Fe	.014 ±.010	.024	.000	[2].01
Al	.012 ±.011	.032	.001	[2].03
B	.01	.02	.00	[2].05
SiO_2	.11 ±.06	.2	.035	[2].17
HCO_3	2.7 ±1.3	4.3	1.2	3.59
NO_3	.2 ±.0	.2	.2	[2].07
SO_4	.06 ±.09	.2	.0	1.14
PO_4	.00 ±.00	.00	.00	[2].03
Cl	.4 ±.2	.7	.2	.47

[1]Mean for four rain and three snow samples.
[2]Value for entire Sierra Nevada.

TABLE 18.—*Chemical constituents in water saturation extracts of two groups of White Mountains soils*

[All analytical values other than pH are in milligrams per liter]

	Mean	Standard deviation	High	Low	Number of analyses
Reed Dolomite					
K	13	±8	43	5.5	23
Na	13	±4	24	7.1	23
Ca	100	±29	150	42	23
Mg	21	±6	33	7.0	23
PO_4	.0082	.0052	.0210	.0021	11
Na/K	1.00				
Ca/Mg	4.8				
Field pH	8.0				saturation paste
Laboratory pH	7.5				saturation paste
Adamellite of Sage Hen Flat					
K	22	±9	94	9.8	23
Na	14	±4	26	7.4	23
Ca	61	±22	110	28	23
Mg	10	±3	17	5.6	22
Fe	.24	±.10	.56	.12	20
Si	10.1	±1.3	14	8.0	21
PO_4	.0150	.0040	.0190	.0110	2
Na/K	.64				
Ca/Mg	6.1				
Field pH	6.8				saturation paste
Laboratory pH	7.0				saturation paste

have lower mean concentrations of most constituents, especially sulfate, than do the Sierra samples. Mn, Fe, Cl, and nitrate are comparable or slightly higher in the White Mountains.

CHEMICAL COMPOSITION OF SOIL WATER

Obtaining representative soil water samples is a considerable problem that has been approached from several angles. Lysimeters and other elaborate devices probably collect the most typical fluids, but they are often difficult to install and maintain and give no indication of geographical variation unless employed in large numbers. In the White Mountains, soils are either dry or frozen except for brief periods during spring snowmelt and after very heavy summer storms, making field collections difficult to obtain. For this study, water saturation pastes of 46 Reed Dolomite soils and adamellite soils of Sage Hen Flat were prepared, and after 1 hour water samples were vacuum-extracted by Buchner funnel in the laboratory. (See section "Supplemental Information" for methods). Saturation, rather than excess water mixtures, was chosen for initial soil moisture content in the belief that this would more closely reflect actual soil water conditions. Distilled water was used in all extractions, the assumption being that any differences between precipitation and distilled water, with regard to the analyzed species, would not be significant in comparison to the soil water concentrations.

Analyses of these extracts, summarized in table 18, indicate that standard deviations within a given soil type are often nearly as large as or larger than differences between soil types. Comparison between some chemical species of the two soil water groups, however, is still possible. The adamellite extracts are lower in Ca and Mg and apparently higher in K and phosphate than the Reed samples. Na is surprisingly low in the adamellite soil water extracts.

The large deviations in soil water composition, which exceed the standard deviations in total soil composition (compare table 19 with tables 12 and 15), imply considerable departures from equilibrium and steady state (rate of ion gains = rate of ion losses) conditions, perhaps accentuated by the relatively short duration of the extraction process. For this reason, soil water extractions may differ to some extent, primarily in degree of variability between sites but probably in ionic proportions as well, from meteoric water that has been in contact with the soil for several days or weeks during snowmelt or after heavy rains.

SOIL pH

Table 19 gives a compilation of field and laboratory pH data for Reed Dolomite soils and adamellite soils of Sage Hen Flat. These data, together with similar information from basalt and sandstone soils in the area, indicate that instrumental laboratory pH values and indicator-determined field pH values are comparable to pH's about 8.0, where the field methods begin to give consistently higher readings. A comparison of the figures for the two soil types shows the Reed soils to have values 0.5–1.5 pH units higher than the adamellite soils.

EXCHANGEABLE CATIONS

Amounts of total extractable soil cations (in milliequivalents per 100 grams of ovendry soil) were ob-

TABLE 19.—*Mean values for total exchangeable cations, percentage exchangeable cations, and pH in Reed Dolomite and adamellite soils of Sage Hen Flat*

	Mean	Standard deviation	Standard deviation (% of mean)	Number of samples
Reed Dolomite soils				
pH:				
Average mean field	8.0	0.1	1	25
Average maximum field	8.2	.1	1	25
Average minimum field	7.9	.01	5	25
Laboratory	7.5	.2	3	25
Exchangeable cations (me/100 g ovendry soil):				
K	.58	.30	52	25
Na	.27	.09	33	25
Ca	32.4	13.3	41	25
Mg	6.1	2.5	41	25
Percent of exchangeable cations:				
K	1.6	.9	56	21
Na	.73	.27	37	21
Ca	80.7	7.6	9	21
Mg	16.9	6.7	40	21
Adamellite soils				
pH:				
Average mean field	6.8	0.5	8	22
Average maximum field	7.6	.6	8	22
Average minimum field	6.2	.5	7	22
Laboratory	7.0	.4	5	22
Exchangeable cations (me/100 g ovendry soil):				
K	.33	.13	40	22
Na	.07	.05	69	22
Ca	7.7	2.5	31	22
Mg	1.09	.34	31	22
Percent of exchangeable cations:				
K	3.8	1.8	47	21
Na	.70	.25	33	21
Ca	83.2	4.2	5	21
Mg	12.2	3.3	27	21

tained by repetitive leaching with 1.0 N NH_4Ac at pH=7.0. (See "Supplemental Information" for details.) Values for exchangeable cations (table 19) were calculated from the total extractable and water-soluble cations as follows:

Exchangeable cations=total (NH_4Ac) extractable cations—cations in water saturation extracts (all values in milliequivalents per 100 grams of dry soil).

The exchangeable cations were then recalculated to 100 percent (table 19). The adamellite soils are much lower than Reed soils in amounts of all exchangeable cations; they are higher in percentage exchangeable K, slightly higher in percentage Ca, comparable in Na percentage, and somewhat lower in percentage Mg.

CHEMICAL COMPOSITION OF SPRING WATERS

Water samples from four springs related to Reed Dolomite and adamellite of Sage Hen Flat were collected during the summer and fall of 1966 and during the summer of 1967. Water samples were filtered through 0.45-μm filters into airtight polyethylene containers. The samples were usually collected near sunrise or sunset to minimize air-water temperature differences, which would affect pH measurements. A part of each sample collected during the summer of 1967 was acidified to pH 2 to prevent precipitation of metals and was used for analysis of Al, Fe, and Mn. Al values are markedly higher for the 1967 samples, reflecting either precipitation of Al in previously collected samples or solution of particles less than 0.45 μm in the acidified parts. There was relatively good agreement of Fe and Al values in the 1967 samples with those reported for granitic waters in the Sierra Nevada by Feth, Roberson, and Polzer (1964). Changes caused by orifice location, diurnal variation, and seasonal fluctuation at a given spring were found to be negligible compared with differences between springs.

WATERS RELATED IN PART TO THE REED DOLOMITE

Poison Creek Spring emerges from the east side of a canyon wall about 400 feet east of the Wyman-Reed contact, which dips about 60° westward at this location. The spring water would appear to be chemically controlled in large part by the dolomite, which crops out continuously for several miles west of the Wyman contact, but the water is also influenced to a lesser degree by the sandstones, shales, and limestones near the orifice. Waters emerge from three orifices (herein designated A, B, and C, from south to north) about 15 feet apart. Discharge from orifice C, the major outlet, averages about 0.1 cfs (cubic feet per second), as measured with a Pygmy current meter.

Cottonwood Spring, the principal source of the south fork of Cottonwood Creek, is in a valley that partially separates the Reed Dolomite from the Cottonwood pluton. The orifice lies within the Reed, though, and the apparent catchment basin is dominated by dolomite. Discharge is quite constant at about 1.8–2.0 cfs.

Analytical data for these two sampling locations are summarized in table 20. The predominant ions are Ca,

TABLE 20.—*Field and laboratory analytical data for two natural waters associated in part with the Reed Dolomite*

[All concentrations in milligram per liter]

	Poison Creek Spring		Cottonwood Spring	
	Mean	Standard deviation	Mean	Standard deviation
Field pH	7.71	0.14	7.72	0.27
Specific conductance K	[1]286		[1]252	
K^+	.99	.03	.81	.01
Na^+	3.35	.09	1.54	.07
Ca^{++}	29	2	24	1
Mg^{++}	14.9	.3	15.9	.1
Ba^{++}	[1]<.5		[1]<.5	
Mn	[1].002		[1].004	
Fe	[1].001		[1].043	
Al	[1].019		[1].013	
SiO_2	13	.5	9.0	.2
B	[1].02		[1].01	
Cl^-	[1].8		[1].6	
Field HCO_3^-	175	7	162	4
NO_3^-	[1].3		[1].3	
SO_4^{-2}	7.8	.7	3.1	.1
PO_4^{-3}	[1].00		[1].12	
Water temperature (°C)	5.8	.3	6.9	1.0
Cation epm	2.84		2.59	
Anion epm	3.06		2.75	
Number of analyses	7		6	

[1]Based on one analysis.

Mg, and bicarbonate; Na and sulfate are quite low. Poison Creek Spring shows the influence of the Wyman beds in its increased Na, K, Si, and sulfate with respect to the Cottonwood samples, and its higher Ca/Mg ratio reflects the presence of limestones near the orifice. The pH of Poison Creek is the same as that of Cottonwood Spring, however, and in most respects the waters of the two springs are similar.

Waters Related Largely to the Adamellite of Sage Hen Flat

Sage Hen Spring and Crooked Creek Spring appear to be almost entirely related to the Sage Hen Flat pluton. Formations adjacent to the adamellites, such as the Wyman Formation, Reed Dolomite, Deep Spring Formation, or Campito Formation could have some slight effect on the chemical composition of these waters. Discharge at Sage Hen Spring is about 0.1 cfs, but fluctuates appreciably. Discharge at Crooked Creek Spring is even smaller, its mean about 0.05 cfs or less.

Analytical data for the two sampling sites related to the adamellite are given in table 21. Crooked Creek Spring has a higher pH than Sage Hen Spring and contains less Mg and slightly less Na. The fact that the two waters, draining the same plutonic body, can be consistently distinguished chemically is an indication of the sensitivity of natural water to variation in bedrock composition and weathering conditions. The adamellite-derived spring waters, however, are virtually identical in most other respects and contrast sharply with those related to dolomite. Waters draining the adamellite are much higher in Na, sulfate, and chloride than are the dolomite waters and much lower in Ca, Mg, and bicarbonate. The pH values of the four spring waters are almost the same except for Crooked Creek Spring, which is more alkaline than either of the springs related to the dolomite.

TABLE 21.—*Field and laboratory analytical data for two natural waters associated with the adamellite of Sage Hen Flat*

[All concentrations in milligrams per liter]

	Crooked Creek Spring		Sage Hen Spring	
	Mean	Standard deviation	Mean	Standard deviation
Field pH	7.96	0.15	7.72	0.11
Specific conductance K	[1]129		[1]127	
K^+	.79	.05	.64	.02
Na^+	6.23	.19	6.56	.16
Ca^{++}	17	1	16	.5
Mg^{++}	.93	.08	1.55	.08
Ba^{++}	[2]<.5		[2]<.5	
Mn	[1].014		[1].000	
Fe	[1].02		[1].019	
Al	[1].014		[1].033	
SiO_2	15.4	.8	16.4	.5
B	[1].015		[1].01	
Cl	[1].9		[1].85	
Field HCO_3^-	61	3	60	1
NO_3^-	[1]3.3		[1].8	
SO_4^{-2}	9.8	.5	9.4	1.1
PO_4^{-3}	[1].145		[1].11	
Water temperature (°C)	5.6	.1	6.5	.1
Cation (epm)	1.22		1.24	
Anion (epm)	1.29		1.22	
Number of analyses	13		7	

[1]Based on two analyses.
[2]Based on one analysis.

Analysis of Chemical Changes

For purposes of analysis and interpretation, the chemical data for natural waters related to both dolomite and adamellite are viewed in the following discussion from three perspectives: (1) Relative mobilities, showing the degree to which the various chemical species are mobilized from bedrock by weathering and released into solution, (2) stability with respect to some important solid and gas phases, including a discussion of water chemistry in relation to several equilibrium reactions, and (3) a chemical comparison of soil water with precipitation and spring waters.

Relative Mobilities

A common means of evaluating the ease with which various chemical constituents are released by weathering from bedrock to ground water is through the calculation of relative mobility:

$$\text{Relative mobility (element X)} = \frac{\text{Percent X of N-element total in water}}{\text{Percent X of N-element total in bedrock}}$$

where N is the number of elements considered. This computation assumes that a given water can be definitely correlated with a given lithology, that the mean analytical values for that lithology are representative, and that the composition of the water with regard to the investigated constituents is entirely a function of contact with the bedrock material. It is likely that the waters sampled in the White Mountains have been affected to some extent by windblown contaminants and the rhyolitic ash, but evidence presented here (see "Relationship of Soil Water to Precipitation and Spring Waters") suggests that major influences on ground-water composition occur after percolation through the soil.

Relative mobilities calculated for Cottonwood Spring with respect to dolomite bedrock (table 22) fall into the sequence Mg > Ca ≫ Fe > Mn. Mobilities of other elements, for example, Si, Al, Ti, Na, and K, are more susceptible to influence by weathering of contaminants than of the bedrock, which contains only trace amounts of these constituents. Interpretation is therefore confined to the carbonate-component elements. The relative mobility sequence of table 22 agrees well with the order of percentage losses from dolomite bedrock to soil (cf. fig. 301), except that the mobility of Fe in dolomite is clearly greater than that of Mn, a relation not evident from solid-phase considerations.

In figure 306, ranges of relative mobilities for eight elements, based on analytical means and standard de-

TABLE 22.—*Relative mobilities for four elements in Cottonwood Spring waters*

	Mg	Ca	Fe	Mn
Concentration in bedrock, percent	12.46	21.52	0.26	0.055
Concentration in Cottonwood Spring water, mg/l	15.9	24	.043	.004
Percent of four-element total (bedrock)	36.33	62.75	.76	.16
Percent of four-element total (spring)	39.79	60.08	.108	.010
Relative mobility	1.095	.957	.142	.063

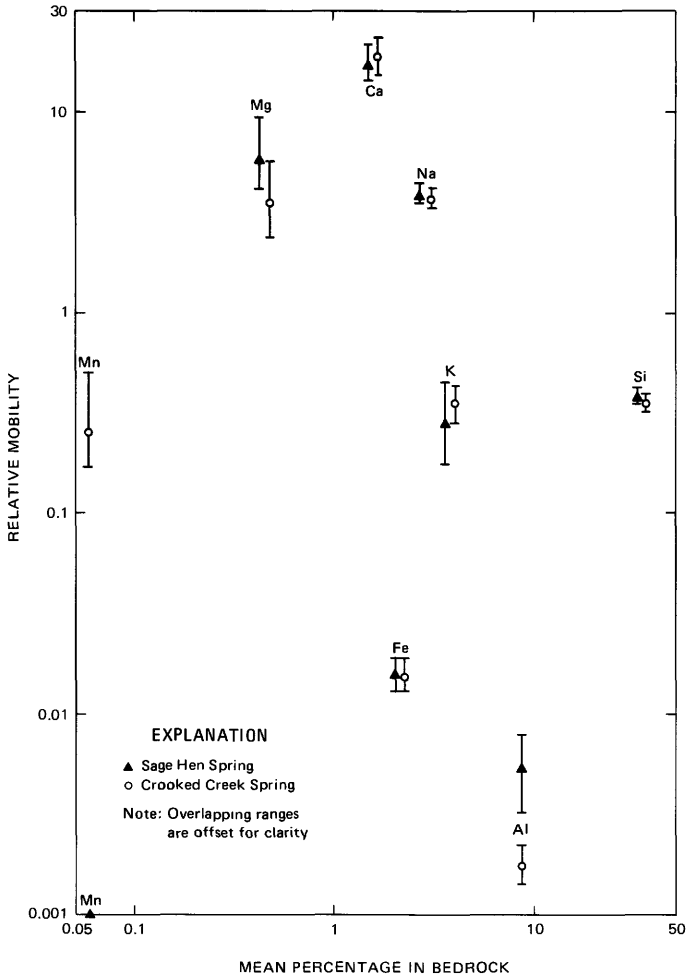

FIGURE 306—Relative mobilities for eight elements in spring waters related to adamellite. Vertical bars indicate ranges of values.

viations at Crooked Creek Spring and Sage Hen Spring, are plotted against mean bedrock percentage on a log-log scale. The horizontal scale serves to emphasize the importance of the various constituents with regard to bedrock weathering and to their net contribution to the ground water. Elements plotting in the upper right of the diagram (Ca, Na, and Si in this case) are mobile constituents present in appreciable quantities in the bedrock and will be liberated in relatively large total amounts to the ground water. Elements that plot toward the lower left (such as Mn) are comparatively immobile, are not abundant in the adamellite, and are therefore released to the ground water in trace amounts.

The apparent sequence of mobilities for the adamellite-draining springs is Ca > Mg ≈ Na ≫ Si ≈ K ≥ Mn ≈ Fe > Al. Values for Mn, and to some extent for Mg, vary considerably between the two springs, making the placement of these elements within the order somewhat uncertain. The results as a whole are in good agreement with those of Feth, Roberson, and Polzer (1964) for quartz monzonite (adamellite) terrane in the Sierra Nevada and are generally similar to losses from bedrock to soil (table 14; fig. 301). The relative positions of Ca, Mg, and Na in the weathering sequence differ, however, between the solid phase and liquid phase perspectives. Considering the problems of soil contamination, one possibility is that carbonate grains may be continually blown into adamellite soils and quickly dissolved, resulting in increased Ca and Mg concentrations in waters draining the pluton. Only a few carbonate fragments were observed in adamellite soils; however, soluble grains (especially those reactive fragments of silt or clay size) would not be expected to persist in nonsoluble soils, and both dolomite and calcite were found in dust trap residues collected within the area (Marchand, 1970). Ruhe (1967, p. 57–59) suggested solution of windblown contaminants to explain the formation of thick caliche horizons in soils formed on low-Ca parent materials in New Mexico.

STABILITY WITH RESPECT TO SOLID AND GAS PHASES[5]

By using means and standard deviations for ion concentrations, pH, and temperature from Cottonwood Spring and Poison Creek Spring, maximum, minimum, and most probable values of ion-activity products (IAP) were calculated for both calcite and dolomite as follows:

$$IAP_c = \left[{}^{a}Ca^{++}\right]\left[{}^{a}CO_3^{-2}\right]$$

and

$$IAP_d = \left[{}^{a}Ca^{++}\right]\left[{}^{a}Mg^{++}\right]\left[{}^{a}CO_3^{-2}\right]^2,$$

where [a] is the ionic activity of the solutions (approximately equal to concentration). A comparison of the spring waters with regard to carbonate equilibria is presented in table 23. All waters are undersaturated with regard to both calcite and dolomite, yet minor amounts of calcium carbonate have precipitated on exposed rocks near all the springs sampled. Calcite lacks saturation by a factor of about 2.5–10 in the dolomite-

[5]Sources for physical constants used in calculations:
K_1 first carbonic acid dissociation; Harned and Davis (1943, p. 2030).
K_2 second carbonic acid dissociation; Harned and Scholes (1941, p. 1708).
KCO_2 graphical solution, using data of Markham and Kobe (1941, p. 449).
A first constant, Debye-Huckel equation; Manov, Bates, Hamer, and Acree (1943, p. 1765).
Kc calcite equilibrium constant; Larson and Buswell (1942, p. 1667).
Kd dolomite equilibrium constant; (Hsu, 1964).

TABLE 23.—*Degree of saturation with respect to calcite and dolomite for four spring waters*

[Ranges of values reflect temperature and compositional extremes. M.P. = most probable value; IAP = ion-activity product]

	Cottonwood Spring	Poison Creek Spring	Crooked Creek Spring	Sage Hen Spring
IAPc:				
Maximum	2.83×10^{-9}	2.51×10^{-9}		
M.P.	1.37×10^{-9}	1.67×10^{-9}	0.746×10^{-9}	0.401×10^{-9}
Minimum	$.682\times10^{-9}$	$.672\times10^{-9}$		
Kc[1]:				
Maximum	7.44×10^{-9}	7.92×10^{-9}		
M.P.	7.69×10^{-9}	7.98×10^{-9}	8.02×10^{-9}	7.79×10^{-9}
Minimum	7.92×10^{-9}	8.02×10^{-9}		
IAPc/Kc:				
Maximum	.381	.317		
M.P.	.178	.209	.093	.052
Minimum	.086	.083		
IAPd:				
Maximum	8.38×10^{-18}	5.09×10^{-18}		
M.P.	2.03×10^{-18}	2.34×10^{-18}	4.99×10^{-20}	2.56×10^{-20}
Minimum	$.528\times10^{-18}$	$.401\times10^{-18}$		
Kd[2]	2.0×10^{-17}	2.0×10^{-17}	2.0×10^{-17}	2.0×10^{-17}
IAPd/Kd:				
Maximum	.419	.254		
M.P.	.103	.117	2.5×10^{-3}	1.28×10^{-3}
Minimum	.026	.020		

[1]From Larson and Buswell (1942, p. 1667).
[2]From Hsu (1964).

TABLE 24.—*Partial pressures of carbon dioxide in four spring waters and a comparison with atmospheric PCO_2*

[M.P. = most probable value]

	Cottonwood Spring	Poison Creek Spring	Crooked Creek Spring	Sage Hen Spring
PCO_2 of water (atm):				
Maximum	5.05×10^{-3}	4.10×10^{-3}		
M.P.	2.66×10^{-3}	2.86×10^{-3}	5.70×10^{-4}	9.79×10^{-4}
Minimum	1.44×10^{-3}	1.98×10^{-3}		
PCO_2 of atmosphere—atm	2.3×10^{-4}	2.3×10^{-4}	2.3×10^{-4}	2.3×10^{-4}
PCO_2(w)/PCO_2(a):				
Maximum	22	18		
M.P.	12	12	2.5	4.2
Minimum	6.3	8.6		

draining waters and by more than 10 in adamellite-derived waters. Cottonwood Spring and Poison Creek Spring are also much closer to dolomite saturation than are their counterparts in the pluton, but all waters are even more undersaturated with respect to dolomite than to calcite.

The undersaturation of calcium carbonate in the Crooked Creek and Cottonwood drainage basins contrasts with the fourfold supersaturation reported by Barnes (1965, p. 92) in the headwater springs of Birch Creek, just south of the study area. The latter drains a mixed terrane in which solution of Wyman limestones, as well as the Reed Dolomite, may have a profound influence on the state of the ground-water calcite reaction.

Partial pressures of carbon dioxide in the four spring waters (table 24) were computed from the following relation:

$$PCO_2(aq)=\frac{(H+)(HCO_3-)}{K_1KCO_2}$$

where

$$K_1=\frac{(H+)(HCO_3-)}{(H_2CO_3)}$$

and

$$KCO_2=\frac{(H_2CO_3)}{PCO_2}.$$

All calculated values for the waters are at least twice that of the atmosphere, and Cottonwood Spring shows CO_2 partial pressures as much as 22 times greater than the air. The two springs related to the dolomite terrain have partial pressures much greater than the springs in the adamellite, yet the pH of all springs is similar. Solution of dolomite would tend to increase PCO_2 but would also increase pH, the net effect being to decrease free CO_2. The explanation for the striking contrast between the two groups of springs must partly lie in the marked vegetational differences between the two lithologies: The adamellites are dominated by relatively dense growth of sagebrush, limber pine, grasses, and perennials, whereas bristlecone pine and sparse low perennials cover most of the Reed terrane. Perhaps photosynthetic rates, and hence root respiration, differ greatly between the two plant communities. In any event, it is apparent that local vegetational changes may play an important role in controlling the pH of ground water and hence in regulating rates of chemical degradation.

For the adamellite-draining springs and adamellite soil water, means and standard deviations were used to compute molalities and activities for Na+, K+, H+, and H_4SiO_4 and to plot the range of each fluid on low-temperature stability diagrams for Na silicates (fig. 307) and K silicates (fig. 308). Plots based on activities did not differ significantly from those based on molality and are not reproduced on the diagrams. Sage Hen Flat pluton water plots within the kaolinite field in both figures, as do most stream and spring waters. The position of the water plots, toward the silica-rich side of the kaolinite field and away from the gibbsite field, tends to support the X-ray diffraction and microprobe evidence that kaolinite is forming as a stable authigenic phase in the adamellite soils. The waters are well above quartz saturation, probably owing to the weathering of Si from feldspars, biotite, and other silicates, in addition to quartz, but are significantly below saturation with amorphous silica.

Major departures from equilibrium are evidenced in adamellite-related waters by oversaturation with respect to quartz and undersaturation with respect to colloidal silica and in waters draining the Reed by undersaturation with regard to dolomite. Such departures, however, do not preclude the existence of steady-state conditions in the spring waters.

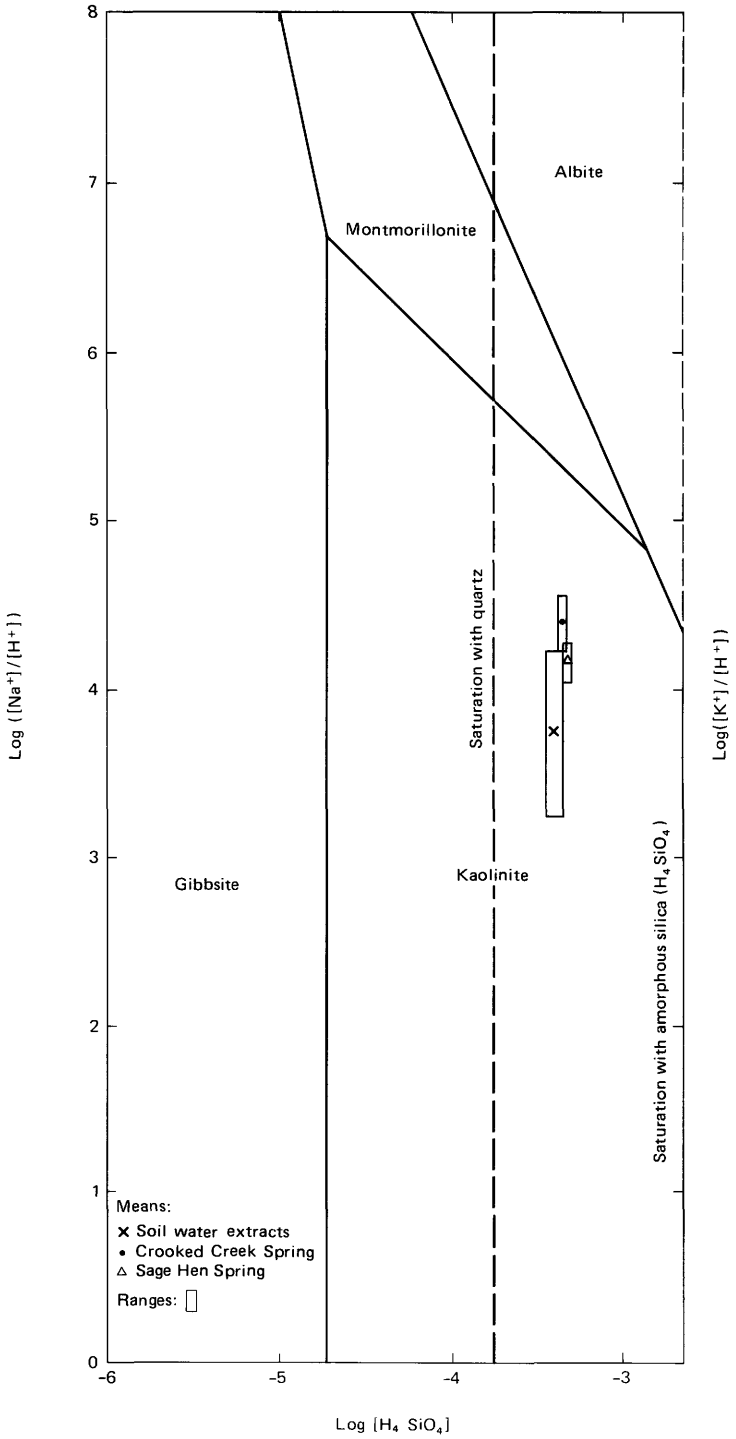

FIGURE 307.—Stability relations of phases in the system Na_2O-Al_2O_3-SiO_2-H_2O at 25°C and 1 atmosphere total pressure as functions of $(Na^+)/(H^+)$ and (H_4SiO_4). After Feth, Roberson, and Polzer (1964, p. 65).

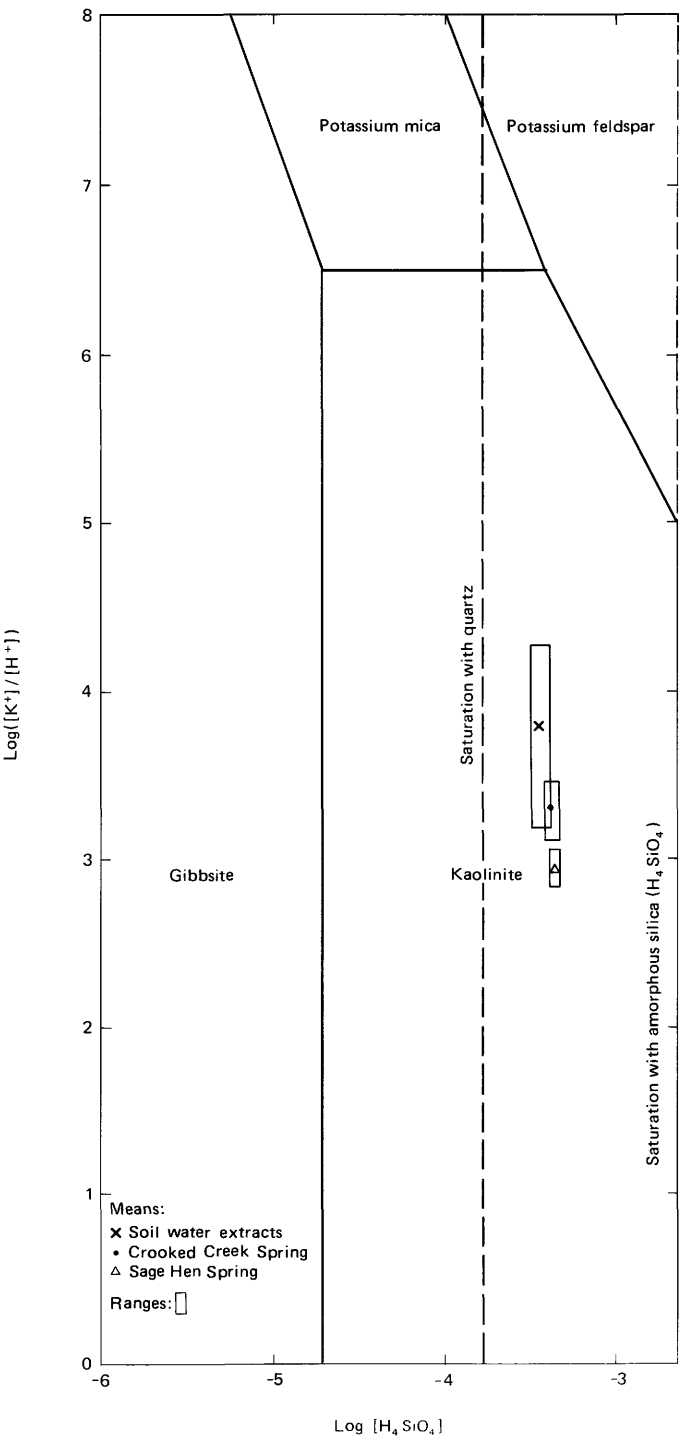

FIGURE 308.—Stability relations of phases in the system K_2O-Al_2O_3-SiO_2-H_2O at 25°C and 1 atmosphere total pressure as functions of $(K+)/(H^+)$ and (H_4SiO_4). After Garrels and Christ (1965, p. 361).

RELATION OF SOIL WATER TO PRECIPITATION AND SPRING WATERS

An important question in the chemistry of natural waters is the space-time dimension of chemical weathering changes. Do most of the chemical additions to rain and snow water occur quickly within the soil, or does the composition of percolating ground waters continue to change, even if the lithology remains the same? Although absolute concentrations of chemical species in the soil water extracts are much higher than those in precipitation and spring water, comparisons are possible through ratios of dissolved constituents.

Figure 309 compares the composition of waters related to the Reed Dolomite in the ternary system Na + K − Ca− Mg.[6] The dolomite soil water extracts are more or less intermediate in composition between precipitation and spring water values, but somewhat higher in percentage Ca than either of the other fluids. A progressive increase in the divalent/monovalent cation ratio occurs from precipitation to soil water to springs. The Ca/Mg ratio increases slightly from about 1.8 in precipitation to a value of nearly 5 (the ratio in bedrock is about 1.6) in soil water, but then decreases substantially from soil water to spring water. This decrease may be in response not only to bedrock composition, but to selective adsorption and removal of Ca by the soil exchange complex. The fact that the spring waters do not plot closer to the bedrock is probably attributable to the weathering of ash and local soil contaminants and to differing relative mobilities of the plotted cations.

Waters related to the adamellite are compared for the same ternary system in figure 310 (bottom). Soil water plots over a wide range and shows a definite increase in Ca/Na + K and Ca/Mg with respect to both precipitation and bedrock. It appears to be closer in composition to spring water than precipitation in terms of Ca concentration. The hydrolysis of plagioclase, solution of secondary calcium carbonate in the soil, and the high mobility of Ca is probably responsible for this trend, which proceeds away from bedrock composition. Also in figure 310 (top), it appears that the Na/K ratio in the soil water extracts has decreased relative to precipitation in response to bedrock and perhaps ash composition. The large increase in Na/K from soil water to ground water is interpreted as the result of K fixation by colloidal adsorption and selective plant uptake, and of high Na mobility. Soil water has a Na/K ratio much closer to precipitation than to spring water, but is quite distinct from both.

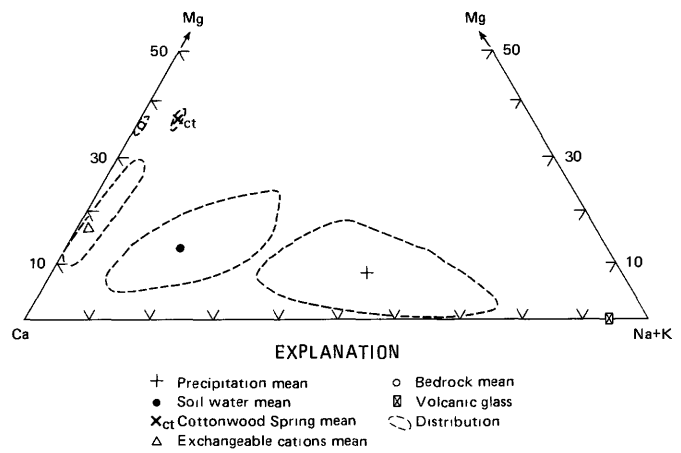

FIGURE 309.—Progressive cation changes from precipitation water to soil and spring waters related to Reed Dolomite. Plots of bedrock, volcanic glass, and exchangeable cations suggest relative influence of these factors.

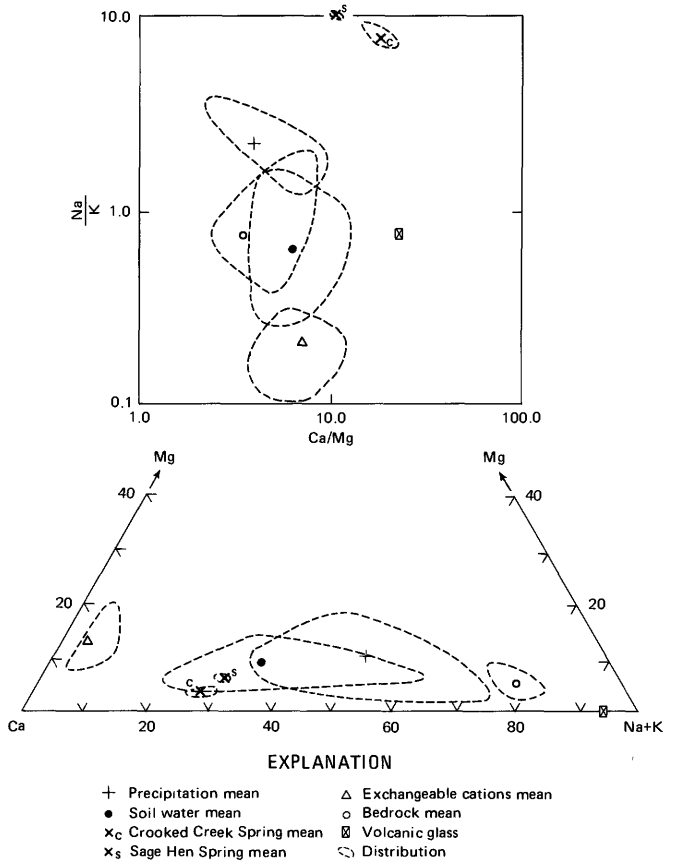

FIGURE 310.—Progressive cation changes from precipitation water to soil and spring waters related to adamellite.

Figure 311 shows regular increases in both Mg/Fe and Ca/Fe from precipitation to soil water to spring water, with soil water plotting approximately intermediate in position between the other two fluids. Both trends are away from bedrock composition and apparently result from low Fe mobility due to precipitation of Fe oxides within the soil.

From precipitation water to soil water to ground water, increases are evident in Si relative to Na+K and Mg+Fe (fig. 312), presumably in response to bedrock composition and possibly also to the rhyolitic ash. Soil water extracts on this diagram plot much closer to precipitation than to spring waters.

The pH value is probably the best single indicator of water chemistry. The median pH of snow samples from the Sierra Nevada is reported as 5.8, close to the value for pure water in equilibrium with atmospheric carbon dioxide (Feth, Rogers, Roberson, 1964, p. 24-25). All soil and ground waters in the White Mountains have much

[6]Values plotted on compositional diagrams in this paper were calculated on a parts per million (milligrams per liter) rather than an equivalents per million basis because the oxidation states of Fe and Mn were not known and a uniform basis between diagrams was desired.

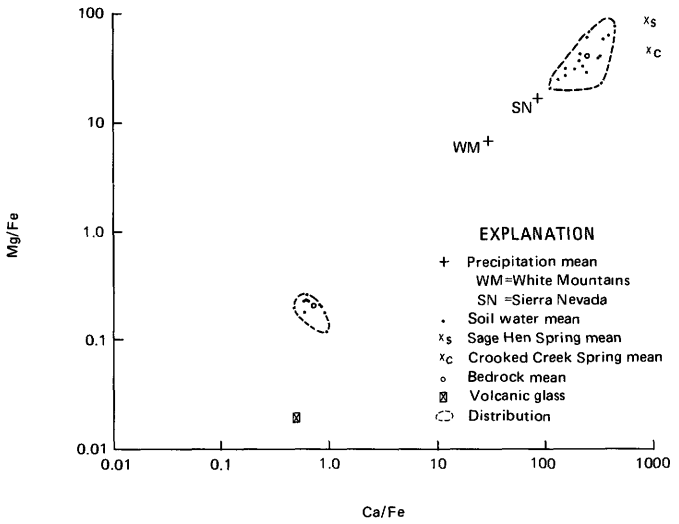

FIGURE 311.—Mg/Fe and Ca/Fe ratio comparisons of waters related to adamellite.

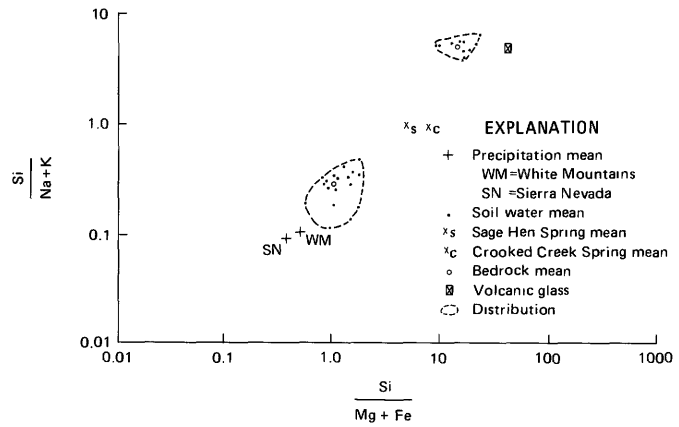

FIGURE 312.—Silica-cation ratio comparisons of adamellite-related waters.

higher pH's (tables 18, 20, 21) than this figure, owing principally to solution and hydrolysis reactions. For the dolomites, soil saturation pH is comparable to spring water pH, but for the adamellite, soil saturation values are intermediate between the pH of precipitation and that of the springs.

Most of the chemical trends just described appear to be controlled by bedrock composition or relative mobility, but the ground waters plot in tight groups distinct from the bedrock, suggesting that a steady-state condition, rather than chemical equilibrium, exists in spring waters that have passed through both lithologies. In the soils, absence of both equilibrium and steady state is manifested by the scatter of soil water points on the compositional diagrams.

Soil water extracts from both dolomite and adamellite terrain are notably distinct in composition from precipitation and spring waters draining the respective lithologies. Total concentrations are much greater in soil saturation extracts than in spring waters owing to the diluting effects of percolating precipitation water on the latter. The contrasting ionic composition of these two groups of fluids imply the existence of weathering reactions at considerable depth and preferential channeling of ground-water flow from certain localized areas of high recharge and possibly of different lithology. Most of the soil water extracts plot in an intermediate position between precipitation and ground water, but some (Na/K for adamellite-related water, for example) soil water plots do not fall in a position between the other two fluids. The pH of dolomite soil water extracts is much closer to spring water than to precipitation, however, suggesting that chemical adjustments in systems having soluble phases occur more rapidly than in those involving silicate or oxide phases.

Precipitation of calcium carbonate, probably sporadic in response to wet and dry seasons, and the contaminating influence of the rhyolitic ash, local aeolian debris, and foreign waters complicate the interpretation of soil water compositions. Also, the preceding conclusions assume that saturation extracts approximate actual soil water, an assumption which may not be entirely valid. A longer period of water contact with the soil might be expected to shift soil water composition closer to that of spring waters and to decrease the variability of extract compositions. A need exists for methods of soil water extraction which will produce fluids clearly representative of the actual soil solution under field conditions.

CHEMICAL FRACTIONATION IN THE BEDROCK-SOIL-WATER-PLANT SYSTEM

Elements released by solution or hydrolysis of mineral grains follow a variety of courses. They may dissolve in the soil water and be flushed out of the system, precipitate as a solid soil phase, become adsorbed on colloidal soil particles, or be utilized by organisms, especially vegetation. Chemical analyses of representative plants from the area, together with data already presented, make possible the location and apportionment of a number of chemical species within the bedrock-soil-water-plant systems of the Reed Dolomite and the adamellite of Sage Hen Flat.

Soil water and exchangeable cation concentrations were converted from milliequivalents per 100 g of soil to grams per cubic centimeter of soil, using milliequivalent weights and mean bulk densities of the total soil. Since the laboratory data apply to only the less-than-2-mm fraction, two sets of figures were calculated for the soil water, one assuming no contributions from the soil gravel fraction (minimum) and a second assuming a contribution from the coarse material proportional to its weight percentage of the whole soil (maximum).

For practical reasons, only a few of the hundreds of

White Mountains plant species could be analyzed. Aboveground parts of sagebrush (*Artemisia arbuscula*), junegrass (*Koeleria cristata*), and sandwort (*Arenaria kingii*), and twigs, needles, and cones of bristlecone pine (*Pinus aristata*) and limber pine (*P. flexilis*) were collected on both dolomite and adamellite. Aboveground parts of flax (*Linum perenne*) were obtained from dolomite terrain. These six species were chosen to represent vegetational groups as follows: *Pinus aristata* and *P. flexilis*—trees; *Artemisia arbuscula*—sagebrush and shrubs; *Koeleria cristata*—grasses; *Arenaria kingii*—noncarbonate-associated herbs; and *Linum perenne*— carbonate-associated herbs. Plant samples were washed with distilled water and ovendried at 104°C prior to ash analysis (table 25; see section "Supplemental Information" for analytical procedures.)

Percentage cover for the preceding groups, estimated at about 20 randomly selected sites on each lithology and then averaged for dolomite and for adamellite, is given in column 12 of table 25. These figures are recalculated to 100 percent in the last column. The percentages of total vegetation (in terms of cover) were then used to obtain weighted averages for each element in plants on each substrate, as follows:

Weighted average Si=(percent Si in species ×) (percent × in total vegetation) + (percent Si in species y) (percent y in total vegetation) + . . . + (percent Si in species N) (percent N in total vegetation),

where N is the total number of species considered. Vegetational concentrations from table 25 were adjusted to a grams per cubic centimeter basis using the weight and percent cover of each plant sampled (giving grams per square centimeter) and dividing by the mean depth of each soil type (giving grams per cubic centimeter of soil). Calculations were made for the individual species and for the weighted averages applicable to each soil type. Since these averages assume continuous vegetative cover, a second pair of weighted averages were computed, adjusting for the actual plant cover. Plots of total soil (uncorrected for contamination), exchangeable cation, soil water, and plant concentrations for adamellite and dolomite terrane are shown in figure 313. The adamellite comparisons, expressed on a percentage basis, are extended to precipitation, bedrock, and spring waters in figure 314. Vegetational concentrations are computed as percentage of soil water plus plant concentration in table 26.

An examination of element totals in figure 313 indicates that constituents released by weathering are concentrated primarily in exchangeable positions (cations only) and secondarily in soil water and plants. Exchangeable cations are adsorbed in the sequence Ca > Mg > K > Na. Cation exchange in soils therefore tends to decrease the Ca/Mg and K/Na ratios with respect to ratios of cations initially made available by weathering. Cation exchange is less important as a fractionation mechanism than these illustrations would imply, because after the exchange complex becomes saturated, no further removal by exchange can occur unless the exchange capacity increases.

Although trends vary to some extent between species, the overall tendency of the White Mountains flora, with respect to soil water (table 26), is to withdraw elements in the sequence P > Fe ≫ K > Ca ≅ Mg > Si ≫ Na. The ratio of plant concentration to soil water concentration is less for the dolomite, but the sequence is the same regardless of lithology. As the result of plant uptake, the soil K/Na ratio is further decreased, and Fe and P are extracted in relatively large quantities. Si is sufficiently soluble at the moderate to high pH's of the adamellite and dolomite soils to become concentrated in the liquid phase, although plant concentrations consti-

TABLE 25.—*Chemical composition (dry weight percentage basis) of some major plant species on Reed Dolomite and adamellite of Sage Hen Flat and weighted averages used for geochemical comparisons*

	Si	Al	Fe	Mn	Mg	Ca	Na	K	P	Number of plants	Number of duplicate analyses	Mean percent cover (see text)	Percent of total vegetation (see text)
Dolomite:													
Pinus aristata	0.0080	0.073	0.015	0.0016	0.17	0.58	0.0053	0.20	0.0480	2	1	17.60	64.9
Pinus flexilis	.0140	.071	.013	.0061	.09	.57	.0133	.23	.0630	1	1	.77	2.8
Artemisia arbuscula	.0300	.60	.062	.0063	.23	.71	.0081	.77	.0874	3	3	1.45	5.4
Koeleria cristata	.0980	.82	.10	.0165	.26	.81	.0066	.27	.0560	3	1	2.74	10.1
Arenaria kingii	.0760	1.1	.108	.0100	.47	3.39	.0219	.69	.0530	4	1	2.43	9.0
Linum perenne	.0549	.42	.040	.0102	.26	.85	.0034	.82	.0745	6	1	2.11	7.8
Weighted average	.0282	.29	.036	.0049	.21	.88	.0072	.33	.0539			(27.10)	(100.0)
Adamellite:													
Pinus aristata	.0120	.051	.010	.0049	.08	.55	.0078	.31	.0690	1	1	.05	.2
Pinus flexilis	.0120	.034	.0068	.0044	.08	.44	.0083	.45	.1100	1	1	2.61	9.6
Artemisia arbuscula	.0600	1.07	.147	.0131	.13	.57	.0118	.80	.0829	4	4	9.85	36.0
Koeleria cristata	.0300	.47	.064	.0064	.09	.34	.0058	.27	.0385	2	1	6.47	23.7
Arenaria kingii	.1200	5.5	.43	.0267	.33	2.52	.0353	.92	.0555	2	1	8.32	30.5
Weighted average	.0665	2.18	.20	.0148	.18	1.10	.0172	.68	.0666			(27.30)	(100.0)

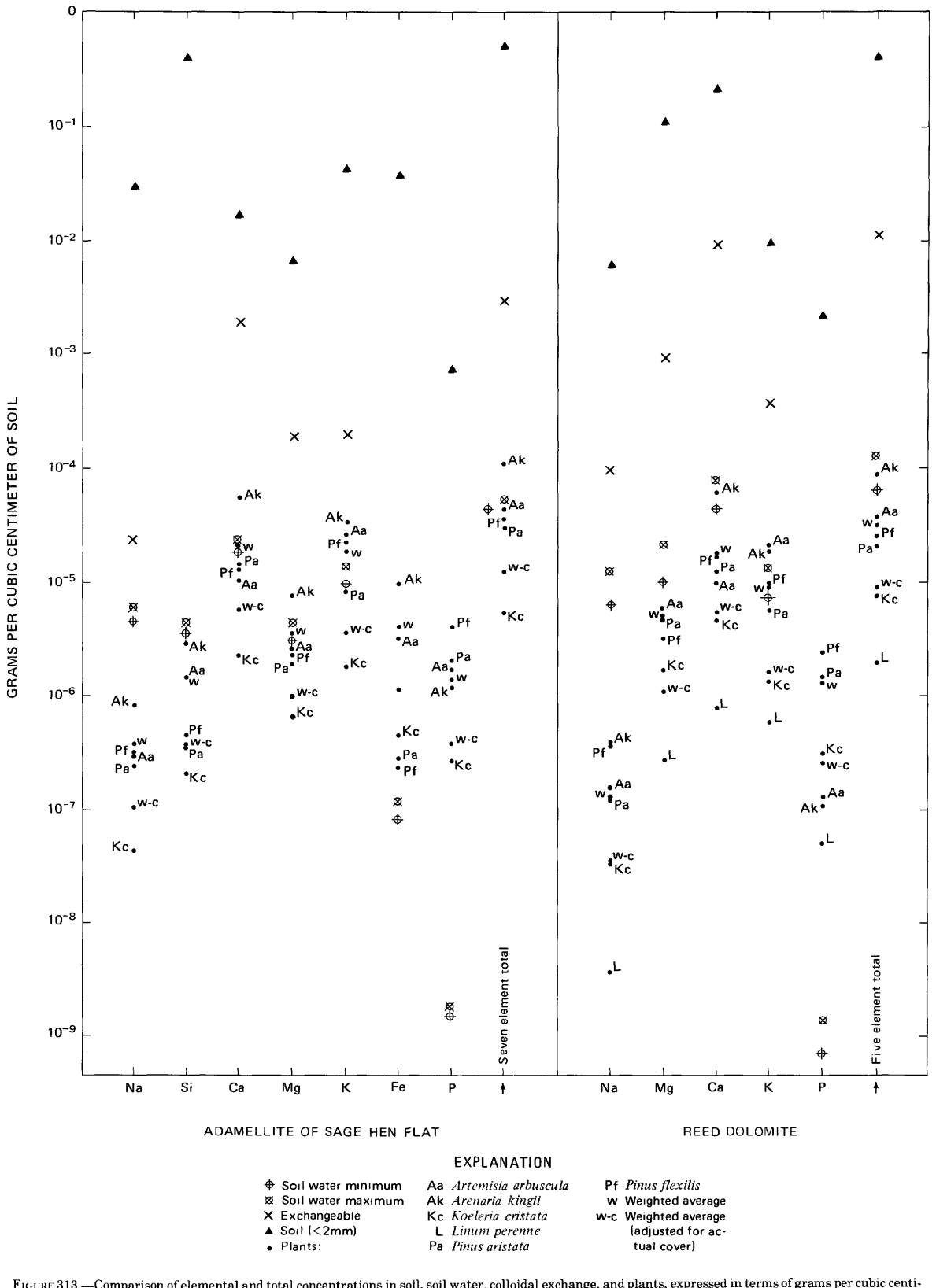

FIGURE 313.—Comparison of elemental and total concentrations in soil, soil water, colloidal exchange, and plants, expressed in terms of grams per cubic centimeter of soil.

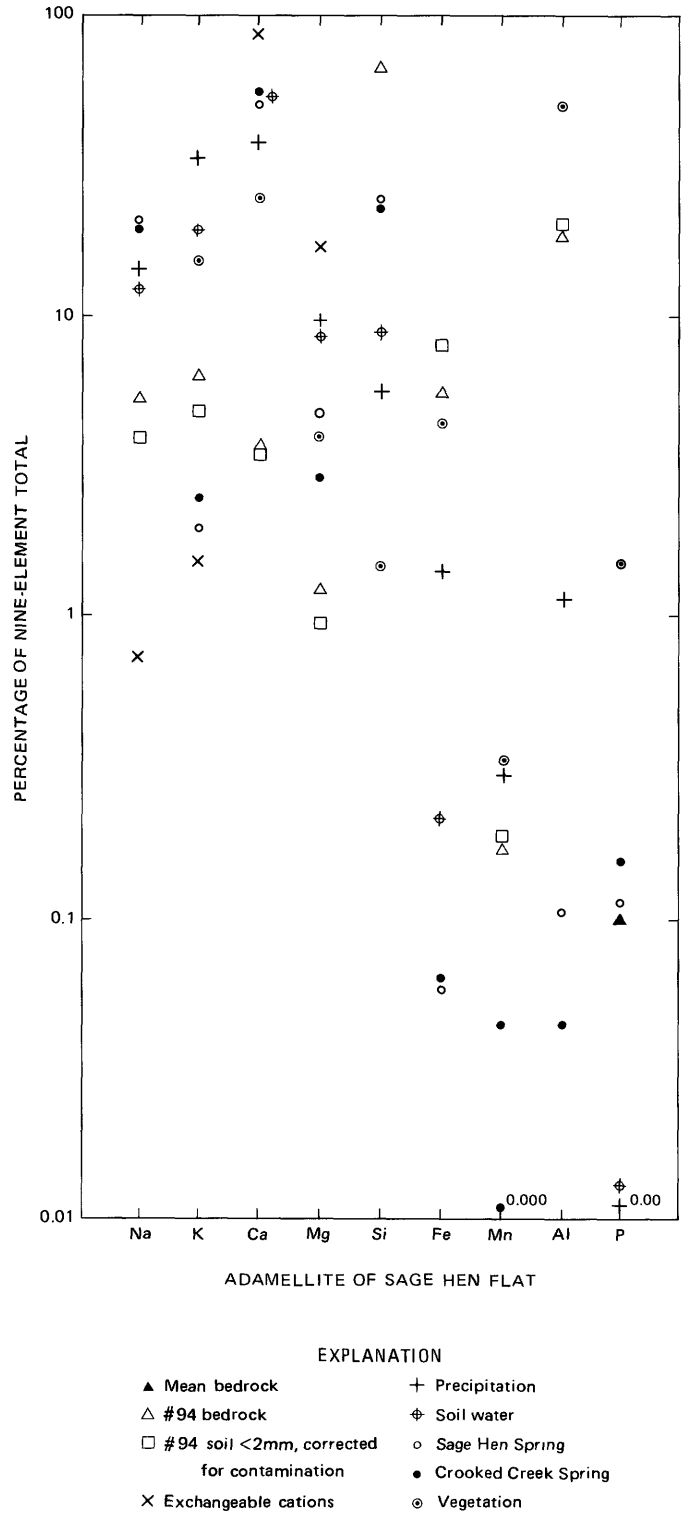

FIGURE 314.—Fractionation of nine elements in the adamellite bedrock-soil-water-plant system based on percentage concentrations.

tute as much as 30 percent of the nonexchangeable total for areas of continuous vegetative cover. Fe and P tend to be quite insoluble under these oxidizing and alkaline soil conditions.

TABLE 26—*Fractionation by plants with respect to soil water for seven elements in adamellite and dolomite terranes*

$$\text{[Elemental percentage} = \frac{\text{Plant concentration (g/cc soil)}}{\text{Plant concentration + soil water concentration (g/cc soil)}} \times 100\text{]}$$

	Si	Ca	Mg	Na
Adamellite:				
Continuous cover	25–30	46–53	47–54	5.9 –7.4
Actual cover	8.3–11	19–23	19–24	1.7 –2.1
Dolomite:				
Continuous cover	------	17–30	17–30	1.1 –2.3
Actual cover	------	5.1–10.0	5.2–10.2	0.31–0.65

	K	Fe	P	Total
Adamellite:				
Continuous cover	51–58	98	~100	47–54
Actual cover	22–27	92	99	20–24
Dolomite:				
Continuous cover	34–51	--	100	18–32
Actual cover	12–22	--	99–~100	5.7–11

The actual extent to which vegetational fractionation occurs is of course dependent on the rate of plant uptake with respect to the rate of leaching. It has been demonstrated (Marchand, 1971) that chemical denudation by plant uptake and litter erosion in this area, although of much less significance than leaching in terms of total chemical removal, may be of considerable importance in the extraction of certain elements, especially metals such as Al, Fe, and Mn. It should also be remembered that elemental concentrations in vegetation represent large static quantities which are unavailable to leaching and which are potentially removable by sporadic accelerated erosion owing to fires or flooding, as well as by normal seasonal denudation.

SUMMARY AND DISCUSSION

The influences of erosion, deposition, vegetation, and microbial activity combine to further complicate an already complex series of chemical and physical alterations (fig. 269) in the weathering processes by which unstable minerals are converted to stable forms under the prevailing surficial conditions, which may themselves change with time. A complete analysis of all aspects of the weathering process is beyond the scope of this paper (the influences of microorganisms, for example, is not evaluated), but the data of the preceding pages suggest the direction and approximate magnitude of some physical, mineralogical, and chemical changes resulting from the weathering of dolomite and biotite adamellite in a present-day semiarid, subalpine climate. These changes involve alterations not only in the solid phases, but in the associated liquid and gas phases as well. Elements released by weathering are fractionated through the effects of plants, colloidal exchange, and leaching.

WEATHERING OF REED DOLOMITE

Field observations and size analyses of soils and bedrock indicate that the initial step of dolomite weathering in the White Mountains involves both physical and chemical breakdown of angular blocks produced by jointing. Polycrystalline soil grains, commonly bounded by cleavages, slowly accumulate from freeze-and-thaw disintegration of these blocks, except in areas of recrystallization near plutonic bodies; here postthermal contraction may have created intergranular stresses, leading to accelerated weathering and spheroidal forms. Chemical weathering is evident throughout the process of grain diminution, but appears to exert a greater effect in the interval between bedrock and soil gravel than between soil gravel and less-than-2-mm soil. Mineralogical decomposition, occurring in the sequence dolomite $\gg$ tremolite, epidote $>$ talc, K-feldspar, plagioclase, biotite $\geq$ apatite $>$ quartz and ilmenite (fig. 294), resulted in percentage chemical losses, from bedrock to soil, of $Mg > Ca > Sr > Mn \overset{?}{\approx} Fe$ (fig. 301). Pure calcite, apparently precipitated during periods of desiccation and partially dissolved during seasonal influx of meteoric waters, occurs as the single verifiably authigenic soil phase, in rinds on spheroidally weathering boulders, on surfaces of soil fragments, and as a discontinuous calcium carbonate soil crust.

Relative mobilities of spring waters with respect to the dolomite bedrock yield the sequence $Mg > Ca \gg Fe > Mn$ (table 22). These findings agree with losses from bedrock to soil, except that they show Fe to be more easily mobilized from dolomite than Mn. Dolomite soil water extracts differ notably in composition from both spring and precipitation waters, probably owing in part to secondary calcite, ash fragments, and local contaminants in the soils. The soil water extracts have pH's much closer to the spring waters than to rain or snow, suggesting a fairly rapid adjustment to soil composition in these soluble soils. Comparisons of ion-activity products with solubility constants indicate that waters draining the terrane are undersaturated with respect to both calcite and dolomite.

Calculated carbon dioxide partial pressures for dolomite-derived waters exceed atmospheric values by more than an order of magnitude and those of waters from the adamellites by several times. The excesses above atmospheric PCO_2 are presumably created by a combination of root respiration, humus oxidation, and other organic processes; the greater PCO_2 values in the dolomite waters must primarily reflect the change in vegetation with substrate, not solution of carbonate.

WEATHERING OF ADAMELLITE OF SAGE HEN FLAT

Weathering in the Sage Hen pluton occurs in several stages. Physical disintegration proceeds by frost riving along intergranular weaknesses caused by cooling and contraction of the rock or possibly by swelling of biotite during initial weathering. Boulders exfoliate and grus accumulates in the A_{11} soil horizon. This coarse material is largely unaltered chemically or mineralogically except for minor Fe oxidation; the principal chemical attack occurs during the transformation of grus to finer sized particles. Primary minerals weather in the sequence plagioclase (An_{25-30}) $>$ hornblende $>$ biotite, epidote $>$ microcline, plagioclase (An_{10-15}), allanite $>$ apatite, chlorite, magnetite $>$ sphene, quartz, muscovite, ilmenite $>$ zircon (fig. 297), resulting in percentage chemical losses, from fresh rock to soil, in the sequence $Rb \overset{?}{>} Na \approx K \approx Mg > Sr > Mn \approx Ca > Ba > Si > Al \gg Fe > Ti$ (fig. 301). X-ray diffractometer and electron microprobe results suggest that kaolinite, and possibly small amounts of vermiculite and montmorillonite, are forming as authigenic alteration products of feldspars, biotite, and other silicates. Microprobe analyses of biotite indicate losses in the sequence $Ba \overset{?}{>} K > Mg > Fe > Si > Al$ (table 8); cations in eightfold to twelvefold coordination appear to be lost most readily, followed by octahedral cations, and finally elements in sixfold and fourfold coordination. Microcline shows some losses of both Na and K, and plagioclase (An_{10-30}) shows changes that imply removal in the sequence $Na > Ca > Si > Al$ (table 10; fig. 300).

Relative mobilities of chemical species in adamellite spring waters indicate that changes with regard to bedrock occur in the sequence $Ca > Mg \approx Na \gg Si \approx K \geq Mn \approx Fe > Al$ (fig. 306). Although this order shows some agreement with bedrock-to-soil losses, it is not entirely consistent with conclusions based on the solid phases alone. The low K mobility is probably the result of plant extraction and fixation within the soil. Plant uptake and litter erosion may explain the low Al content of spring waters. It is suggested that Mg and especially Ca are augmented in waters draining the pluton owing to the solution of fine-grained carbonate particles continually blown into the adamellite terrane. If this latter hypothesis is correct, the chemistry of ground waters is extremely sensitive to the presence of small quantities of soluble materials, including those foreign to the area. The fact that waters from two springs draining the adamellite can be chemically distinguished is another indication of such sensitivity. Both soil and spring waters associated with the pluton plot within the kaolinite stability field (figs. 307, 308) and are supersaturated with quartz but undersaturated with respect to colloidal silica. Proportions of solutes in adamellite soil water extracts appear to be roughly intermediate between precipitation and spring water in the adamellite terrane.

GENERAL WEATHERING RELATIONSHIPS

Observations in the White Mountains, as well as in warmer and wetter regions, suggest that physical weathering of a given lithology may be chiefly a function of the nature and spacing of initial physical weaknesses, particularly intergranular openings, cleavages, fissility, and planar weaknesses, especially joints, which may serve as avenues for fluids. The process of physical breakdown, which tends to precede chemical weathering, may be as closely related to lithologic features as to external conditions. Thermal history or inherent properties such as grain size, grain adhesion or cohesion, crystallographic properties of mineral constituents, bedding characteristics, or jointing may be more critical in affecting rates of physical weathering than climate.

Chemical weathering of any mineral is a function of the chemical composition and crystalline structure of the mineral and of the chemical environment in which weathering occurs. Ca, Mg, Fe, Mn, and Sr, for example, are all lost more readily from dolomite than from silicates and oxides in the adamellite. Dolomite-to-soil percentage losses of Fe are about the same as for Mn, but adamellite Mn losses are much greater than those of Fe. In nonsoluble lithologies such as the adamellite of Sage Hen Flat, chemical losses tend to adhere to the general pattern of alkali metals > alkaline earth metals > nonmetals > metals.

Precipitation water undergoes major chemical changes upon entering the soil, but significant additional modifications occur during percolation to springs. The state of both soil and spring waters with respect to calcite, dolomite, and silica saturation preclude chemical equilibrium in the natural waters studied. This result is not surprising since chemical weathering, which supplies most of the constituents to the waters, is itself an open-system disequilibrium process. It is noteworthy, however, that although steady-state conditions are definitely not attained in soil waters, spring waters closely approximate constant composition. Contact with weathering materials over a considerable space-time interval is apparently necessary for the achievement of a steady state, but this interval may be decreased somewhat in the case of mobile constituents in readily weatherable minerals. The existence of steady-state spring water compositions indicates another area of applicability of the "dynamic equilibrium" concept suggested by Hack (1960) and others in regard to surficial processes.

Elements removed from lattice sites in primary minerals undergo fractionation by (1) formation of secondary phases—primarily clay minerals, calcium carbonate, and various insoluble precipitates, (2) adsorption on colloidal mineral or organic particles, (3) plant uptake, and (4) solution. Quantitative information concerning fractionation of elements into secondary phases is not available for the two lithologies studied here (Al, Si, Fe, Mn, P, and Ca probably undergo fixation to some extent, in this form), but nine principal elements appear to apportion themselves between vegetation, colloidal exchange, and solution as follows (figs. 313, 314; table 25):

Na,	soln $\gg$ exch > veg
Si,	soln $\gg$ veg
Ca,	exch > soln > veg
Mg,	exch > soln $\overset{?}{=}$ veg
K,	veg $\gg$ soln > exch
Fe, Mn, P,	veg $\gg$ soln
Al,	veg $\ggg$ soln

Constituents entering authigenic phases or exchangeable positions are retained within the soil and are removed only through soil erosion or change in chemical environment. Elements taken up by plants are recycled through the soil to the extent that decomposition takes precedence over litter erosion. Evidence presented elsewhere (Marchand, 1971) suggests that, in this area at least, most elements are eventually dissolved and carried out of the soil by deep percolation. Results from the preceding study indicate that removal by plant uptake and litter erosion, although probably not significant in terms of total chemical denudation, may play some part in the total extraction of P and K from the bedrock and soil and undoubtedly accounts for appreciable parts of the chemical denudation of Al, Fe, and Mn. Another effect of vegetation in the weathering process may lie in the conversion of relatively insoluble constituents to more soluble chemical forms in which they could be carried out of the system. Plant uptake, litter fall, and decomposition may thus facilitate leaching, but data are lacking to evaluate the quantitative importance of this aspect of the geochemical cycle.

REFERENCES CITED

Anderson, G. H., 1937, Granitization, albitization, and related phenomena in the northern Inyo Range of California-Nevada: Geol. Soc. America Bull., v. 48, no. 1, p. 1–74.

Anderson, G. H., and Maxson, J. H., 1935, Physiography of the northern Inyo Range [abs.]: Geol. Soc. America Proc., 33d, Berkeley 1934, Cordilleran Sec., p. 318.

Barnes, Ivan, 1964, Field measurement of alkalinity and pH: U.S. Geol. Survey Water-Supply Paper 1535–H, 17 p.

———1965, Geochemistry of Birch Creek, Inyo County, California, a travertine depositing creek in an arid climate: Geochim. et Cosmochim. Acta, v. 29, no. 2, p. 85–112.

Bateman, P. C., and Wahrhaftig, Clyde, 1966, Geology of the Sierra Nevada, *in* Geology of northern California: California Div. Mines and Geol. Bull. 190, p. 107–172.

Beaty, C. B., 1959, Slope retreat by gullying [California-Nevada]: Geol. Soc. America Bull., v. 70, p. 1479–1482.

———1960, Gradational processes in the White Mountains of California and Nevada: Ph.D. thesis, Univ. California, Berkeley, 260 p.

Bower, C. A., Reitemeier, R. F., and Fireman, M., 1952, Exchangeable cation analysis of saline and alkali soils: Soil Sci., v. 73, no. 4, p. 251–261.

Bower, C. A., and Wilcox, L. V., 1965, Soluble salts, *in* Methods of soil analysis; Part 2, Chemical and microbiological properties: Madison, Wis., Am. Soc. Agronomy (Agronomy, no. 9), p. 933–951.

Brewer, Rey, 1964, Fabric and mineral analysis of soils: New York, John Wiley and Sons, Inc., 470 p.

Cady, J. G., 1951, Reck weathering and soil formation in the North Carolina Piedmont region: Soil Sci. Soc. America Proc., v. 15, p. 337–342.

Carmichael, I. S. E., 1967, The iron-titanium oxides of salic volcanic rocks and their associated ferromagnesian silicates: Contr. Mineralogy and Petrology, v. 14, no. 1, p. 36–64.

Cloud, P. E., Jr., and Nelson, C. A., 1966, Phanerozoic-cryptozoic and related transitions—new evidence: Science, v. 154, no. 3750, p. 766–770.

Dalrymple, G. B., 1963, Potassium-argon dates of some Cenozoic volcanic rocks of the Sierra Nevada, California: Geol. Soc. America Bull., v. 74, no. 4, p. 379–390.

Deer, W. A., Howie, R. A., and Zussman, J., 1962a, Reck-forming minerals; Volume 3, Sheet silicates: New York, John Wiley and Sons, Inc., 270 p.

———1962b, Rock-forming minerals; Volume 1, Ortho- and ring-silicates: New York, John Wiley and Sons, Inc., 333 p.

———1963a, Reck-forming minerals; Volume 2, Chain silicates: New York, John Wiley and Sons, Inc., 379 p.

———1963b, Rock-forming minerals; Volume 4, Framework silicates: New York, John Wiley and Sons, Inc., 435 p.

Emerson, D. O., 1966, Granitic rocks of the Mt. Barcroft quadrangle, Inyo batholith, California-Nevada: Geol. Soc. America Bull., v. 77, no. 2, p. 127–152.

Feth, J. H., Roberson, C. E., and Polzer, W. L., 1964, Sources of mineral constituents in water from granitic rocks, Sierra Nevada, California and Nevada: U.S. Geol. Survey Water-Supply Paper 1535–I, 70. p.

Feth, J. H., Rogers, S. M., and Roberson, C. E., 1964, Chemical composition of snow in the northern Sierra Nevada and other areas: U.S. Geol. Survey Water-Supply Paper 1535–J, 39. p.

Folk, R. L., 1965, Petrology of sedimentary rocks: Austin, Texas, Hemphill's, 159 p.

Gallick, C. M., 1964, Geology of a part of the Blanco Mountain quadrangle, Inyo County, California: M. A. thesis (unpub.), Univ. California, Los Angeles.

Garrels, R. M., and Christ, C. L., 1965, Solutions, minerals, and equilibria: New York, Harper and Row, 450 p.

Goldich, S. S., 1938, A study in rock-weathering: Jour. Geology, v. 46, p. 17–58.

Hack, J. T., 1960, Interpretation of erosional topography in humid temperate regions (Bradley volume): Am. Jour. Sci., v. 258–A, p. 80–97.

Hall, M. L., 1964, Intrusive truncation of the Precambrian-Cambrian succession in the White Mountains, California: M. A. thesis, Univ. California, Berkeley, 90 p.

Harned, H. S., and Davis, Raymond, Jr., 1943, The ionization constant of carbonic acid in water and the solubility of carbon dioxide in water and aqueous salt solutions from 0° to 50° C.: Am. Chem. Soc. Jour., v. 65, p. 2030–2037.

Harned, H. S., and Scholes, S. R., Jr., 1941, The ionization constant of HCO_3 from 0° to 50° C.: Am. Chem. Soc. Jour., v. 63, p. 1706–1709.

Hay, R. L., 1959, Origin and weathering of late Pleistocene ash deposits on St. Vincent, B. W. I.: Jour. Geology, v. 67, no. 1, p. 65–87.

———1966, Zeolites and zeolitic reactions in sedimentary rocks: Geol. Soc. America Spec. Paper 85, 130 p.

Helley, E. J., 1966, Sediment transport in the Chowchilla River basin: Mariposa, Madera, and Merced Counties, California: Ph. D. thesis (unpub.), Univ. California, Berkeley, 153 p.

Hsu, K. J., 1964, Solubility of dolomite estimated on the basis of the chemical composition of Florida ground waters [abs]: Geol. Soc. America Spec. Paper 76, p. 84–85; Ground Water, v. 2, no. 1, p. 56.

Johnson, C. M., and Ulrich, Albert, 1959, Analytical methods for use in plant analyses: California Agr. Expt. Sta. Bull. 766, Part 2, p. 26–77.

Jones, L. H., and Thurman, D. A., 1957, The determination of aluminum in soil, ash, and plant materials using Eriochrome Cyanine R. A.: Plant and Soil, v. 9, p. 131–142.

Kesseli, J. E., and Beaty, C. B., 1959, Desert flood conditions in the White Mountains of California and Nevada: U.S. Army Quartermaster Research and Eng. Center, Tech. Rept. EP–108, 107 p.

Kilmer, V. J., 1965, Silicon, *in* Methods of soil analysis; Part 2, Chemical and microbiological properties: Madison, Wis., Am. Soc. Agronomy (Agronomy, no. 9), p. 959–962.

Knopf, Adolf, 1918, A geologic reconnaissance of the Inyo Range and the eastern slope of the southern Sierra Nevada, California: U.S. Geol. Survey Prof. Paper 110, 130 p.

Krauskopf, K. B., 1968, A tale of ten plutons: Geol. Soc. America Bull., v. 79, no. 1, p. 1–18.

———1971, Geologic map of the Mount Barcroft quadrangle, California-Nevada: U.S. Geol. Survey Geol. Quad. Map GQ–960.

LaMarche, V. C., Jr., 1967, Spheroidal weathering of thermally metamorphosed limestone and dolomite, White Mountains, California, *in* Geological Survey research, 1967: U.S. Geol. Survey Prof. Paper 575–C, p. C32–C37.

———1968, Rates of slope degradation as determined from botanical evidence, White Mountains, California: U.S. Geol. Survey Prof. Paper 352–I, p. 341–377.

Larson, T. E., and Buswell, A. M., 1942, Calcium carbonate saturation index and alkalinity interpretations: Am. Water Works Assoc. Jour., v. 34, no. 11, p. 1667–1684.

McKee, E. H., and Nash, D. B., 1967, Potassium-argon ages of granitic rocks in the Inyo batholith, east-central California: Geol. Soc. America Bull., v. 78, no. 5, p. 669–680.

Major, Jack, 1967, Potential evapotranspiration and plant distribution in Western States with emphasis on California, *in* Shaw, R. H., ed., Symposium on ground level climatology, 1965, Berkeley, Calif.: Am. Assoc. Adv. Sci. Pub. 86, p. 93–126.

Manov, G. G., Bates, R. G., Hamer, W. J., and Acree, S. F., 1943, Values of the constants in the Debye-Huckel equation for activity coefficients: Am. Chem. Soc. Jour., v. 65, p. 1765.

Marchand, D. E., 1968, Chemical weathering, soil formation, and geobotanical correlations in a portion of the White Mountains, Mono and Inyo Counties, California: Ph. D. thesis, Univ. California, Berkeley, 376 p.

———1970, Soil contamination in the White Mountains, eastern California: Geol. Soc. America Bull., v. 81, no. 8, p. 2497–2505.

———1971, Rates and modes of denudation, White Mountains, eastern California: Am. Jour. Sci., v. 270, p. 109–135.

———1973, Edaphic control of plant distribution in the White Mountains, eastern California: Ecology, v. 54, no. 2, p. 233–250.

Markam, A. A., and Kobe, K. A., 1941, The solubility of carbon dioxide and nitrous oxide in aqueous salt solutions: Am. Chem. Soc. Jour., v. 63, p. 449.

Maxson, J. H., 1935, Pre-Cambrian stratigraphy of the Inyo Range [abs.]: Geol. Soc. America Proc., 33d, Berkeley 1934, Cordilleran Sec., p. 314.

Mead, W. J., 1915, Occurrence and origin of the bauxite deposits of Arkansas: Econ. Geology, v. 10, p. 28–54.

Morrison, R. B., 1964, Lake Lahontan: Geology of southern Carson Desert, Nevada: U.S. Geol. Survey Prof. Paper 401, 156 p.

Munz, P. A., and Keck, D. D., 1959, A California flora: Berkeley, Univ. California Press, 1681 p.

Nelson, C. A., 1962, Lower Cambrian-Precambrian succession, White-Inyo Mountains, California: Geol. Soc. America Bull., v. 73, p. 139–144.

———1963, Preliminary geologic map of the Blanco Mountain quadrangle, Inyo and Mono Counties, California: U.S. Geol. Survey Mineral Inv. Field Studies Map MF–256.

———1966, Geologic map of the Blanco Mountain quadrangle, Inyo and Mono Counties, California: U.S. Geol. Survey Geol. Quad. Map GQ–529.

Nelson, C. A., and Perry, L. J., 1955, Late Precambrian-early Cambrian strata, White-Inyo Mountains, California [abs]: Geol. Soc. America Bull., v. 66, no. 12, Part 2, p. 1657–1658.

Nicholls, J. W., 1965, Summary of the climatic conditions and geologic history of the White Mountains region, California: Space Sci. Lab. Pub., Univ. California, Berkeley.

Olsen, S. R., and Dean, L. A., 1965, Phosphorus, *in* Methods of soil analysis; Part 2, Chemical and microbiological properties: Madison, Wis., Am. Soc. Agronomy (Agronomy, no. 9), p. 1035–1049.

Pace, Nello, 1963, Climatological data summary for the decade 1 January 1953 through 31 December 1962 from the Crooked Creek Laboratory (10,150 ft) and the Barcroft Laboratory (12,470 ft): Berkeley, Univ. California, White Mountain Research Sta. rept., 52 p.

Pittman, E. D., 1958, Geology of the northwestern portion of the Blanco Mountain quadrangle, California: M. S. thesis (unpub.), Univ. California, Los Angeles, 103 p.

Powell, D. R., 1963, The physical geography of the White Mountains, California-Nevada: M. A. thesis (unpub.), Univ. California, Berkeley.

Rosenblum, Samuel, 1956, Improved techniques for staining potash feldspars: Am. Mineralogist, v. 41, nos. 7–8, p. 662–664.

Ruhe, R. V., 1967, Geomorphic surfaces and surficial deposits in southern New Mexico: New Mexico Bur. Mines and Mineral Resources Mem. 18, 65 p.

Sherman, G. D., and Uehera, Goro, 1956, The weathering of olivine basalt in Hawaii and its pedogenic significance: Soil Sci. Soc. America Proc., v. 20, p. 337–340.

Spurr, J. E., 1903, Descriptive geology of Nevada south of the fortieth parallel and adjacent portions of California: U.S. Geol. Survey Bull. 208, p. 206–212.

Taylor, M. E., 1966, Precambrian mollusc-like fossils from Inyo County, California: Science, v. 153, no. 3732, p. 198–201.

Taylor, R. L., 1965, Cenozoic volcanism, block faulting, and erosion in the northern White Mountains, Nevada: M. A. thesis (unpub.), Univ. California, Berkeley, 95 p.

Wahrhaftig, Clyde, 1965, Stepped topography of the southern Sierra Nevada, California: Geol. Soc. America Bull., v. 76, no. 10, p. 1165–1190.

Waring, R. H., and Hermann, R. K., 1966, A modified Piche evaporimeter: Ecology, v. 47, no. 2, p. 308–310.

Warshaw, C. M., and Roy, Rustum, 1961, Classification and a scheme for the identification of layer silicates: Geol. Soc. America Bull., v. 72, p. 1455–1492.

Wolfenden, E. B., 1965, Geochemical behavior of trace elements during bauxite formation in Sarawak, Malaysia: Geochim. et Cosmochim. Acta, v. 29, p. 1051–1062.

Wooley, J. T., and Johnson, C. M., 1957, Silicon determination in ashed plant material: Agr. and Food Chemistry, v. 5, no. 11, 872. p.

SUPPLEMENTAL INFORMATION

METHODS, REPRODUCIBILITY, AND ACCURACY

Field procedures for the collection of data and samples have been discussed in the text. Several temporary field impregnations were obtained from soil pits with Quickmont (available from E. V. Roberts and Associates, Culver City, Calif.) and later fully impregnated under vacuum with leucite. The advantage of the field impregnation is that natural orientation and textures are maintained. Bedrock and soil samples were treated in the laboratory as outlined in figures 315 and 316.[7]

Fresh bedrock chips and soil samples (soil gravel, less than 2 mm) were crushed with a tungsten carbide mortar and pestle and ground to −50 mesh in a tungsten carbide ball mill. Each fraction was then split and made into an X-ray fluorescence pellet. The values of table 27 (top), representing chips of the same sample, ground in different mortars and separately prepared, indicate no significant source of error in the grinding, splitting, or pellet-making operations. The replicate analyses of the table suggest precision of about ± 0–6 percent of the analyzed value and generally below 2 percent for values above 2.0 percent. Table 28 compares X-ray fluorescence results with those of wet chemistry (unpub. data of Ken-ichiro Aoki) and those for Na and K by flame photometer (by Joaquin Hampel; see "Introduction"). Agreement is good in some cases and very poor in others. Lighter elements such as Na, Mg, Al, and Si are not as easily excited by X-rays as heavier elements and are most susceptible to error. Where samples approximate the composition of well-analyzed standards, however, X-ray results appear to be both precise and accurate. The values of Hampel were used for Na and K, but all other figures were taken from X-ray determinations (except values of Aoki used as X-ray standards).

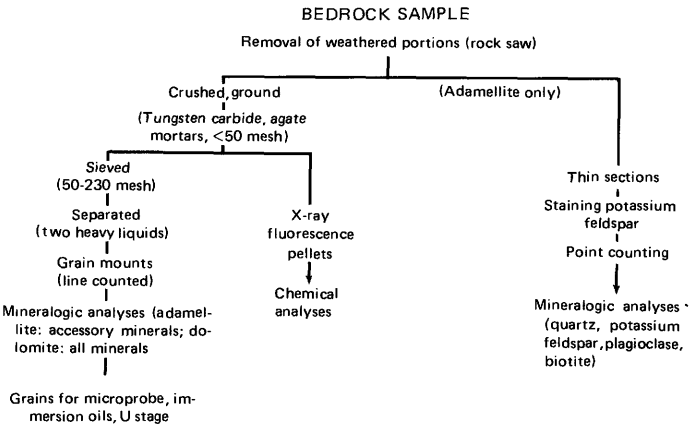

FIGURE 315.—Flowsheet for laboratory treatment of bedrock samples.

Thin sections of five adamellite bedrock samples were stained for K-feldspar (Rosenblum, 1956) and point counted to determine quartz, K-feldspar, plagioclase, and biotite percentages. Mineralogical analyses of crushed bedrock (50–230 mesh) and less-than-2-mm-sand (greater than 62 μm, crushed to -50 mesh), fine sand and very fine sand fractions of soils were obtained from line counts of grain mounts after removal of organic matter with 2 percent hydrogen peroxide (soils only) and two successive heavy liquid separations. For the dolomite samples, liquids of specific gravity 2.69 (bromoform plus alcohol) and 2.95 (tetrabromoethane) were used; liquids having densities of 2.88 (bromoform) and 3.3 (methylene iodide) were used for adamellite samples. A minimum of 900 grains, and usually more than

[7]The following parameters were determined for the less-than-2-mm fraction of many soil samples for purposes outside the scope of this paper: Phosphorus in 10:1 water extracts, permanent wilting point (soil moisture at 15-atm tension), moisture equivalent (soil moisture at 1/3-atm tension), available water (mositure equivalent minus permanent wilting point), percentage carbonate, and total carbon.

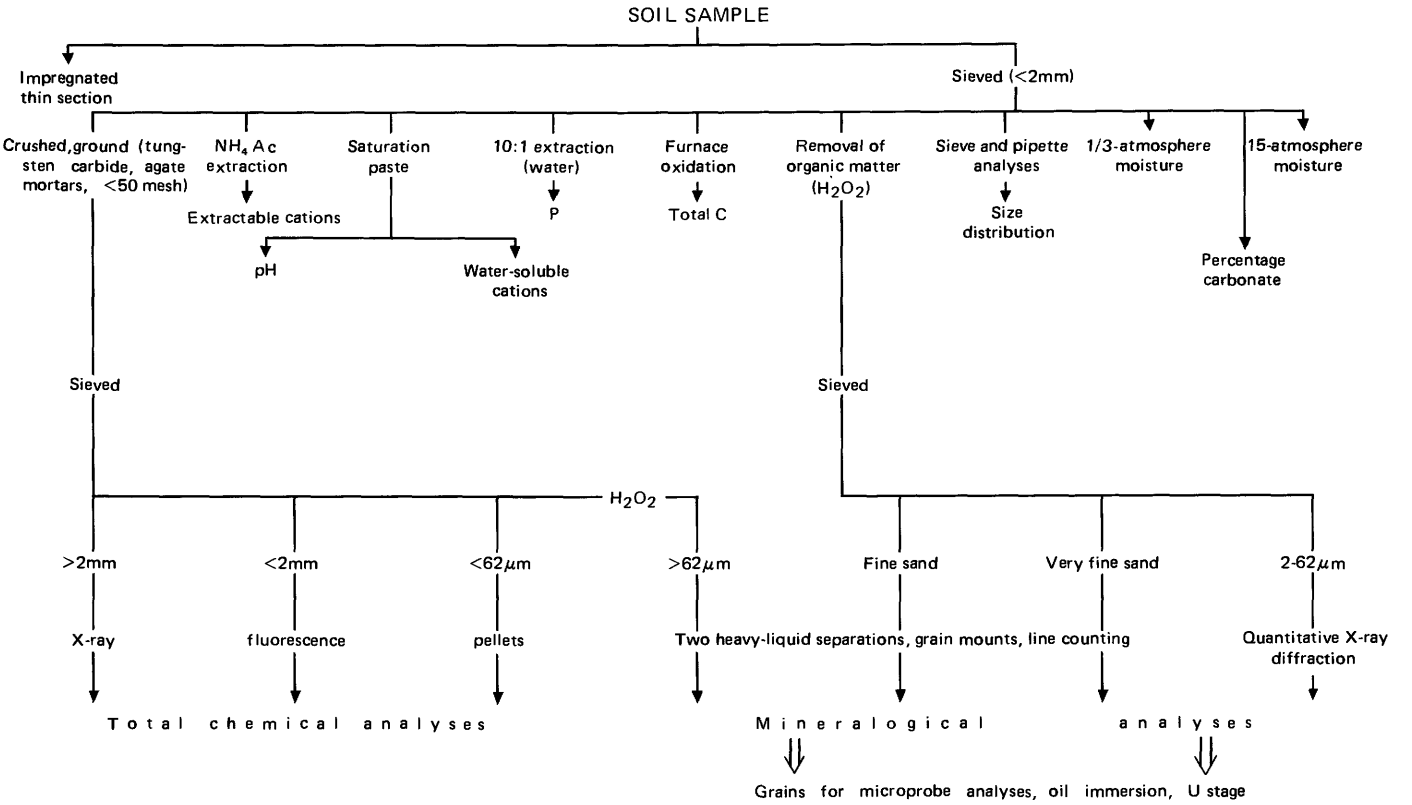

FIGURE 316.—Flowsheet for laboratory treatment of soil samples.

TABLE 27.—*Reproducibility of X-ray fluorescence analyses*

[Values yielded by opposite sides of the same pellet, except sample 58]

	Fe	Mn	Ca	Sr	Rb
	(weight percent)			(ppm)	
58 (agate)	0.22	0.06	21.86	59.3	0.0
58 (tungsten carbide)	.22	.06	21.99	59.5	.0
47 soil	3.26	------	------	------	------
47 soil	3.26	------	------	------	------
52 soil	------	------	------	------	43.1
52 soil	------	------	------	------	44.1
64 soil	------	------	22.98	------	------
64 soil	------	------	23.31	------	------
66 soil	------	------	22.76	------	------
66 soil	------	------	23.00	------	------
68 soil	------	------	------	166	------
68 soil	------	------	------	167	------
97	1.32	------	------	------	------
97	1.32	------	------	------	------
98	------	.042	------	------	------
98	------	.045	------	------	------

1,500 grains, per sample was counted. The statistical analysis of Brewer (1964, p. 46–50) indicates that counts of 1,500 grains yield results within about 5 percent probable error for major constituents and less than 15 percent for minor minerals. Mineral densities used to compute weight percentages from grain mounts were obtained by direct measurement or from chemical composition information.

Line-counted samples were used as standards for quantitative X-ray diffraction analyses of silt fractions. Both standards and samples were finely ground in a mortar, mounted on glass slides with the aid of acetone, and X-rayed under identical conditions on the same day. Abundances were based on peak heights above background. Glass was assumed to make up the difference between totals and 100 percent, an assumption verified by many visual estimations of silt-glass percentage under the polarizing microscope. Probable error is estimated at less than 15 percent of the given value.

Laboratory soil pH measurements were made with a Beckman Zeromatic pH meter on water-saturation pastes. Replicate analyses of samples yielded results within 0.1 pH unit. Similar pastes were extracted by the Buchner funnel method of Bower and Wilcox (1965, p. 935). Replicate analyses of 19 saturation extract samples indicate reproducibility at the level of ±25 percent of the stated value. Soil samples were extracted with NH_4Ac solutions at pH 7.0, using the centrifuging method of Bower, Reitemeier, and Fireman (1952, p. 253), and analyzed for total extractable Na, K, Ca, and Mg. Results are reproducible to within 20 percent of the stated values. Na and K in water and NH_4Ac extracts were analyzed by flame photometry. Ca, Mg, and Fe in soil extracts were determined by atomic absorption spectrophotometry. Si was analyzed using colorimetric procedures described by Kilmer (1965, p. 959–962). P in water-saturation extracts was determined by the methods of Olsen and Dean (1965, p. 104–107).

Plant samples from the field and greenhouse were washed with distilled water and ovendried at 104°C. Into 30-milliliter digestion flasks, 0.2000–0.5000 grams of each dry sample was weighed. Five milliliters of concentrated HNO_3 and $HCLO_4$ were added, and the samples were digested overnight in a sand bath. The samples were then heated on Kjeldahl burners until they appeared colorless and $HCLO_4$ fumes were evident. The solutions were cooled and diluted to 100 milliliters in volumetric flasks with 10 milliequivalents per liter $SrCl_2$ (to mask interferences). Aliquots were taken for subsequent analysis. K, Na, Ca, Mg, Fe, and Mn were analyzed by atomic absorption spectrophotometry. P was determined colorimetrically by the molybdenum blue method described by Johnson and Ulrich (1959), using stannous chloride as a reducing agent. Al was determined by the Eriochrome Cyanine R. A. method of Jones and Thurman (1957). The methods of Wooley and Johnson (1957, p. 872) were employed in the dry ashing and Si analysis of plants. Absolute limits of precision are ±20 percent of the given value, but analytical results are within ±10 percent in all but a few cases.

The preceding discussion has been confined to methods and precision of measurements for any given sample. Statistical computer data (table 29) permit a comparison of various physical and chemical soil parameters with regard to variation within a given soil type. Geographic patterns of variation within and between soil types were not assessed. The figures of table 29, based on samplings of from 12 to 25 sites per soil type, indicate seven general groups of soil parameter variation for this area, decreasing in reliability as follows:

TABLE 28.—*Comparison of analytical results for some adamellite of Sage Hen Flat (samples 92, 98) and Reed Dolomite samples, as analyzed by X-ray fluorescence (XRF), wet chemistry (Ken-ichior Aoki), and flame photometry (Joaquim Hampel)*

	52 bedrock			52 soil, < 2 mm			54 bedrock			54 soil, < 2 mm			54 soil, > 2 mm	
	XRF	Aoki	Hampel	XRF	Aoki	Hampel	XRF	Aoki	Hampel	XRF	Aoki	Hampel	XRF	Hampel
SiO_2	0.17	0.16	------	41.19	23.01	------	0.55	0.81	------	[1]35.74	35.74	------	1.95	------
TiO_2	------	Trace	------	------	.44	------	.03	.03	------	.47	.50	------	.01	------
Al_2O_3	.13	.16	------	11.48	7.87	------	.40	.47	------	[1]9.89	9.89	------	.08	------
Total Fe as Fe_2O_3	.23	.23	------	3.78	3.56	------	.39	.39	------	[1]3.14	3.14	------	.53	------
MnO	.05	.04	------	.21	.17	------	.07	.05	------	[1].16	.16	------	.09	------
MgO	20.47	21.29	------	6.96	8.86	------	20.75	21.76	------	[1]8.44	8.44	------	18.54	------
CaO	30.79	31.24	------	9.16	22.09	------	29.74	30.29	------	[1]14.14	14.14	------	30.92	------
Na_2O	.04	.03	0.04	1.00	.46	0.48	<.01	.08	0.04	.72	.16	1.55	<.01	0.07
K_2O	.00	.02	.02	1.81	.82	.98	.01	.07	.03	------	1.63	1.88	.07	.06

	68 bedrock		68 soil, > 2 mm		64 bedrock		92 bedrock		92 soil, < 2 mm		98 soil, < 2 mm		
	XRF	Hampel	XRF	Hampel	XRF	Aoki	XRF	Aoki	XRF	Aoki	XRF	Aoki	Hampel
SiO_2	0.09	------	1.49	------	0.75	0.59	65.83	67.20	65.93	65.40	66.93	69.65	------
TiO_2	.01	------	.04	------	------	0.03	------	.53	------	.63	.50	.43	------
Al_2O_3	.12	------	.61	------	.19	.12	------	16.33	------	15.77	------	14.57	------
Total Fe as Fe_2O_3	.39	------	.51	------	.33	.46	3.96	3.12	4.73	3.54	2.67	2.50	------
MnO	.12	------	.12	------	.03	.03	.10	.06	.11	.05	.04	.04	------
MgO	19.83	------	19.83	------	7.20	7.42	1.05	.77	[1]1.15	1.15	.79	.65	------
CaO	30.41	------	30.41	------	39.69	46.87	2.37	2.86	2.14	2.32	1.60	1.63	------
Na_2O	<.01	.03	<.01	.08	<.01	.07	3.44	3.73	3.31	3.35	2.84	3.24	3.39
K_2O	.00	.01	.08	.07	.05	.06	3.88	.11	3.77	3.82	3.69	3.53	3.63

[1]Valve of Aoki used for standard.

TABLE 29.—*Variation in measured parameters of four White Mountains soil types*

	Reed Dolomite		Basalt		Adamellite of Sage Hen Flat		Andrews Mountain Sandstone		Range of percent standard deviation
	Number of samples	Percent standard deviation from mean	Number of samples	Percent standard deviation from mean	Number of samples	Percent standard deviation from mean	Number of samples	Percent standard deviation from mean	
Total extractable K	25	51	18	20	22	37	19	26	20–51
Total extractable Na	25	31	18	20	22	62	19	23	20–62
Total extractable Ca	25	41	18	16	22	32	19	22	16–14
Total extractable Mg	25	40	18	23	22	31	19	18	18–40
K in water-saturation extracts	21	78	17	42	21	83	12	55	42–83
Na in water-saturation extracts	21	35	17	53	21	28	12	59	28–59
Ca in water-saturation extracts	21	39	17	49	21	40	12	51	39–51
Mg in water-saturation extracts	21	36	17	42	21	36	12	37	36–42
Percent exchangeable K	21	56	17	19	21	47	12	31	19–56
Percent exchangeable Na	21	37	17	19	21	33	12	17	17–37
Percent exchangeable Ca	21	9	17	2	21	5	12	3	2– 9
Percent exchangeable Mg	21	40	17	12	21	27	12	13	12–40
Sum of exchangeable cations	21	32	17	15	21	29	12	14	14–32
P in 10:1 water extracts	18	73	17	67	21	59	15	111	59–111
High field pH	25	1	18	8	22	8	19	8	1– 8
Low field pH	25	5	18	5	22	7	19	8	5– 8
Mean field pH	25	1	18	7	22	8	19	8	1– 8
Laboratory pH	25	3	18	4	22	5	17	7	3– 7
Soil moisture at ⅓-atm tension	17	28	16	9	22	16	16	14	9–28
Soil moisture at 15-atm tension	23	45	17	24	22	25	17	30	24–45
Available water	17	28	16	21	22	12	15	18	12–28
Soil depth on topographic highs	24	27	17	22	21	22	17	14	14–27
Bulk density	24	34	17	20	21	17	----	----	17–34
Percent fragments greater than 2 mm	14	20	----	----	14	61	19	16	16–61

1. Laboratory and field pH
2. Available water, ⅓-atmosphere moisture, soil depth on topographic highs
3. Exchangeable cations, bulk density
4. Total extractable cations, 15-atmosphere moisture
5. Percentage of soil gravel fragments
6. Cations in water-saturation extracts
7. 10:1 available phosphorus

Many soil surveys and soil descriptions include only one or two analyses of these soil properties for each soil series. Information presented here would suggest that although a few pH and ⅓-atmosphere moisture determinations may suffice to characterize properties of a soil series as a whole, most other parameters range widely within a given soil type and cannot be accurately evaluated by a few analyses. The White Mountains soils are, of course, lithosols and therefore may show more variation than finer textured soils formed on alluvium or strongly developed soils on almost any parent material. Nonetheless it is unlikely that analyses at one type locality are sufficient to describe accurately properties of a soil series having any appreciable lateral extent.

☆ U.S. GOVERNMENT PRINTING OFFICE: 1974—543–583/93